Thermodynamic and Transport Properties of Non-Magnetic Particles in Magnetic Fluids

by

Saurabh Tejwani

B.Tech., Chemical Engineering – Indian Institute of Technology, Bombay, India, 2004

M.S., Chemical Engineering Practice - Massachusetts Institute of Technology, Cambridge, MA 2006

Submitted to the Department of Chemical Engineering in partial fulfillment of the requirements for the degree of

Doctor of Philosophy
at the
Massachusetts Institute of Technology
July 2009

Signature of Author.....
Department of Chemical Engineering
July 14, 2009

Certified by.....
T. Alan Hatton
Ralph Landau Professor of Chemical Engineering Practice
Thesis Supervisor

Certified by.....
Kenneth A. Smith
Gilliland Professor of Chemical Engineering
Thesis Supervisor

Accepted by.....
William M. Deen
Carbon P. Dubbs Professor of Engineering
Chairman, Committee for Graduate Students

Thermodynamic and Transport Properties of Non-Magnetic Particles in Magnetic Fluids

by

Saurabh Tejwani

Submitted to the Department of Chemical Engineering on July 14, 2009

in partial fulfillment of the requirements for the degree of

Doctor of Philosophy in Chemical Engineering

Abstract

Magnetic composites, obtained on associating magnetic fluid with non-magnetic particles, offer interesting opportunities in separations, assemblies and other applications, where the microstructure of the composite can be altered reversibly by an external field without altering the composition. The goal of our work in this area is to develop computational and simulation tools to assist in the in-depth understanding of the thermodynamic and transport properties of such non-magnetic nanoparticles immersed in magnetic fluids under varying magnetic field conditions. Also, in this work we have studied the relaxation and magnetization characteristics of magnetic nanoparticle clusters in presence of low external magnetic fields.

Theoretical analysis of such a complex system is difficult using conventional theories, and hence we have used Monte Carlo Simulations to explore these effects. We simulated the interactions between non-magnetic particles (1000 nm) and magnetic nanoparticles (10 nm and 20 nm diameter) dispersed in organic phase. We observed that the presence of the non-magnetic particle in the system induces magnetic non-homogeneity. The magnetic nanoparticles present in the equatorial place of the non-magnetic particle with reference to the applied magnetic field have a higher magnetization as compared to the particles in the polar region. This effect was much more dominant for 20 nm particles than 10nm particles, because the magnetic inter-particle interactions are much stronger for the larger particles. We have also studied the effect of radial distance from the non-magnetic particle on the magnetization and radial distribution function characteristics of the magnetic nanoparticles.

We have evaluated the magnetophoretic forces the non-magnetic particles experience when subjected to magnetic field gradient. We have identified such forces arising from the inter-particle interactions between the magnetic nanoparticles. These forces were found to be significant for larger magnetic particles, smaller non-magnetic particles and lower magnetic fields.

Diffusion coefficients were evaluated for non-magnetic nanoparticles in magnetic fluids using Brownian Dynamics Simulation. The chain-like structures formed by magnetic nanoparticles introduce anisotropy in the system with the diffusion coefficients higher along the direction of applied external magnetic field and lower in the perpendicular direction. It was observed that the anisotropy increases with higher magnetic particle concentration and larger non-magnetic particles. Anisotropy is negligible for small sized magnetic particles for which the inter-particle interaction is smaller, increases with increasing magnetic particle size and becomes constant thereafter. Results were compared with theoretical predictions.

Néel Relaxation was studied for magnetic nanoparticle clusters. Chain-like, spherical and planar clusters were evaluated for the relaxation times. For chain-like structures the relaxation times increase significantly on increasing the chain length and particle size. For spherical clusters the relaxation times were fairly similar to that of individual magnetic nanoparticles. Hence, such a fast relaxation makes them ideal candidates for HGMS separations, since they will be released quickly from the magnetic wires during the elution step. Also, we studied the magnetization characteristics of rectangular and hexagonal packing arrangements of magnetic clusters in presence of remnant fields. The hexagonal arrangement revealed a novel oscillatory behavior. A theoretical model was developed to predict the magnetic particle size beyond which the oscillations are observed.

Thesis Supervisor: T. Alan Hatton
Title: Ralph Landau Professor of Chemical Engineering

Thesis Supervisor: Kenneth A. Smith
Title: Gilliland Professor of Chemical Engineering

Acknowledgements

I would like to sincerely thank my advisers Prof. T. Alan Hatton and Prof. Kenneth A. Smith for their guidance and support, and made this work possible. They always encouraged me to think creatively and independently. I am indebted to Alan for the valuable inputs he gave when it seemed I had reached a dead end. Ken's never ending quest for details took my understanding to the next level. I am also thankful to my committee members, Prof. Gregory Rutledge and Prof. Patrick Doyle for their helpful suggestions throughout the course of the project.

It would have been very difficult to finish this work without the help of past and current members of Hatton Group. Dr. Harpreet Singh and Dr. Lino Gonzalez helped me get acquainted with the subject and were there for my questions. Thanks to Fei Chen, for having all the valuable discussion. Fei and I have worked together all through the course of this project and it has been the most pleasurable experience, professionally and personally. I would also like to mention a note of thanks to Dr. Lev Bromberg, Dr. Smeet Deshmukh and Dr. Tatsushi Isojima for introducing me to the experimental techniques. A special thanks to Abhinav Akhoury, Sanjoy Sircar, Nate Aummock, A.V.N Ravikanth, Himanshu Dhamankar, Vaibhav Somani, and Asha Parekh for all the friendly chats and discussions.

I am thankful to my friends and family for all the help. Thanks to my roommate Yogesh Ramadass, for getting me involved with all kinds of sports. I am grateful to my brother, Gaurav Tejwani and my sister-in-law Charu Tejwani for the constant love and support. I would not have even been at MIT, if not for the help and support of my father, Dr. Suresh Tejwani and my mother, Rashmi Tejwani. I dedicate this thesis to them.

Table of Contents

List of Figures

Chapter 1

1. Introduction

The goal of this thesis is to understand the interactions between magnetic nanoparticles and non-magnetic particles. We have evaluated transport and thermodynamic properties of non-magnetic nanoparticles in magnetic fluids using Monte Carlo simulations and stochastic dynamics simulations. We have considered non-magnetic particles of the size of few nanometers, almost similar in size as that of magnetic nanoparticles. Hence, we treat the magnetic particles discretely as compared to the continuum approximation considered previously [1, 2]. Another area looked in this study is the Néel relaxation of magnetic nanoparticle clusters and magnetic characterization of particle clusters in remnant magnetic fields.

1.1 Magnetic fluids

1.1.1 Applications

Magnetic fluids are stable colloidal suspensions of sub-domain magnetic metal particles (3-15 nm) in a carrier liquid. Their history dates back to the early 1930's when Bitter [3] and Elmore [4] synthesized the first magnetic colloid. However the type of magnetic fluids used these days have their origins in the early 1960's [5]. Nanoparticles of magnetite (Fe_3O_4) and maghemite γFe_2O_3 are the most studied magnetic nanoparticles due to their ease of synthesis and chemical modification and their non-toxicity. Industrial applications for magnetic fluids include seals, dampers, and moving coil loud speakers [5]. Magnetic fluids have been employed in adsorptive non-magnetic particle separations [6-10]. These separations have become widespread in the field of biology, biotechnology, biomedicine [11] and applications include cell sorting, RNA and DNA isolation [12], separation and purification [13, 14]. Recently these particles have also been employed

toxin removal [15-17] and water purification [18-21]. Magnetic nanoparticles have been employed in data storage [22], magneto-optical areas [23-26], catalysis [27-29], oxygen transfer [30], and bio-medicine [31-36]. Researchers have designed various kinds of on-chip and integrated magnetic particle manipulators and separators [37, 38]. Pamme [39] has used magnetic nanoparticles for mixing fluid streams, as valves, and as support for bio-reactions in microchannels.

1.1.2 Stability of magnetic fluids

An important component of these ferrofluids is the presence of adsorbed long chain molecular species on the particle surface (Figure 1-1). The magnetic fluid is considered stable, if it can overcome the van der Waals forces of attraction responsible for agglomeration. Also the magnetic particles interact with each other by another interparticle force, which is the magnetic dipole-dipole interaction. The magnetic dipole-dipole interaction is dominant at long separation distances, while the van der Waals interaction dominates at short distances [5]. The repulsion caused by this surfactant or the polymer prevents aggregation between particles even under the presence of strong magnetic fields.

All stabilizing polymers or surfactants require a means of attachment to the nanoparticles. A common method of stabilizer attachment to the particles is through the incorporation of a functional group that forms an electrostatic or covalent bond to the particle surface. For magnetite-based magnetic fluids, the most common functional group for attachment is carboxylic acid, which is known to form a strong *d*-orbital chelation to iron atoms on the magnetite surface [40, 41]. This attachment mechanism was used in the earliest magnetic fluids [42, 43], which consisted of fatty acid-stabilized magnetite nanoparticles in kerosene, where the carboxyl head group of the fatty acid attached to the magnetite surface and the alkyl tail provided steric stabilization.

The repulsive forces are steric in nature for organic magnetic fluid, and are steric and electrostatic for water based magnetic fluids. Usually, water based magnetic fluids are considered more stable that organic magnetic fluids. Stability of these magnetic colloids has been an exciting area of research in the recent past [44-46].

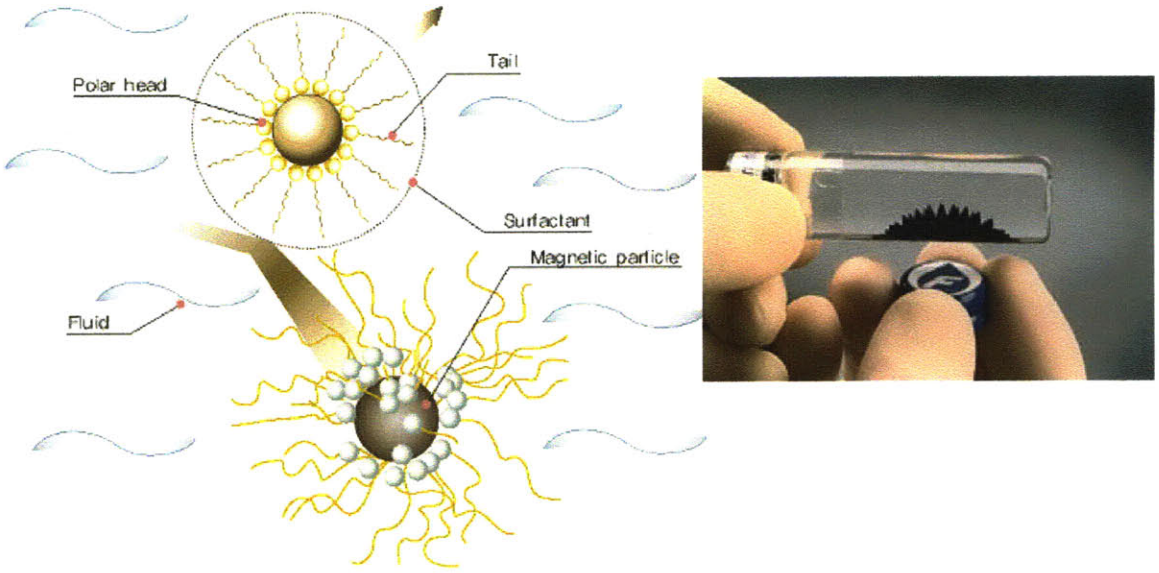

Figure 1-1: Magnetic fluids: The image on the left shows a microscopic image of magnetic fluid with the long chain molecular species attached to the magnetic nanoparticles. The image on right shows the macroscopic behavior of such a magnetic fluid under an externally applied magnetic field. (Source: http://www.ferrofluidics.de/images/fluid_demo.jpg)

Under ambient conditions, the suspended particles are subject to significant Brownian motion, which prevents the particles from settling. This Brownian motion leads to a zero net magnetic moment of the ferrofluid in absence of an externally applied magnetic field because the moments of all the individual particles are randomly oriented (for e.g. at 298K, the dipole vector of an 8 nm magnetite nanoparticle changes direction after every 10^{-8} s). Also, the magnetic domains of the particles rotate randomly, termed as Néel Relaxation. However, if an external magnetic field is applied to the magnetic fluid, the magnetic particles will try to align themselves so that their magnetic moments line up with the applied magnetic field as shown in Figure 1-2. For this reason, magnetic fluids are said to exhibit superparamagnetism [5]. Removing the applied magnetic field from the particles will instantly reduce the overall net magnetic moment of the fluid to zero, making it possible to use these magnetic nanoparticles for a number of repetitive separation cycles.

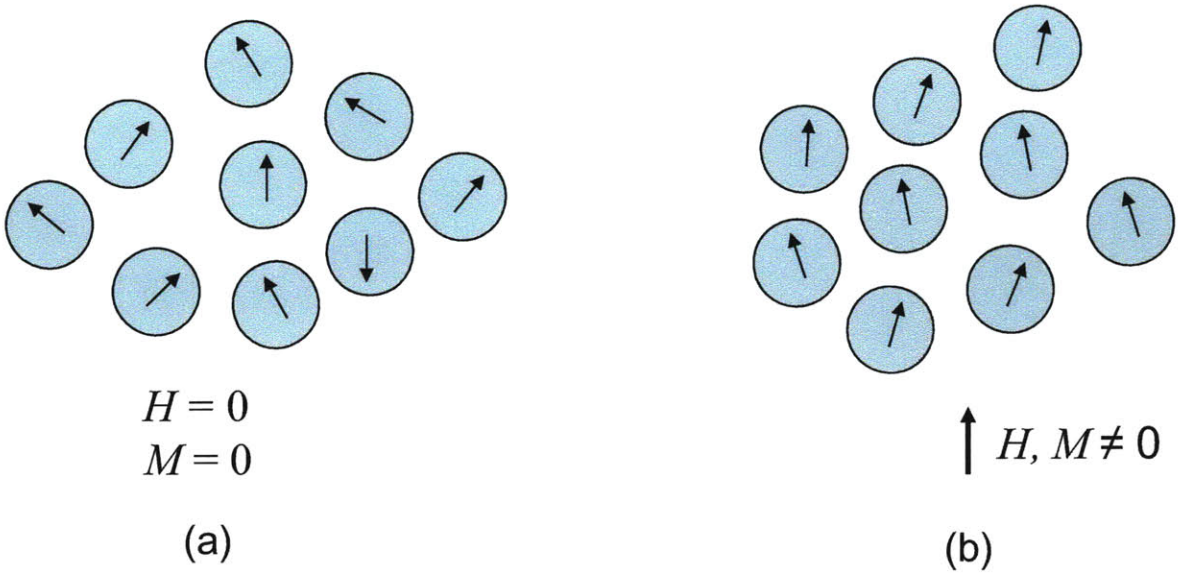

Figure 1-2: Dipoles for the magnetic nanoparticles are randomly oriented in absence of a magnetic field (a). They tend to align themselves preferentially in the direction of the applied magnetic field (b).

1.1.3 Structure of magnetic fluids

Various researchers have tried to understand the behavior and structure of these magnetic fluids due to their significance in technological applications as well as for the fundamental physics [47-49]. Most of the computational studies in the 1980's and the 1990's involved 2-dimensional simulations of the magnetic fluids due to the limited computational power available. Chantrell observed the formation of chain like structure in cobalt nanoparticles [50]. In zero applied field, the particles form open loop structure with no spatial orientation. In large applied field of 10kOe, the particles form long chains which are oriented along the applied field direction as shown in Figure 1-1. They also showed that the formation of such structures leads to a decrease in the initial susceptibility of the system. These interactions decrease with a decrease in the size of the nanoparticle [51]. Also these simulations were carried out for varying temperatures and it was found that for each particle diameter the initial susceptibility obeyed the Curie-Weiss law [52], which states that the initial susceptibility varies inversely with temperature.

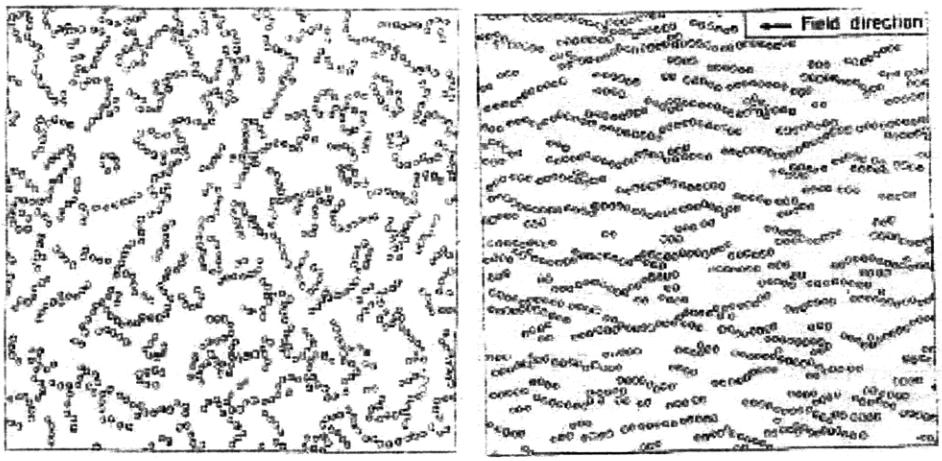

(a) (b)

Figure 1-3: Configuration of cobalt nanoparticles in zero applied field (a) and in the presence of large applied field (b) [50].

However, all these simulations did not include any cluster moves. It is impossible to reproduce the correct aggregate structure of these magnetic particles using the conventional Monte Carlo algorithm. Satoh introduced a new method to capture aggregate structures of these nanoparticles by using a cluster moving Monte Carlo algorithm [53]. This new algorithm involved performing a cluster move after a certain number of particles moves. The criterion of acceptance was the same as described by the Metropolis algorithm. This algorithm violated the detailed balance equation. The new algorithm by Satoh represented a more realistic picture than the previous works as shown in Figure 1-4. Also, Satoh incorporated the electrostatic forces of interaction between the magnetic nanoparticles, which play an important role in the stability of aqueous magnetic fluids. Davis incorporated 'reversal moves' so as to satisfy the detailed balance when performing cluster moves to study magnetic anisotropy in dilute thin films [54].

Satoh carried out two dimensional Monte Carlo simulations to capture thick chainlike clusters of ferromagnetic particles in colloidal dispersions [55]. The simulations were carried out in 2-dimensions, to save computation times, so as to simulate thick and large clusters, similar to those observed experimentally. Also they made an attempt to capture the internal structure by plotting pair correlation functions for these chains as shown in

Figure 1-5. Later, they also carried out these simulations for 3-dimensional system [56] and similar results were obtained.

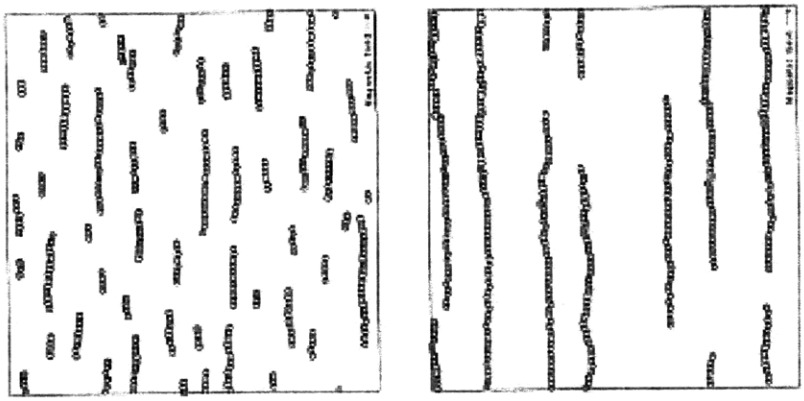

(a) (b)

Figure 1-4: Simulation results obtained for highly interacting particles (λ=15) without cluster moves (a) and with cluster moves (b) [53].

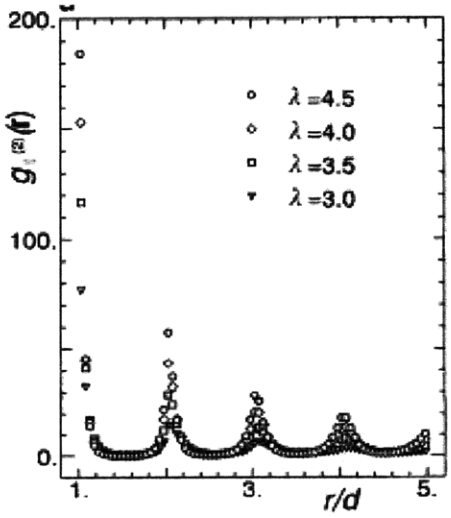

Figure 1-5: Pair correlation functions in the direction parallel to the field direction [55]

The simulations discussed above are very time consuming. Satoh and Chantrell [56] used the concept of secondary particles (as shown in Figure 1-6a) to speed up calculations for the formation of thick chain like clusters. The secondary particles are composed of highly

interacting primary particles. To simulate the thick chain like clusters only the interaction of these secondary particles was considered as shown in Figure 1-6b. However the mechanism of the formation of these particles was not considered in their work. The simulations were performed for various sizes of secondary particles. The attractive forces were found to get stronger as the clusters became longer and were composed of larger secondary particles.

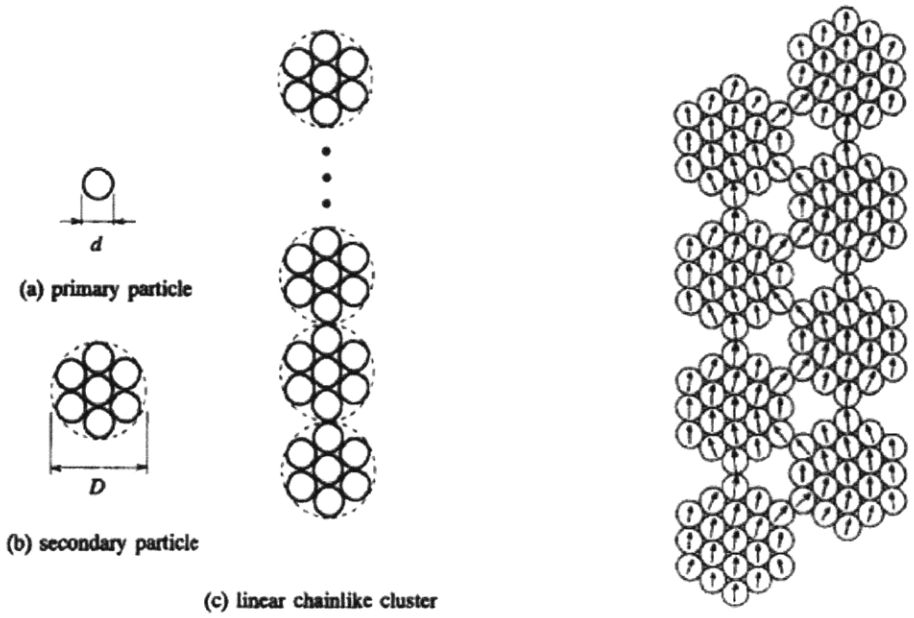

Figure 1-6: Secondary particles, linear chainlike structures (a) and the interactions of these secondary particles (b) [56].

The effect of size distribution on ferrofluid configuration was studied by Bhatt [57]. The Monte Carlo simulations were performed for log-normal and flat top profiles for the magnetic nanoparticles. They observed that in absence of magnetic field, the agglomerates were formed from smaller particles (d<10 nm) as compared to larger particles. However they failed to justify their results.

Kruse however predicted an increase in agglomeration probability with an increase in size [58], but a large fraction of small particles also take part in agglomeration. The work

also discussed the choice of Hamaker constant and its effect on convergence of the Monte Carlo simulations. The probability distribution of the agglomerate size was found to decay exponentially which is in agreement with theoretical distributions. Very recently, Aoshima studied the effect of the variation of the standard deviation in particle size in a polydisperse system in a 2-dimensional system [59]. He observed necklace-like structures for smaller values of the standard deviation (~0.2) and clumplike structures for larger values of the standard deviation (~0.35). Large complicated network structures were formed for stronger magnetic interactions.

1.2 Magnetic and non-magnetic particles

Particles can be classified as ferromagnetic, which have a very high magnetic susceptibility, paramagnetic, which have a low magnetic susceptibility and diamagnetic, which have a negative magnetic susceptibility and can be considered non-magnetic for all practical reasons, when subjected to a magnetic field. A high magnetic field alone, although necessary for separating paramagnetic particles, is not sufficient; there must also be a high field gradient. When a uniform magnetic field is applied to a magnetized particle, the forces acting on the two poles of the particle are equal and opposite, resulting in a net zero force. Only if the applied field differs in intensity at the two sides of the particles, a net magnetic force will act on the particle. That means that the applied field must have a gradient, a spatial variation that is appreciable in terms of the dimensions of the magnetized particle.

A particle in an inhomogeneous magnetic field experiences several forces. The relative importance of these forces depends primarily on the type of magnetic separation and the size of the particle. Forces that act on the particle are the magnetic force, viscous drag force of the surrounding fluid medium, the gravity force, the inertial forces on the particle, the thermal diffusion and inter-particle interactions forces.

1.3 Magnetic separations

Magnetic separations have been employed in water treatment, mineral and other industries in the past. Recently high gradient magnetic separations has been employed in

separation of proteins [6-8, 60, 61], peptides [62], cells [63, 64], organic compounds [15, 16, 65], heavy metal ions [66], etc. These separations can be broadly categorized into two categories. In the most common type of magnetic separations one of the non-magnetic entities is either physically or chemically attached preferentially to the magnetic nanoparticles. The suspension is then passed through a high gradient magnetic separation (HGMS) column under the presence of a magnetic field. The magnetic nanoparticles along with the bound non-magnetic particle species are trapped in the HGMS column, while rests of species are eluted out (see Figure 1-7). Following this step the bound non-magnetic species can be separated from the magnetic particles and the magnetic particles can be recovered for the next cycle.

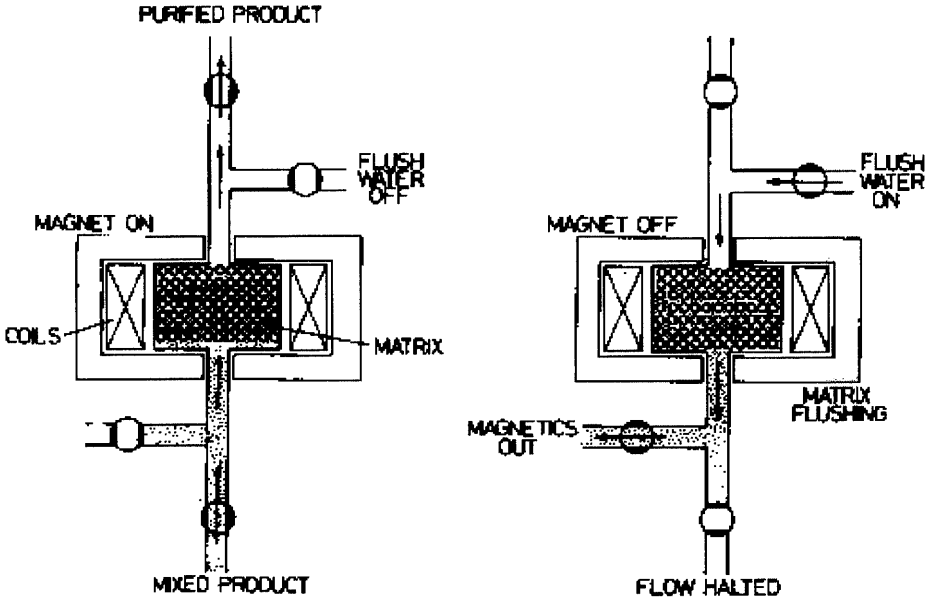

Figure 1-7: Cycles in high gradient magnetic separation [2].

A HGMS column usually consists of magnetically susceptible wires or spheres packed in a column placed inside an elecotromagnet [61, 67]. One of the challenges one faces in the design of magnetic nanoparticles is that the particles should be large enough so that they get trapped in the HGMS column in separation phase, yet should be easily removed in the elution phase when the magnetic field is switched off. In other words, they should have high net magnetic moment, but should have small relaxation times. Ditsch [7, 60] has used magnetic nanoparticle clusters to achieve the same effect. Having multiple smaller

(8-10 nm) particles in the cluster ensures that the clusters are entrapped in the HGMS column, yet are removed easily when the magnetic field is removed. However in case the chemical and biological properties of the non-magnetic species are identical, these separations become difficult.

Another kind of separation has the medium rather than the particles to be separated to be magnetic. These have been termed magnetic separations of the second kind [68]. The magnetic fluid is used to generate a "magnetic pressure", which is utilized to move the non-magnetic species in the direction opposite to the magnetic field gradient. Fateen [2] studied the forced diffusion of polystyrene beads in magnetic fluids. Fateen validated his work experimentally by using digital imaging techniques to study the dynamic evolution of the concentration profile of fluorescently-tagged polymer beads. He also performed a feasibility study by designing a simple separation device to isolate 200 nm from 500 nm particles. Gonzalez [1, 69] studied the focusing and trapping of sub-micron non-magnetic particles in magnetic fluids under the presence of magnetic fields. He developed a microchip that produced spatially increasing magnetic field gradients that trapped polystyrene beads in different locations of the chip, based on the relative size of the beads. Brownian dynamic simulations were used to match his experimental results with theoretical predictions.

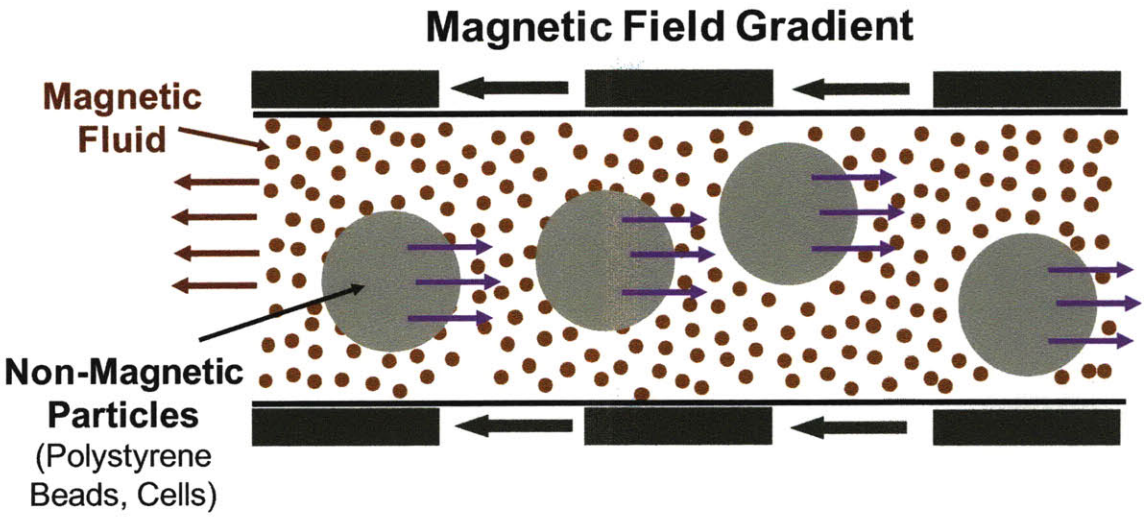

Figure 1-8: On application of a magnetic field gradient, magnetic particles move in the direction of the applied gradient, while the non-magnetic particles move in the opposite direction [1].

Watarai studied the magnetophoretic behavior of polystyrene latex micro-particles [9, 10, 70] and red blood cells [70] in paramagnetic metal ion solution of aqueous Manganese (II) Chloride. Bashtovoi [71] has studied the effect of magnetophoresis and Brownian diffusion on levitation of non-magnetic bodies in magnetic fluid. He studied the variation in magnetic particle concentration and its influence on the pressure distribution and pressure forces under the influence of non-uniform magnetic fields. Gao and co-workers [72] have evaluated the magnetophoretic forces on non-spherical non-magnetic particles. They have also evaluated these forces when an alternating currents magnetic field applied to electrically conducting particles produces eddy currents.

1.4 Assemblies using magnetic fluid

Another interesting application of magnetic fluid involves transporting and assembling non-magnetic particles, often termed as 'magnetic holes', into regular patterns such as chain like alignments and triangle-lattice alignments [73, 74]. Davies et al. [75] carried out Monte Carlo simulations with the ferrofluid as a continuum and magnetic holes having negative susceptibilities [76]. Skejltorp [77, 78] demonstrated the application of

magnetic fluid to orient biological assemblies. He experimentally studied one and two dimensional crystallization of magnetic holes by chaining polystyrene beads in modest magnetic fields. Chainlike structures were observed when the external magnetic field was applied parallel to the plane of magnetic fluid film and regular two dimensional triangular structures were obtained when the external magnetic field was applied perpendicular to the plane of the magnetic fluid film as shown in Figure 1-10. Skjeltorp further carried out experiments with non-spherical particles [78]. On using pear-shaped particles, application of an external magnetic field perpendicular to the layer produced a triangular structure with a preferential up-down arrangement.

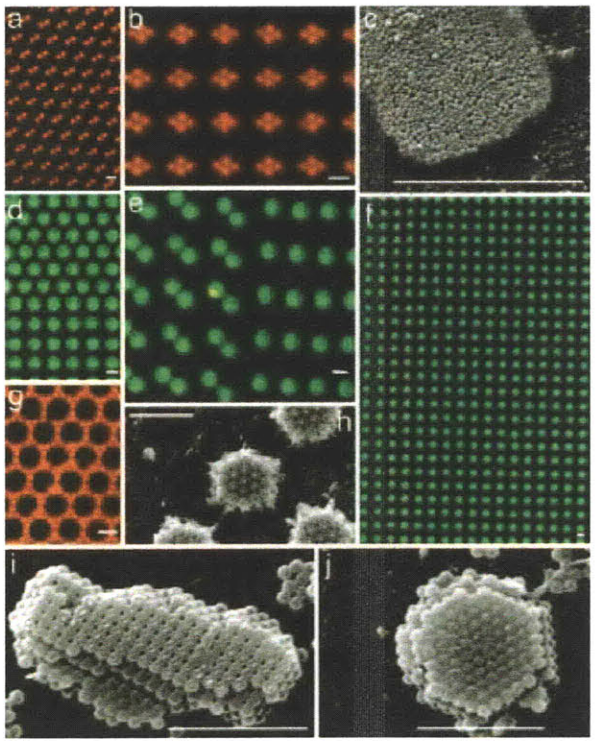

Figure 1-9: Assembly of non-magnetic particles in magnetic fluids [74].

Toussaint worked out an interaction model for magnetic holes in a ferrofluid layer and was able to give an explanation for the finite equilibrium separation between the particles [79]. He also studied the stability of such systems. Miguel and Rubi worked on the dynamics of magnetic colloidal particles and holes [80]. They were able to justify the experimental observation of rotation of the magnetic holes in the direction opposite to

that of the applied field. Again these calculations assume that the non-magnetic particle is considerably larger in size in comparison to the magnetic nanoparticles.

Arrangement of these non-magnetic and magnetic particles is of considerable importance with some of the applications in display elements and nanowire transistors [81]. Manipulation of materials can also be guided by a program of magnetic information in a substrate. A unique advantage offered by this method is a large degree of control over the particle motion [74].

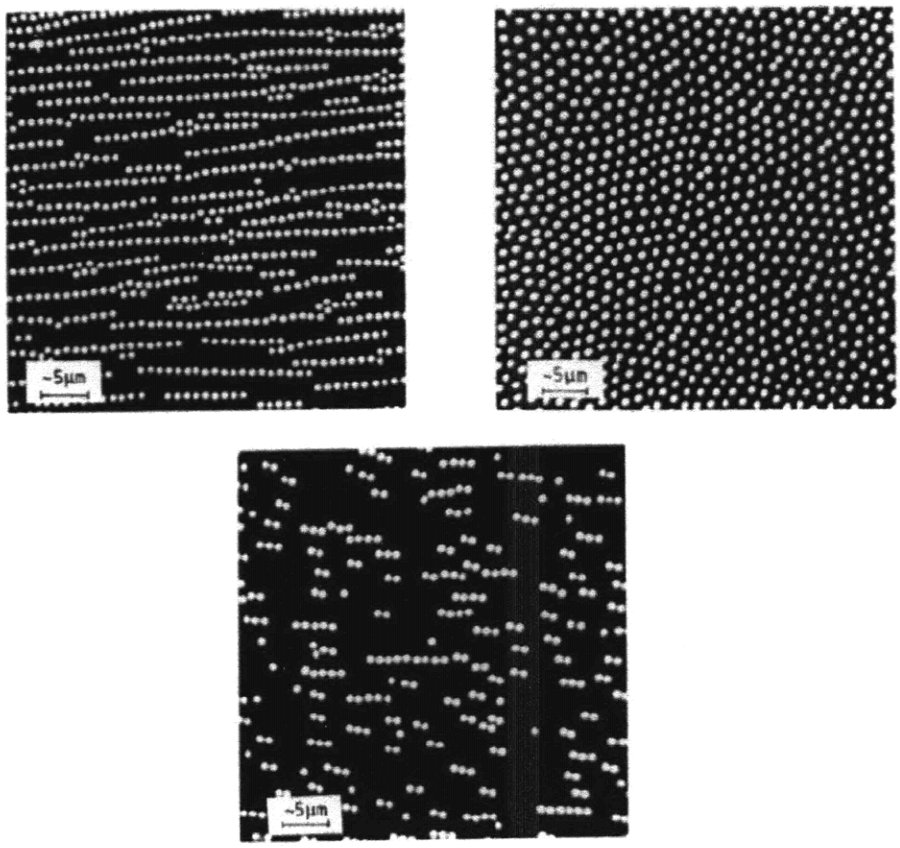

Figure 1-10: Assemblies formed by polystyrene beads at varying concentrations. The two figures at top are for a monolayer of polystyrene at high volume concentration (magnetic field parallel and perpendicular to the plane of the sample respectively). The figure at the bottom is for a monolayer of polystyrene at low volume concentrations [82].

In the previous works, the magnetic holes considered have been a few microns in size, where the magnetic fluid can be treated as a continuum and the diffusion is not important. There is a need for an integrated equilibrium and dynamic analysis when magnetic nanoparticles and magnetic nanoparticles are of similar sizes and the continuum approximation is no longer valid. In our work, we have evaluated the thermodynamic and transport properties of non-magnetic particles in magnetic fluids.

1.5 Outline of the Thesis

The work in this is primarily divided into two sections. Chapters 2, 3, and 4 focus on the interaction of magnetic and non-magnetic nanoparticles, while Chapters 5 and 6 relate to the magnetization behavior of magnetic nanoparticle clusters. In Chapter 2, we study the effect of non-magnetic particles on the magnetization behavior of the magnetic nanoparticles. We have performed Monte-Carlo simulations to show the non-homogeneity in the magnetization behavior around the non-magnetic particle. In Chapter 3, we have evaluated the forces non-magnetic particles experience when subjected to a magnetic field gradient. We evaluate the gradient of chemical potential with the variation in magnetic field, by using Monte-Carlo Simulations. In Chapter 4, we evaluate the diffusion coefficients of the non-magnetic particles in magnetic fluids using Brownian dynamics simulations.

In Chapter 5, we carry out Stochastic Dynamics Simulations to evaluate the Néel relaxation behavior of stationary magnetic particle clusters. In Chapter 6, we have evaluated the magnetization behavior of magnetic particles in rectangular and hexagonal packed clusters in presence of low magnetic fields. Finally, in Chapter 7 we present our conclusions from this work and recommendations for future work.

1.6 Bibliography

1. Gonzalez, L.A., *Negative Magnetophoresis of Submicron Species in Magnetic Nanofluids*. 2009, Massachusetts Institute of Technology: Cambridge.

2. Fateen, S., *Magnetophoretic Focusing of Submicron Particles Dispersed in a Polymer-Based Magnetic Fluid*, in *Doctoral Thesis*. 2002, MIT: Cambridge.

3. Bitter, F., *On inhomogeneities in the magnetization of ferromagnetic materials.* Phys. Rev., 1931. **38**: p. 1903.

4. Elmore, W.C., *Ferromagnetic colloid for studying magnetic structures.* Phys. Rev., 1938. **54(4)**: p. 309-10.

5. Rosensweig, R.E., *Ferrohydrodynamics*. 1985: Cambridge University Press: Cambridge.

6. Bucak, S., Jones, D.A., Laibinis, P.E., and Hatton, T.A., *Protein separations using colloidal magnetic nanoparticles.* Biotechnology Progress, 2003. **19**(2): p. 477-484.

7. Ditsch, A., Lindenmann, S., Laibinis, P.E., Wang, D.I.C., and Hatton, T.A., *High-gradient magnetic separation of magnetic nanoclusters.* Industrial & Engineering Chemistry Research, 2005. **44**(17): p. 6824-6836.

8. Hubbuch, J.J. and Thomas, O.R.T., *High-gradient magnetic affinity separation of trypsin from porcine pancreatin.* Biotechnology And Bioengineering, 2002. **79**(3): p. 301-313.

9. Watarai, H. and Namba, M., *Magnetophoretic behavior of single polystyrene particles in aqueous manganese(II) chloride.* Analytical Sciences, 2001. **17**(10): p. 1233-1236.

10. Watarai, H., Suwa, M., and Iiguni, Y., *Magnetophoresis and electromagnetophoresis of microparticles in liquids.* Analytical And Bioanalytical Chemistry, 2004. **378**(7): p. 1693-1699.

11. Gupta, A.K. and Gupta, M., *Synthesis and surface engineering of iron oxide nanoparticles for biomedical applications.* Biomaterials, 2005. **26**(18): p. 3995-4021.

12. Liu, C.J., Lien, K.Y., Weng, C.Y., Shin, J.W., Chang, T.Y., and Lee, G.B., *Magnetic-bead-based microfluidic system for ribonucleic acid extraction and reverse transcription processes.* Biomedical Microdevices, 2009. **11**(2): p. 339-350.

13. Hatch, G.P. and Stelter, R.E., *Magnetic design considerations for devices and particles used for biological high-gradient magnetic separation (HGMS) systems.* Journal Of Magnetism And Magnetic Materials, 2001. **225**(1-2): p. 262-276.

14. Chung, S.H., Hoffmann, A., Guslienko, K., Bader, S.D., Liu, C., Kay, B., Makowski, L., and Chen, L., *Biological sensing with magnetic nanoparticles using Brownian relaxation (invited).* Journal Of Applied Physics, 2005. **97**(10).

15. Bromberg, L. and Hatton, T.A., *Decomposition of toxic environmental contaminants by recyclable catalytic, superparamagnetic nanoparticles.* Industrial & Engineering Chemistry Research, 2007. **46**(10): p. 3296-3303.

16. Bromberg, L. and Hatton, T.A., *Nerve agent destruction by recyclable catalytic magnetic nanoparticles.* Industrial & Engineering Chemistry Research, 2005. **44**(21): p. 7991-7998.

17. Zhao, X.L., Shi, Y.L., Wang, T., Cai, Y.Q., and Jiang, G.B., *Preparation of silica-magnetite nanoparticle mixed hemimicelle sorbents for extraction of several typical phenolic compounds from environmental water samples.* Journal Of Chromatography A, 2008. **1188**(2): p. 140-147.

18. Huang, S.H. and Chen, D.H., *Rapid removal of heavy metal cations and anions from aqueous solutions by an amino-functionalized magnetic nano-adsorbent.* Journal Of Hazardous Materials, 2009. **163**(1): p. 174-179.

19. Li, H.D., Li, Z., Liu, T., Xiao, X., Peng, Z.H., and Deng, L., *A novel technology for biosorption and recovery hexavalent chromium in wastewater by bio-functional magnetic beads.* Bioresource Technology, 2008. **99**(14): p. 6271-6279.

20. Rocher, V., Siauque, J.M., Cabuil, V., and Bee, A., *Removal of organic dyes by magnetic alginate beads.* Water Research, 2008. **42**(4-5): p. 1290-1298.

21. Yantasee, W., Warner, C.L., Sangvanich, T., Addleman, R.S., Carter, T.G., Wiacek, R.J., Fryxell, G.E., Timchalk, C., and Warner, M.G., *Removal of heavy metals from aqueous systems with thiol functionalized superparamagnetic nanoparticles.* Environmental Science & Technology, 2007. **41**(14): p. 5114-5119.

22. Frolov, G., *Film carriers for super-high-density magnetic storage.* Technical Physics, 2001. **46**(12): p. 1537.

23. Hasmonay, E., Depeyrot, J., Sousa, M.H., Tourinho, F.A., Bacri, J.C., Perzynski, R., Raikher, Y.L., and Rosenman, I., *Magnetic and optical properties of ionic ferrofluids based on nickel ferrite nanoparticles.* Journal Of Applied Physics, 2000. **88**(11): p. 6628-6635.

24. Hasmonay, E., Depeyrot, J., Sousa, M.H., Tourinho, F.A., Bacri, J.C., and Perzynski, R., *Optical properties of nickel ferrite ferrofluids.* Journal Of Magnetism And Magnetic Materials, 1999. **201**: p. 195-199.

25. Hasmonay, E., Dubois, E., Neveu, S., Bacri, J.C., and Perzynski, R., *Alternating magneto-birefringence of ionic ferrofluids in crossed fields.* The European Physical Journal B - Condensed Matter and Complex Systems, 2001. **21**(1): p. 19.

26. Martin, J.E., Hill, K.M., and Tigges, C.P., *Magnetic-field-induced optical transmittance in colloidal suspensions.* Physical Review E, 1999. **59**(5): p. 5676-5692.

27. Teunissen, W., de Groot, F.M.F., Geus, J., Stephan, O., Tence, M., and Colliex, C., *The structure of carbon encapsulated NiFe nanoparticles.* Journal Of Catalysis, 2001. **204**(1): p. 169-174.

28. Teunissen, W. and Geus, J.W., *Catalyst supports based on encapsulated magnetic metal particles.* Science And Technology In Catalysis 1998, 1999. **121**: p. 185-190.

29. Hu, A.G., Yee, G.T., and Lin, W.B., *Magnetically recoverable chiral catalysts immobilized on magnetite nanoparticles for asymmetric hydrogenation of aromatic ketones.* Journal Of The American Chemical Society, 2005. **127**(36): p. 12486-12487.

30. Olle, B., Bucak, S., Holmes, T.C., Bromberg, L., Hatton, T.A., and Wang, D.I.C., *Enhancement of oxygen mass transfer using functionalized magnetic nanoparticles.* Industrial & Engineering Chemistry Research, 2006. **45**(12): p. 4355-4363.

31. Majewski, P. and Thierry, B., *Functionalized magnetite nanoparticles - Synthesis, properties, and bio-applications.* Critical Reviews In Solid State And Materials Sciences, 2007. **32**(3-4): p. 203-215.

32. Ito, A., Shinkai, M., Honda, H., and Kobayashi, T., *Medical application of functionalized magnetic nanoparticles.* Journal Of Bioscience And Bioengineering, 2005. **100**(1): p. 1-11.

33. Neuberger, T., Schopf, B., Hofmann, H., Hofmann, M., and von Rechenberg, B., *Superparamagnetic nanoparticles for biomedical applications: Possibilities and limitations of a new drug delivery system.* Journal Of Magnetism And Magnetic Materials, 2005. **293**(1): p. 483-496.

34. Kopelman, R., Koo, Y.E.L., Philbert, M., Moffat, B.A., Reddy, G.R., McConville, P., Hall, D.E., Chenevert, T.L., Bhojani, M.S., Buck, S.M., Rehemtulla, A., and Ross, B.D., *Multifunctional nanoparticle platforms for in vivo MRI enhancement and photodynamic therapy of a rat brain cancer.* Journal Of Magnetism And Magnetic Materials, 2005. **293**(1): p. 404-410.

35. Kalambur, V.S., Han, B., Hammer, B.E., Shield, T.W., and Bischof, J.C., *In vitro characterization of movement, heating and visualization of magnetic nanoparticles for biomedical applications.* Nanotechnology, 2005. **16**(8): p. 1221-1233.

36. Jordan, A., Scholz, R., Wust, P., Fahling, H., and Felix, R., *Magnetic fluid hyperthermia (MFH): Cancer treatment with AC magnetic field induced excitation of biocompatible superparamagnetic nanoparticles.* Journal Of Magnetism And Magnetic Materials, 1999. **201**: p. 413-419.

37. Ahn, C.H., Allen, M.G., Trimmer, W., Jun, Y.N., and Erramilli, S., *A fully integrated micromachined magnetic particle separator.* Journal Of Microelectromechanical Systems, 1996. **5**(3): p. 151-158.

38. Pamme, N. and Manz, A., *On-chip free-flow magnetophoresis: Continuous flow separation of magnetic particles and agglomerates.* Analytical Chemistry, 2004. **76**(24): p. 7250-7256.

39. Pamme, N., *Magnetism and microfluidics.* Lab On A Chip, 2006. **6**(1): p. 24-38.

40. Mikhailik, O.M., Povstugar, V.I., Mikhailova, S.S., Lyakhovich, A.M., Fedorenko, O.M., Kurbatova, G.T., Shklovskaya, N.I., and Chuiko, A.A., *Surface-Structure Of Finely Dispersed Iron Powders.1. Formation Of Stabilizing Coating.* Colloids And Surfaces, 1991. **52**(3-4): p. 315-324.

41. Mikhailik, O.M., Povstugar, V.I., Mikhailova, S.S., Fedorenko, O.M., Kurbatova, G.T., Shklovskaya, N.I., and Chuiko, A.A., *Surface-Structure Of Finely Dispersed Iron Powders.2. Specific Features Of Stabilizing Coating Structure.* Colloids And Surfaces, 1991. **52**(3-4): p. 325-330.

42. Khalafalla, S. and Reimers, G., *Preparation of dilution-stable aqueous magnetic fluids.* Magnetics, IEEE Transactions on, 1980. **16**(2): p. 178.

43. Papell, S.S., *Low Viscosity Magnetic Fluid Obtained by the Colloidal Suspension of Magnetic Particle.* 1965: United States.

44. Hu, Y.H., Liu, J.P., Xu, J., and Wang, D.Z., *Dispersion mechanism of nano-magnetite coated with oleate in aqueous carrier.* Journal Of Central South University Of Technology, 2008. **15**(5): p. 663-668.

45. Lopez-Lopez, M.T., Zugaldia, A., Gomez-Ramirez, A., Gonzalez-Caballero, F., and Duran, J.D.G., *Effect of particle aggregation on the magnetic and magnetorheological properties of magnetic suspensions.* Journal Of Rheology, 2008. **52**(4): p. 901-912.

46. Tombacz, E., Bica, D., Hajdu, A., Illes, E., Majzik, A., and Vekas, L., *Surfactant double layer stabilized magnetic nanofluids for biomedical application.* Journal Of Physics-Condensed Matter, 2008. **20**(20).

47. Dormann, J.L., Ezzir, A., Cherkakoui, R., Nogues, M., Lucari, F., dOrazio, F., Godinho, M., Tronc, E., Jolivet, J.P., and Fiorani, D., *Static and dynamical properties of gamma-Fe2O3 nanoparticles.* Journal De Physique Iv, 1997. **7**(C1): p. 509-512.

48. Puntes, V.F., Krishnan, K.M., and Alivisatos, A.P., *Colloidal nanocrystal shape and size control: The case of cobalt.* Science, 2001. **291**(5511): p. 2115-2117.

49. Sun, S.H., Murray, C.B., Weller, D., Folks, L., and Moser, A., *Monodisperse FePt nanoparticles and ferromagnetic FePt nanocrystal superlattices.* Science, 2000. **287**(5460): p. 1989-1992.

50. Chantrell, R.W., Bradbury, A., Popplewell, J., and Charles, S.W., *Particle Cluster Configuration in Magnetic Fluids.* Journal of Physics D-Applied Physics, 1980. **13**(7): p. L119-L122.

51. Chantrell, R.W., Bradbury, A., Popplewell, J., and Charles, S.W., *Agglomerate Formation in a Magnetic Fluid.* Journal of Applied Physics, 1982. **53**(3): p. 2742-2744.

52. Menear, S., Bradbury, A., and Chantrell, R.W., *A Model Of The Properties Of Colloidal Dispersions Of Weakly Interacting Fine Ferromagnetic Particles.* Journal Of Magnetism And Magnetic Materials, 1984. **43**(2): p. 166-176.

53. Satoh, A., *A New Technique For Metropolis Monte-Carlo Simulation To Capture Aggregate Structures Of Fine Particles - Cluster-Moving Monte-Carlo Algorithm.* Journal Of Colloid And Interface Science, 1992. **150**(2): p. 461-472.

54. Davis, S.W., McCausland, W., McGahagan, H.C., Tanaka, C.T., and Widom, M., *Cluster-based Monte Carlo simulation of ferrofluids.* Physical Review E, 1999. **59**(2): p. 2424-2428.

55. Satoh, A., Chantrell, R.W., Kamiyama, S.I., and Coverdale, G.N., *Two-dimensional Monte Carlo simulations to capture thick chainlike clusters of ferromagnetic particles in colloidal dispersions.* Journal Of Colloid And Interface Science, 1996. **178**(2): p. 620-627.

56. Satoh, A., Chantrell, R.W., Kamiyama, S., and Coverdale, G.N., *Three dimensional Monte Carlo simulations of thick chainlike clusters composed of ferromagnetic fine particles.* Journal Of Colloid And Interface Science, 1996. **181**(2): p. 422-428.

57. Bhatt, P., Mehta, R.V., Bhatnagar, S.P., Upadhyay, R.V., and Srinivas, D., *Effect of size distribution on ferrofluid configuration: A Monte Carlo simulation.* Indian Journal Of Engineering And Materials Sciences, 1998. **5**(6): p. 356-360.

58. Kruse, T., Spanoudaki, A., and Pelster, R., *Monte Carlo simulations of polydisperse ferrofluids: Cluster formation and field-dependent microstructure.* Physical Review B, 2003. **68**(5).

59. Aoshima, M. and Satoh, A., *Two-dimensional Monte Carlo simulations of a polydisperse colloidal dispersion composed of ferromagnetic particles for the case of no external magnetic field.* Journal Of Colloid And Interface Science, 2004. **280**(1): p. 83-90.

60. Ditsch, A., Yin, J., Laibinis, P.E., Wang, D.I.C., and Hatton, T.A., *Ion-exchange purification of proteins using magnetic nanoclusters.* Biotechnology Progress, 2006. **22**(4): p. 1153-1162.

61. Moeser, G.D., Roach, K.A., Green, W.H., Hatton, T.A., and Laibinis, P.E., *High-gradient magnetic separation of coated magnetic nanoparticles.* Aiche Journal, 2004. **50**(11): p. 2835-2848.

62. Safarik, I. and Safarikova, M., *Magnetic techniques for the isolation and purification of proteins and peptides.* BioMagnetic Research and Technology, 2004. **7**(2).

63. SafarIk, I. and SafarIková, M., *Use of magnetic techniques for the isolation of cells.* Journal of Chromatography B: Biomedical Sciences and Applications, 1999. **722**(1-2): p. 33.

64. Norina, S.B., Kim, J., and Soh, K.S., *Gradient magnetic field effects on separation, Fourier-spectra and motion of chromatin particles and cells.* International Journal Of Applied Electromagnetics And Mechanics, 2007. **25**(1-4): p. 419-427.

65. Moeser, G.D., Roach, K.A., Green, W.H., Laibinis, P.E., and Hatton, T.A., *Water-based magnetic fluids as extractants for synthetic organic compounds.* Industrial & Engineering Chemistry Research, 2002. **41**(19): p. 4739-4749.

66. Ebner, A.D., Ritter, J.A., and Navratil, J.D., *Adsorption of cesium, strontium, and cobalt ions on magnetite and a magnetite-silica composite.* Industrial & Engineering Chemistry Research, 2001. **40**(7): p. 1615-1623.

67. Gerber, S. and Briss, R.R., *High Gradient Magnetic Separation.* 1983, Chichester; New York: Research Studies Press.

68. Khalafalla, S.E., *Magnetic Separation Of 2nd Kind - Magnetogravimetric, Magnetohydrostatic, And Magnetohydrodynamic Separations.* Ieee Transactions On Magnetics, 1976. **12**(5): p. 455-462.

69. Gonzalez, L., Fateen, S.E.K., Smith, K., and Hatton, T.A., *Magnetophoresis of Nonmagnetic, Submicrometer Particles in Magnetic Fluids.* Singapore-MIT Alliance (SMA) Symposium, 2004.

70. Watarai, H., Monjushiro, H., Tsukahara, S., Suwa, M., and Iiguni, Y., *Migration analysis of micro-particles in liquids using microscopically designed external fields.* Analytical Sciences, 2004. **20**(3): p. 423-434.

71. Bashtovoi, V.G., Polevikov, V.K., Suprun, A.E., Stroots, A.V., and Beresnev, S.A., *The effect of magnetophoresis and Brownian diffusion on the levitation of bodies in a magnetic fluid.* Magnetohydrodynamics, 2008. **44**(2): p. 121-126.

72. Gao, Y., Jian, Y.C., Zhang, L.F., and Huang, J.P., *Magnetophoresis of nonmagnetic particles in ferrofluids.* Journal Of Physical Chemistry C, 2007. **111**(29): p. 10785-10791.

73. Hirota, N., Takayama, T., Beaugnon, E., Saito, Y., Ando, T., Nakamura, H., Hara, S., Ikezoe, Y., Wada, H., and Kitazawa, K., *Control of structures of feeble magnetic particles by utilizing induced magnetic dipoles.* Journal Of Magnetism And Magnetic Materials, 2005. **293**(1): p. 87-92.

74. Yellen, B.B., Hovorka, O., and Friedman, G., *Arranging matter by magnetic nanoparticle assemblers.* Proceedings Of The National Academy Of Sciences Of The United States Of America, 2005. **102**(25): p. 8860-8864.

75. Davies, P., Popplewell, J., Martin, G., Bradbury, A., and Chantrell, R.W., *Monte-Carlo Simulations Of The Structure Of Magnetic Fluid Composites.* Journal Of Physics D-Applied Physics, 1986. **19**(3): p. 469-&.

76. Skjeltorp, A.T., *Colloidal Crystals In Magnetic Fluid.* Journal Of Applied Physics, 1984. **55**(6): p. 2587-2588.

77. Skjeltorp, A.T., *One-Dimensional And Two-Dimensional Crystallization Of Magnetic Holes.* Physical Review Letters, 1983. **51**(25): p. 2306-2309.

78. Skjeltorp, A.T., *Ordering Phenomena Of Particles Dispersed In Magnetic Fluids.* Journal Of Applied Physics, 1985. **57**(8): p. 3285-3290.

79. Toussaint, R., Akselvoll, J., Helgesen, G., Skjeltorp, A.T., and Flekkoy, E.G., *Interaction model for magnetic holes in a ferrofluid layer.* Physical Review E, 2004. **69**(1).

80. Miguel, M.C. and Rubi, J.M., *On the dynamics of magnetic colloidal particles and holes.* Physica A, 1996. **231**(1-3): p. 288-294.

81. Duan, X.F., Huang, Y., Cui, Y., Wang, J.F., and Lieber, C.M., *Indium phosphide nanowires as building blocks for nanoscale electronic and optoelectronic devices.* Nature, 2001. **409**(6816): p. 66-69.

82. Charles, S.W., *Alignment Of Biological Assemblies Using Magnetic Fluids - A Review.* Journal Of Magnetism And Magnetic Materials, 1990. **85**(1-3): p. 277-284.

Chapter 2

2 Non-homogenous magnetization by induction of non-magnetic entities in a magnetic fluid

2.1 Introduction

Manipulation of suspensions of nonmagnetic particles immersed in magnetic fluids is of interest to us. It is known that, when subjected to a magnetic field gradient, these non-magnetic particles experience a force of magnitude

$$F_m = \mu_O V_p (M_p - M_f) \underline{\nabla} H \tag{2.1}$$

where M_f and M_p describe the magnetization of the fluid and of particles, respectively, V_p is the particle volume, μ_0 is the permeability of free space and H is the magnetic field strength. Generally, $M_p = 0$, and thus the force acts on the non-magnetic particles so that they migrate in the direction of decreasing field strength. These phenomena can offer interesting opportunities in separations of biological entities that are non-magnetic (viruses, cell organelles, etc.), and in the fractionation of fine particles (also non-magnetic) [1, 2], which rely on the different rates of migration of different sized particles. Similar effects can be harnessed to drive the formation of particle assemblies and other nanostructures where the microstructure of the composite suspension can be altered reversibly by an external field without altering the composition [3, 4]. Arrangement of these nonmagnetic and magnetic particles is of considerable importance with applications in, e.g., display elements and nanowire transistors [5]. In the presence of a magnetic field, these materials can exhibit anisotropies in various properties, including dielectric

permittivities, viscosities and refractive indices [6], that can be exploited in a range of electro-optical [7-10] and other applications.

Davies et al. [11] carried out Monte Carlo simulations of magnetic holes with negative susceptibilities [3] dispersed in a ferrofluid as a continuum. Toussaint worked out an interaction model for magnetic holes in a ferrofluid layer and was able to reproduce the experimentally-observed finite equilibrium separation between the particles [12]. He also studied the stability of such systems. Miguel and Rubi worked on the dynamics of magnetic colloidal particles and holes [13] and were able to rationalize the experimental observation of rotation of the magnetic holes in the direction opposite to that of the applied field. These calculations and simulations assumed that the non-magnetic particle is considerably larger in size than the magnetic nanoparticles.

In the analyses and work reported to date, the magnetic fluid has been treated as a continuum; however, when dealing with nonmagnetic particles comparable in size to the magnetic nanoparticles or near the boundaries of the non-magnetic particles, this approximation may not be valid, and the thermodynamic and transport properties of these systems need to be evaluated with allowance for these effects. The goal of our work is, therefore, to develop computational and simulation tools to provide an in-depth understanding of the thermodynamic and dynamic properties of such systems under varying magnetic field conditions. In this chapter, we have used Monte Carlo simulations to show that the introduction of non-magnetic particles to a magnetic fluid can lead to the development of non-homogenous magnetization characteristics for the system.

2.2 Monte Carlo Simulations

For nonmagnetic particles with sizes of a few microns or more, it is reasonable to assume that the magnetic fluid, consisting as it does of a stable suspension of ~10-20 nm nanoparticles, can be treated as a continuum [14]. However, when the nonmagnetic entities are similar in size to the magnetic nanoparticles (of the order of a few tens of nanometers, for instance, in the size range of viruses) or near the boundaries of the non-magnetic particles, the continuum approximation may no longer be valid. A statistical

analysis which includes the role of inter-particle interactions may be required. This analysis has been carried out in this work by performing Monte Carlo simulations.

We simulated the system, as shown in Figure 2-1, in which we probed the equilibrium distribution and magnetization of magnetic nanoparticles surrounding a stationary 100 nm nonmagnetic particle when subjected to an external magnetic field. The magnetic nanoparticles are 10-20 nm in diameter, which is the size range over which inter-particle magnetic forces start to become significant, and is also representative of the sizes normally obtained during the nanoparticle synthesis. We considered 1000 magnetic particles in a cubic simulation box with a volume fraction of the magnetic nanoparticles of about 1%.

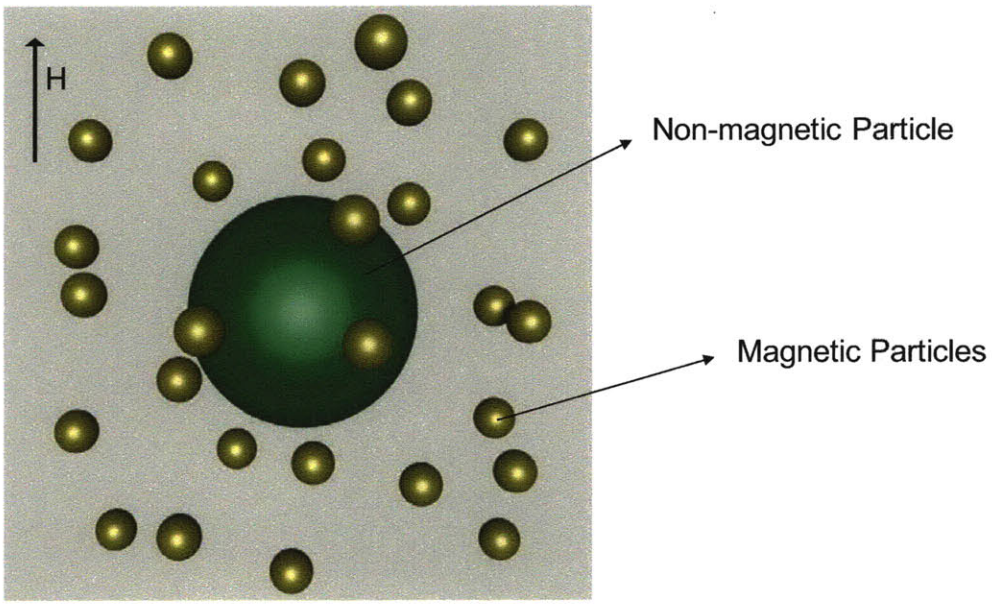

Figure 2-1: The simulation box consisting of the stationary nonmagnetic particle in the center and the mobile magnetic nanoparticles in the medium.

2.2.1 Methodology

The conventional Markov chain three-dimensional Monte Carlo method for an NVT ensemble was used for these simulations. Two types of moves, single particle and cluster, were considered. Single particle moves involve translation of the particle and orientation of its magnetic dipole [15]. The cluster moves involve translation of the intact cluster and

rotation about a randomly chosen particle. This method of rotation is as rigorous as rotating about the center of mass, yet it is more computationally efficient as there is no need to calculate the center of the mass of the cluster.

When the particles aggregate through attractive particle-particle interaction, most of the moves for the single particles in the cluster are rejected as they are not favorable energetically. It is often difficult to explore the different possible conformations of such aggregates, because they are separated by high energy barriers [16]. Hence, a cluster move involves collectively changing particle co-ordinates for a group of magnetic nanoparticles, without changing the interactions within the cluster, even though the interaction of the cluster with the remainder of the system changes. A new algorithm (see Appendix) was also developed for identification of clusters, which is more efficient for larger systems.

These simulations do not include any moves which would lead to a fissure of clusters. Hence, it is important to ensure that the growth of the clusters takes place only by single particle moves and not by cluster moves, so that the detailed balance equation [17] is satisfied. A detailed balance equation requires that, at equilibrium, each pair of configurations be in dynamic balance [16], i.e.

$$N(o)\pi(o \rightarrow n) = N(n)\pi(n \rightarrow o) \tag{2.2}$$

Here the '*o*' subscript refers to the old state and '*n*' subscript refers to the new state and $\pi(o \rightarrow n)$ refers to the transition probability to go from configuration '*o*' to '*n*. $N(n)$ is the probability density that the system will assume any particular configuration, $\boldsymbol{r}^N$. It is given by

$$N(\boldsymbol{r}^N) = \frac{\exp(-\beta U(\boldsymbol{r}^N))}{\int \exp(-\beta U(\boldsymbol{r}^N)) d\boldsymbol{r}^N} \tag{2.3}$$

where β is the reciprocal temperature ($1/kT$) and U is the energy of a system. Thus, on average, the number of accepted trial moves that result in the system leaving the state '*o*' and proceeding to state "n" must be equal to the number of accepted trial moves from

state 'n' to state 'o'. Violation of the detailed balance equation can easily arise in the context of cluster moves, as e.g., in the work of Satoh et al. [16, 18, 19]. Fateen [36] has shown that this can lead to significant errors in the predicted sizes of the aggregates.

The Metropolis criterion [20] was used for acceptance or rejection of the moves generated in the simulation. The acceptance ratio is defined as

$$acc(o \rightarrow n) = \min[1, \exp(-\beta \Delta U)] \tag{2.4}$$

where ΔU is the change in the energy of the system on going from the old configuration to the new configuration and is defined as

$$\Delta U = U(n) - U(o) \tag{2.5}$$

In order to decide whether to accept or to reject the move, a random number is generated in the interval [0, 1]. If the value of the generated random number is less than $acc(o \rightarrow n)$, the move is accepted. In other words, all moves which lead to minimization of the total energy (for which $acc(o \rightarrow n) = 1$) are accepted; but moves which lead to an increase in total energy may be either accepted or rejected. The bias toward rejection increases as ΔU increases.

An important criterion that should be satisfied by the simulation is that it be ergodic, which implies that all accessible points in the configuration space should be attainable in a finite number of Monte Carlo steps. This is a necessary condition in order to generate states with the correct probability distributions [21]. Some of the transition probabilities of the Markov process can be zero, but that there should be at least one path of non-zero transition probability between any two given states.

Periodic boundary conditions were used to simulate the infinite bulk surroundings, thereby constraining our study to uniform external magnetic fields. The minimum image convention [17] was used for calculation of interaction energies, such that each particle 'sees' at most just one image of every other particle in the system, repeated infinitely via the periodic boundary conditions. The interactions of a given particle are calculated with the closest particle or image. The system was initialized by assuming that the positions of

the magnetic nanoparticles and the directions of their magnetic dipoles were distributed randomly in the medium. Since the system is ergodic, the final results are independent of the initial conditions.

2.2.2 Simulation parameters

The acceptance criterion, defined as the ratio of the number of accepted moves to the total number of attempted moves, used for the simulations was selected to be in the range of 0.3 to 0.5 [22], by adjusting the step size during the translational moves of the magnetic nanoparticles and the orientation of their dipoles. The maximum step size for single particle translational move was one fifth of a diameter of the magnetic nanoparticle (d) and the cluster translational moves were limited to a single particle diameter of the magnetic nanoparticle. In both cases, the dipole/orientation move was restricted to no more than $\pi/10$ radians. The simulations were carried out for room temperature conditions (298K) in an NVT ensemble. In the following simulations 6,000,000 equilibration steps and 20,000,000 sampling steps were used. One hundred and eight codes were executed simultaneously to expedite the calculations.

2.2.3 Energy models

The magnetic nanoparticles were modeled as hard spheres coated with soft layers of chemisorbed surfactants and the large particle was assumed to be a hard polystyrene bead, as shown in Figure 2-2 and Figure 2-3. The inter-particle interactions considered in the energy model were magnetic dipole-dipole interactions, entropic repulsion, and Van der Waals forces of attraction. These inter-particle interactions were assumed to be pair-wise additive. The interactions of these particles with the external applied field were also included in the model.

The magnetic contributions to the energy field were those due to dipole-dipole interactions

$$u_{ij}^{\ m} = kT\lambda\frac{d^3}{r_{ij}^{\ 3}}\left(\boldsymbol{n}_i.\boldsymbol{n}_j - \frac{3}{r_{ij}^{\ 2}}(\boldsymbol{n}_i.\boldsymbol{r}_{ij})(\boldsymbol{n}_j.\boldsymbol{r}_{ij})\right) \tag{2.6}$$

and those due to the interactions of the dipoles with the applied field

$$u_i^H = -kT\xi \boldsymbol{n}_i.\boldsymbol{H} \tag{2.7}$$

where $\boldsymbol{n}_i$ is the unit vector of the magnetic dipole of particle i. λ and ξ are dimensionless parameters defined by

$$\lambda = \frac{m^2}{4\pi\mu_0 d^3 kT} \tag{2.8}$$

$$\xi = \frac{mH}{kT} \tag{2.9}$$

respectively, with the magnetic moment, m, defined by

$$m = \mu_0 MV \tag{2.10}$$

The distance r_{ij} is the magnitude of the vector $\boldsymbol{r}_{ij}$ drawn from the center of particle 'i' to the center of particle 'j', V is the volume of the particle, H is the applied field strength, M is the saturation magnetization of that material, and μ_0 is the permeability of free space. The value of λ for a 10nm magnetite particle is 1.31, while that of a 20nm particle is 10.5.

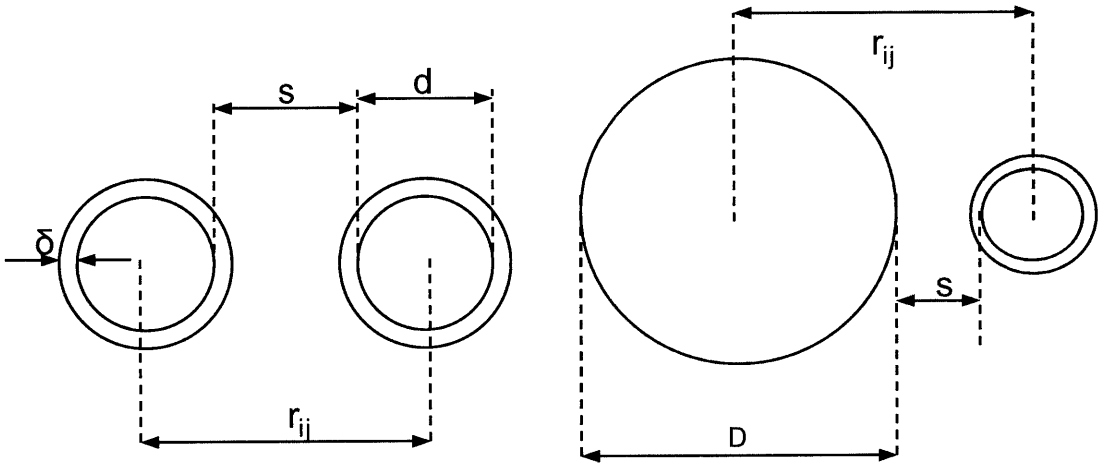

Figure 2-2: Dimensions involved in the model

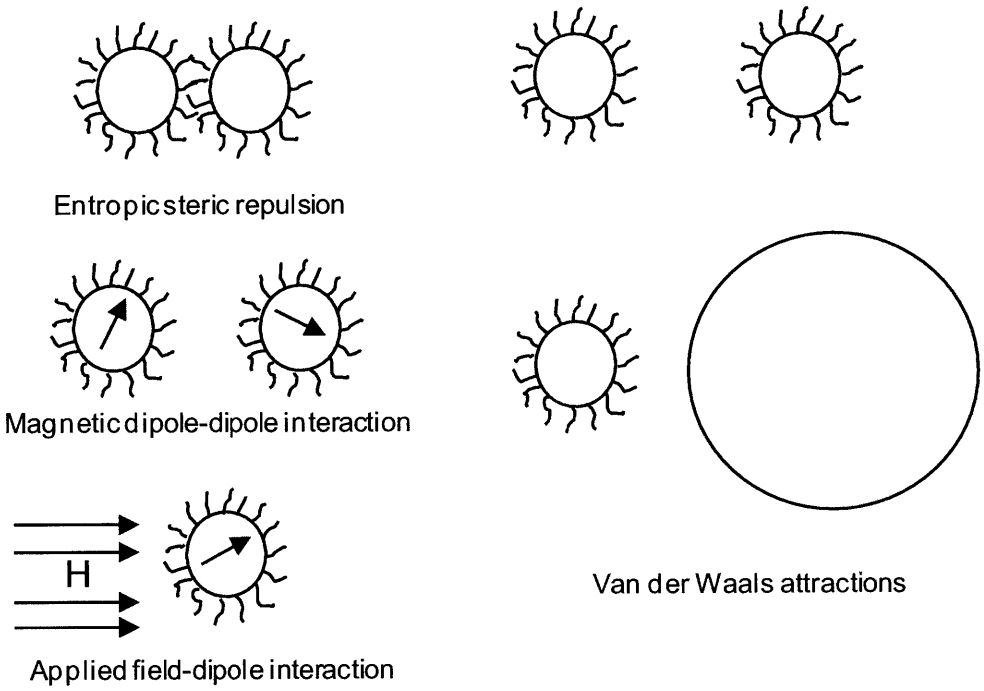

Figure 2-3: Force model

Van der Waals forces of interaction also play an important role in agglomeration. The interaction between two spheres of unequal sizes can be expressed as [23]:

$$u^{vdw} = -\frac{A}{6}\left[\frac{2R_1R_2}{f_1(R_1,R_2,s)} + \frac{2R_1R_2}{f_2(R_1,R_2,s)} + \ln\left(\frac{f_1(R_1,R_2,s)}{f_2(R_1,R_2,s)}\right)\right] \quad (2.11)$$

where,

$$f_1(R_1,R_2,s) = s^2 + 2R_1s + 2R_2s$$

$$f_2(R_1,R_2,s) = s^2 + 2R_1s + 2R_2s + 4R_1R_2$$

and A is the Hamaker constant which is calculated as discussed below. R_1 and R_2 are the radii of the two particles, and s is the separation of the surfaces along the line of centers. The negative sign in front of the equation signifies that this force is attractive in nature. The values of Hamaker constants are known only approximately. In a given system, particles of two different materials interact across a medium with an effective Hamaker constant [23]

$$A_{312} = (A_{33}^{1/2} - A_{11}^{1/2})(A_{22}^{1/2} - A_{11}^{1/2}) \tag{2.12}$$

which captures the interactions between two bodies of types 2 and 3 in a medium of type 1 where A_{ii} is the Hamaker constant of type i. Hence, it is possible to have negative values for effective Hamaker constants, depending on the choice of medium. It was also assumed that the surfactant layer does not contribute to the Van der Waals force of attraction since we assume that the surfactant chains are similar in nature to the solvent molecules. For our simulations Hamaker constants were taken to be 20×10^{-20} J for magnetite, 9.8×10^{-20} J for the non-magnetic polystyrene sphere, and 5.4×10^{-20} J for the medium (kerosene) [23].

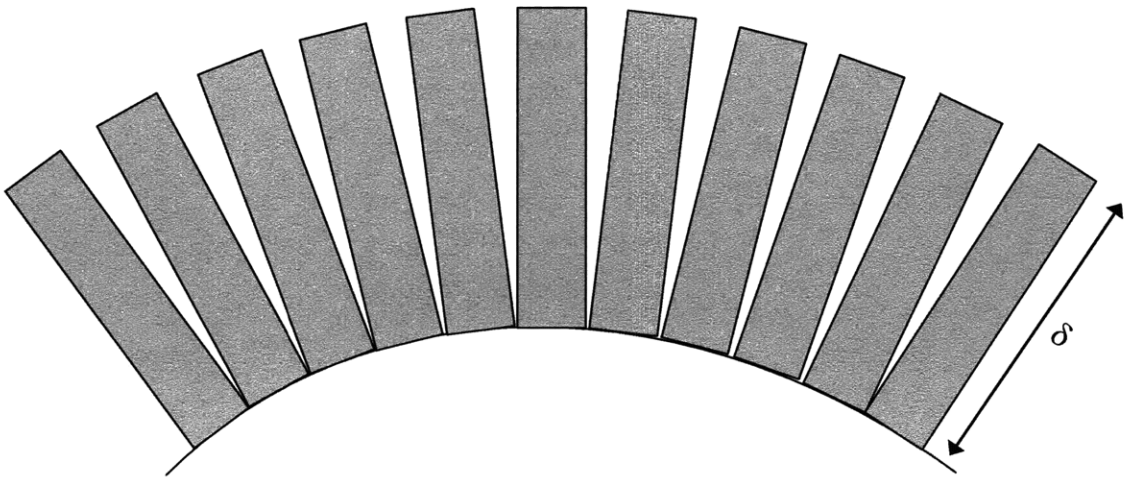

Figure 2-4: Arrangement of polymer layers on the particle surface

Various models are available to capture the entropic repulsion energy. In this work, we considered the statistical mechanics of a rigid rod attached to a universal hinge[24]. It is assumed that one of the ends of the surfactant molecule is attached on the particle surface, while the other end is free, as shown in Figure 2-4. On the surface of the particle, the molecules are close-packed. The inter-particle repulsion is due to the decrease in the number of possible configurations when the two particles approach each other. The entropic energy is then [18]

$$u^{er} = 2\pi kTd^2 N_s \left[2 - \frac{l+2}{t} \ln\left(\frac{1+t}{1+\frac{l}{2}} \right) - \frac{l}{t} \right] \tag{2.13}$$

where $l=2s/d$ and $t=2\delta/d$ (symbols s, d and δ are defined in Figure 2-2), and N_s is the number of adsorbed surfactant molecules per unit area. Note, however, that s cannot approach zero, because the surfactant layer becomes fully dense at some non-zero value of s. The volume of the surfactant molecules, for a close-packed surface, is given by

$$V_S = \pi d^2 \delta \tag{2.14}$$

Since the total volume of the particle plus the surfactant molecules is conserved, the minimum thickness of the surfactant layer is given by

$$\frac{\pi}{6}(d+2\alpha)^3 = \frac{\pi}{6}d^3 + \pi d^2 \delta \tag{2.15}$$

The real root of the above equation gives the value of α.

$$\frac{2\alpha}{d} = \left(\frac{6\delta}{d} + 1 \right)^{1/3} - 1 \tag{2.16}$$

Thus, the entropic repulsion term is given by

$$u^r = \begin{cases} \infty & r < d + 2\alpha \\ u^{er} & d + 2\alpha < r < d + 2\delta \\ 0 & r > d + 2\delta \end{cases} \tag{2.17}$$

From our results we gathered that the inter-particle magnetic interaction forces are the most dominant forces. For the particles simulated in our system we have taken the value of δ to be 2nm. It was also assumed that a surfactant head occupies an area of 1nm×1nm on the magnetic nanoparticle [24, 25]. The model for the entropic repulsion term does not

influence the results obtained significantly. A simple volume exclusion model would have yielded very similar results.

The simulations were run for suitably long periods of time to achieve system equilibrium. The length of this period is called the equilibration time (τ_{eq}). The total energy of the system was used as the criterion to determine whether the system had equilibrated. Once equilibrium was attained, the quantities of interest were measured over another suitably long period of time (sampling phase) and averaged over this period.

2.3 Results

In this work we have simulated the effect of the nonmagnetic particle on the magnetization characteristics of the magnetite nanoparticle under varying magnetic field conditions. We have also examined the effect the nonmagnetic particle has on the structural properties of the magnetic particles around it. These simulations have been performed for two sets of magnetic particle sizes (10 nm and 20 nm) to the study the effect of importance of magnetic inter-particle interactions on the results obtained. In the following simulations one hundred eight codes were executed simultaneously to expedite the calculations. A 3-dimensional graphical representation of the results was provided by POVRAY®.

2.3.1 Variation with azimuthal angle

Figure 2-5 shows the variation of the normalized magnetization of the magnetic nanoparticles close to the nonmagnetic particle as a function of the azimuthal angle θ, defined relative to the plane perpendicular to the applied magnetic field (Figure 2-6). The particles considered in these calculations are within a shell of thickness three times the diameter of the magnetic particle around the nonmagnetic particle. The normalized magnetization is defined as the ensemble average of the cosine of the angle the dipole makes with the applied magnetic field. It is also important to note that these individual dipoles have a fixed magnetic moment magnitude dependent on the materials magnetic properties. The nonmagnetic particle introduces non-homogeneity to the system with the average normalized magnetization at the equator ($\theta = 0°$) being considerably higher than

it is at the poles (θ = 90°). The results are plotted for various ξ values, representing varying magnetic field strengths.

This observation of non-homogenous magnetization can be explained by noting that any two given magnetized particles are in a lower energy state (Equation (2.6)) if they are aligned along the magnetic field (e.g. Particles A and C in Figure 2-6) than if they lie adjacent to each other (e.g. Particles A and B in Figure 2-6). The magnetic particles next to the bead within its equatorial plane (θ = 0°) have no particles on the side adjacent to the bead, and hence they are more stable, leading to higher magnetization values. The opposite is true for the particles occupying the polar regions adjacent to the top and bottom of the nonmagnetic particle (θ = ±90°). These nanoparticles have no neighboring particle on one side along the direction of applied field, and therefore have lower stability and lower normalized magnetization values.

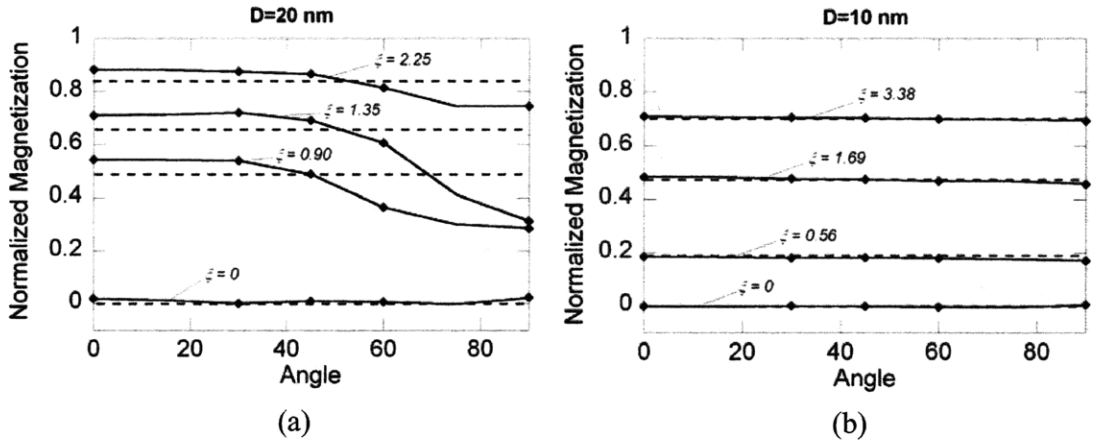

Figure 2-5: Plot of normalized magnetization against the angular position with reference to the nonmagnetic particle (0° representing the equatorial position and 90° representing the poles) for magnetic nanoparticles with a diameter of (a) 20nm (λ=10.5) and (b) 10nm (λ=1.31). The dotted lines represent the bulk magnetization values for the given magnetic field.

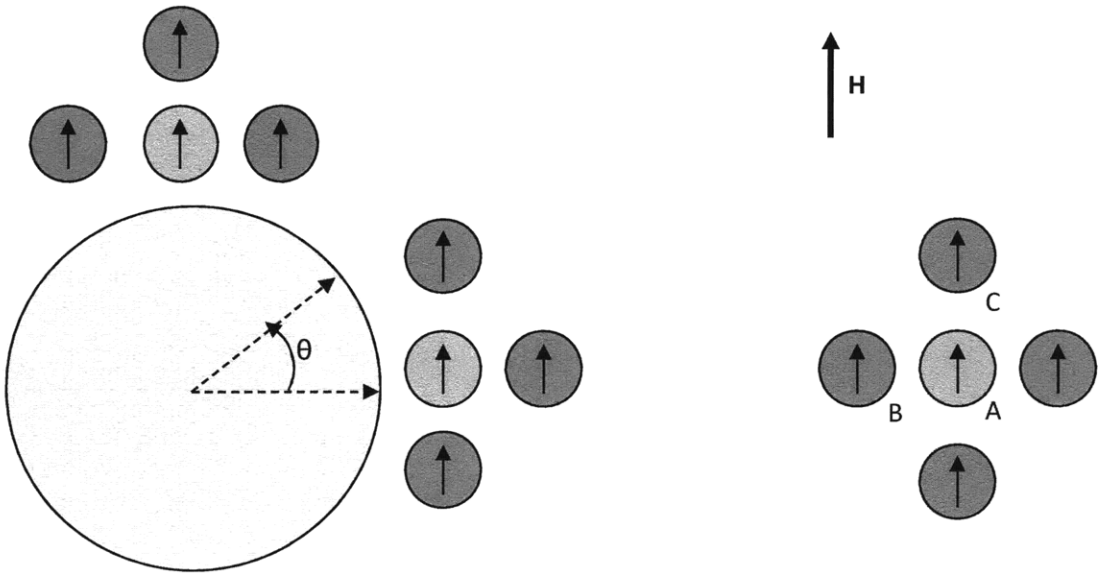

Figure 2-6: The effect of the nonmagnetic particle on the magnetization of the magnetic nanoparticles.

Figure 2-5b shows the variation of the normalized magnetization of 10 nm particles around the nonmagnetic particle. The magnetic interparticle interactions, represented by λ, for these particles are approximately 8 times weaker than those of 20 nm diameter particles, and consequently the non-homogeneity effects are much smaller. These results corroborate the hypothesis that the inter-particle interactions are responsible for the anisotropic magnetization behavior observed.

The equilibrium structures of the two magnetic nanoparticle suspensions considered here are visualized in Figure 2-7. On application of the magnetic field the 20nm diameter magnetic nanoparticles align themselves to form chain like structures that must curl round the non-magnetic particle (Figure 2-7b). In contrast, the 10nm diameter magnetic nanoparticles do not form such structures (Figure 2-7d) because the magnetic inter-particle interaction forces are weak relative to the Brownian forces.

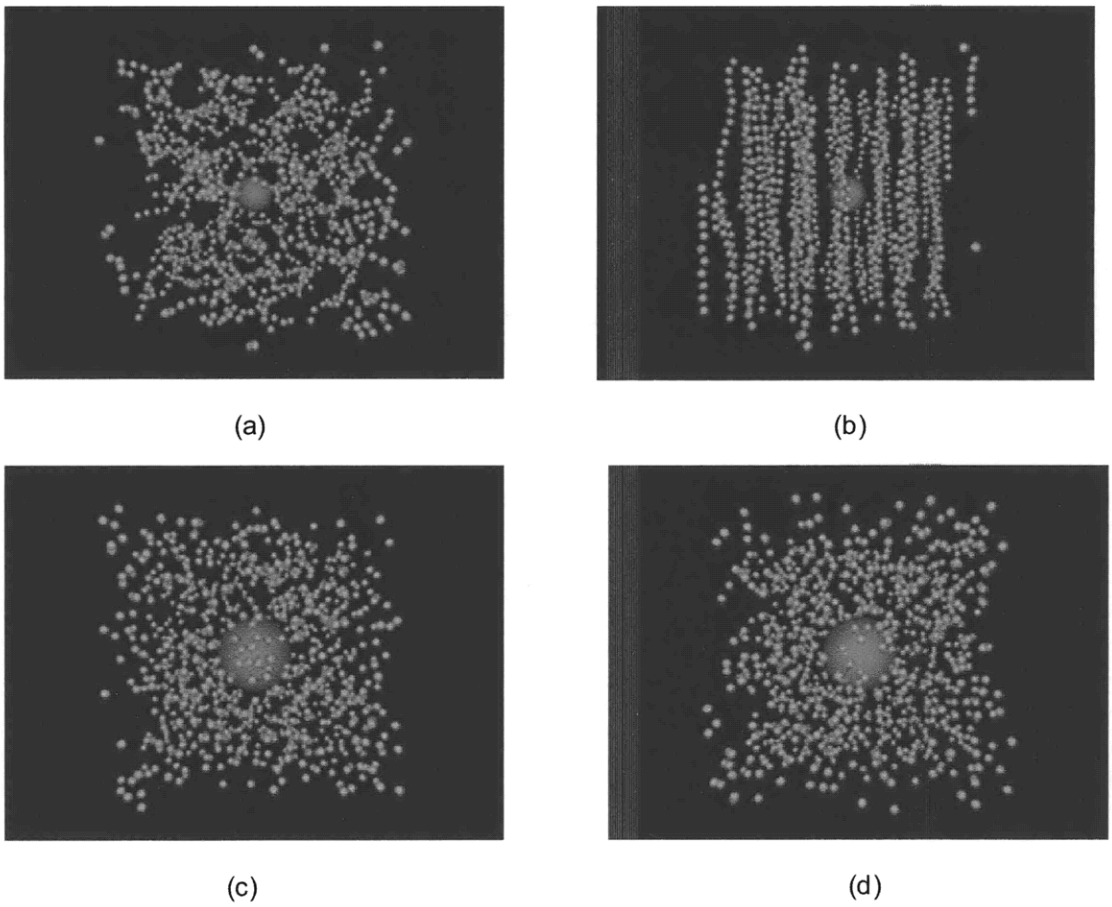

Figure 2-7: Equilibrium structures: Dark grey sphere is the nonmagnetic particle (100nm in diameter). Light grey spheres are the magnetic particles. (a) 20nm diameter, H = 0T, (b) 20 nm diameter, $\mu_0 H$ =0.007 T, (c) 10nm diameter, H = 0T and (d) 10 nm diameter, $\mu_0 H$ =0.06 T.

2.3.2 Variation in the equatorial plane

Figure 2-8 shows the variation of the normalized magnetization of the magnetic particles with normalized radial distance (r_n) from the nonmagnetic particle in the equatorial plane ($\theta = 0°$ plane). The normalized radial distance is defined as:

$$r_n = \left(\frac{r - r_c}{d} \right) \tag{2.18}$$

where r is the distance between the centre of the magnetic particle and the centre of nonmagnetic particle, r_c is the closest distance of approach between the magnetic and nonmagnetic particles and d is the diameter of the magnetic particle.

These variations are in agreement with the results shown in Figure 2-5, exhibiting higher values of magnetization in the perpendicular direction as compared to the bulk magnetization values. These trends are more significant for the 20 nm diameter magnetic nanoparticles than for the 10 nm diameter magnetic nanoparticles. Also, the magnetization values decrease slowly to the bulk normalized magnetization values with increasing distance from the nonmagnetic nanoparticles surface.

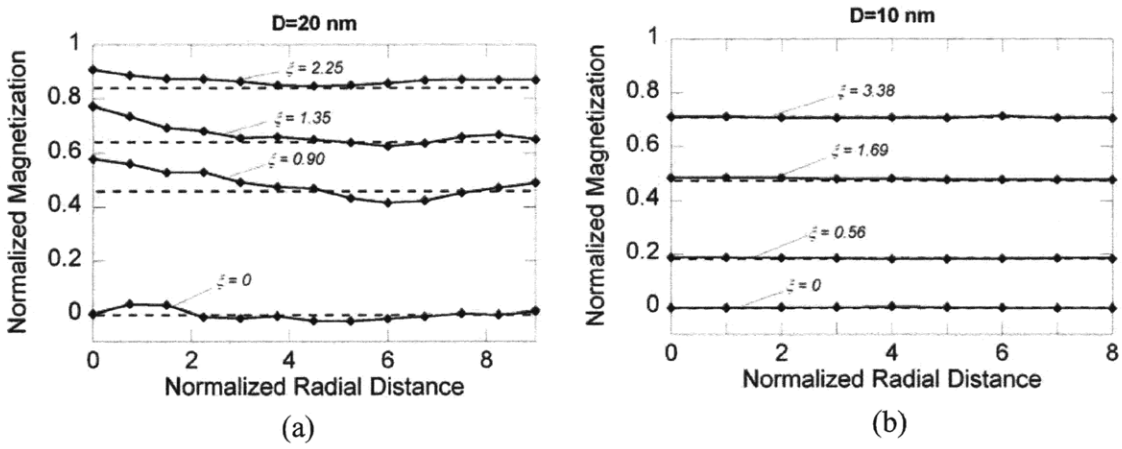

Figure 2-8: Radial variation in normalized magnetization in the direction perpendicular to the magnetic field (θ=0°) for magnetic nanoparticles with a diameter of (a) 20nm (λ=10.5) and (b) 10nm (λ=1.31).

2.3.3 Variation along the polar axis

The variation in the magnetization of the magnetic nanoparticles with distance from the poles of the nonmagnetic particle (θ = 90°) is shown in Figure 2-9. The magnetization in the vicinity of the nonmagnetic nanoparticles is smaller than in the bulk values. Again, these trends are stronger for the 20 nm diameter magnetic nanoparticles than for the 10 nm diameter magnetic nanoparticles.

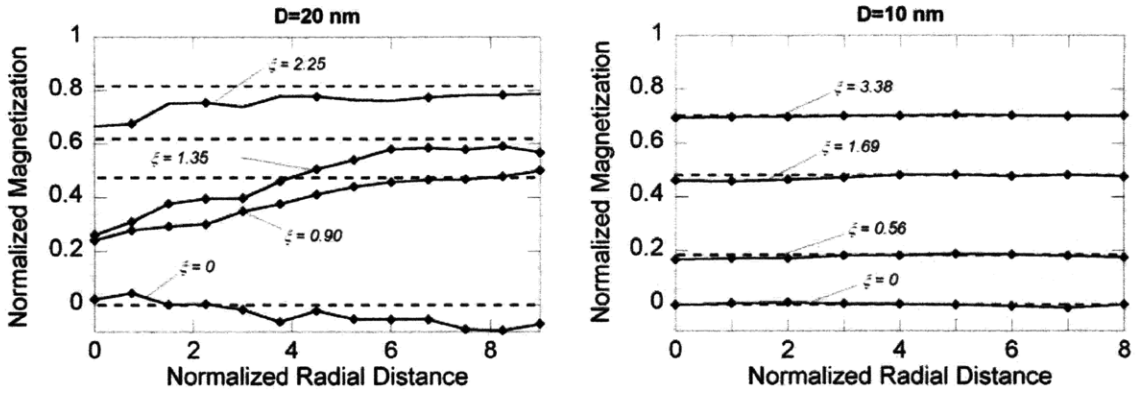

Figure 2-9: Radial variation in normalized magnetization in the direction parallel (θ=90°) to the magnetic field for magnetic nanoparticles with a diameter of (a) 20nm (λ=10.5) and (b) 10nm (λ=1.31).

From the zero magnetic field strength data in Figure 2-8 and Figure 2-9, it is clear that the noise for the θ = 90° region is significantly greater than for the θ = 0° case. This is because the sampling space for the θ = 90° region (a cylinder extending above and below the particle), is a lot smaller than the sampling space for the θ = 0° plane (a disk extending along the equatorial plane).

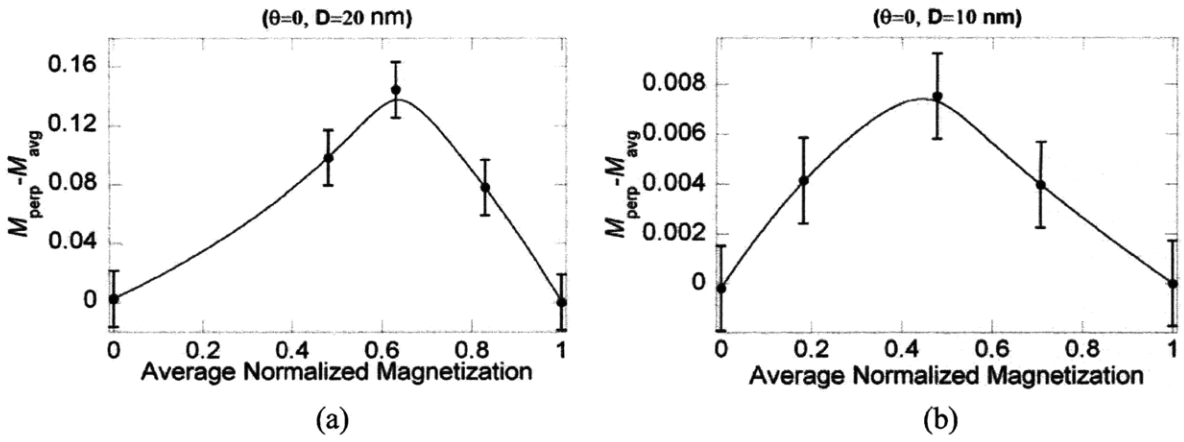

Figure 2-10: Difference in Magnetization in θ=0° plane and the average normalized magnetization values for the bulk plotted against average normalized magnetization for magnetic nanoparticles with a diameter of (a) 20 nm (λ=10.5) and (b) 10 nm (λ=1.31).

The deviation in the magnetization of the nanoparticles adjacent to the non-magnetic bead in the equatorial plane from that of the nanoparticles in the bulk fluid far from the beads is shown in Figure 2-10 as a function of increasing average normalized magnetization, which can be related directly to an increasing applied magnetic field strength. It is clear that the non-homogeneity in magnetization of the nanoparticles near the bead vanishes both for very low field strengths and very high field strengths, and passes through a maximum at some intermediate field strength. The reason for such behavior is that at zero field strength, corresponding to zero average normalized magnetization values, all the dipoles are completely randomly distributed through Brownian rotational and translational diffusion, while at very high field strengths, corresponding to a normalized magnetization value of one, all dipoles are oriented along the magnetic field irrespective of their actual position within the system. Hence, this anisotropic behavior becomes significant in a magnetic separation device near the edges or physical constraints in the device where the magnetic field strengths are low.

The presence of the nonmagnetic particle affects the energetics of the system. If the magnetic inter-particle interactions are strong and the system is subjected to a magnetic field gradient nonmagnetic particles will experience chemical potential driving forces apart from the magnetophoretic forces. These forces have been neglected for systems

where continuum approximation is valid [1, 26]. The evaluation of forces could be important for nano-sized nonmagnetic particles when the continuum approximation breaks down, and this would be the topic of interest for our next chapter.

2.3.4 Radial distribution functions

Figure 2-11a shows the radial distribution function (rdf) from the centre of the 100 nm non-magnetic particles in the equatorial plane. The rdf values are greater near the nonmagnetic bead due to the stabilization effect, as discussed previously, and increase with an increasing applied magnetic field intensity, in accord with the effects of field strength on nanoparticle stabilization. The rdf for the case with no magnetic field should be a constant function, however because of the statistical fluctuations there is a small decrease in the region close to the nonmagnetic particle. A similar rdf function for the 10nm diameter magnetic nanoparticles is shown in Figure 2-11b. In this case, however, these trends are very weak and the effects of applied field strength are small.

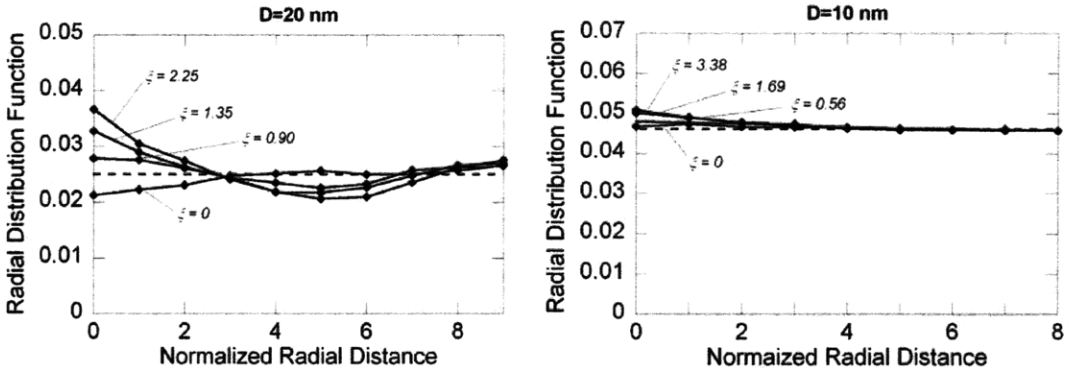

Figure 2-11: Radial distribution function in the direction perpendicular (θ=0°) to the magnetic field for magnetic nanoparticles with a diameter of (a) 20nm (λ=10.5) and (b) 10nm (λ=1.31).

2.4 Conclusions

We have determined the equilibrium magnetization profiles for magnetic nanoparticles in the vicinity of a nonmagnetic particle. The introduction of this nonmagnetic nanoparticle introduces non-homogeneity in the system with normalized magnetization values that are higher in the equatorial regions than in the polar region. The radial distribution functions

for the magnetic nanoparticles show that they are more stable in the equatorial plane than in the polar region around the nonmagnetic particles. All these effects were more pronounced for the 20 nm than for the 10 nm diameter magnetic nanoparticles, since the larger particles have much stronger magnetic interparticle interactions than do the smaller particles. These effects are stronger at moderate magnetic field strengths, when all the dipoles are not completely aligned along the magnetic field.

In contrast to the previous works, this study does not consider the magnetic medium as a continuum, but the magnetic nanoparticles are considered discretely. The understanding of the thermodynamic and transport properties of these nonmagnetic particles immersed in magnetic fields is important in the development of many nano-scale operations, including chemical and biological separations and self assembly systems in which the continuum approximation may not hold.

2.5 Bibiliography

1. Gonzalez, L.A., *Negative Magnetophoresis of Submicron Species in Magnetic Nanofluids*. 2009, Massachusetts Institute of Technology: Cambridge.

2. Fateen, S., *Magnetophoretic Focusing of Submicron Particles Dispersed in a Polymer-Based Magnetic Fluid*, in *Doctoral Thesis*. 2002, MIT: Cambridge.

3. Skjeltorp, A.T., *Colloidal Crystals In Magnetic Fluid.* Journal Of Applied Physics, 1984. **55**(6): p. 2587-2588.

4. Skjeltorp, A.T., *Ordering Phenomena Of Particles Dispersed In Magnetic Fluids.* Journal Of Applied Physics, 1985. **57**(8): p. 3285-3290.

5. Duan, X.F., Huang, Y., Cui, Y., Wang, J.F., and Lieber, C.M., *Indium phosphide nanowires as building blocks for nanoscale electronic and optoelectronic devices.* Nature, 2001. **409**(6816): p. 66-69.

6. Kruse, T., Spanoudaki, A., and Pelster, R., *Monte Carlo simulations of polydisperse ferrofluids: Cluster formation and field-dependent microstructure.* Physical Review B, 2003. **68**(5).

7. Hasmonay, E., Depeyrot, J., Sousa, M.H., Tourinho, F.A., Bacri, J.C., and Perzynski, R., *Optical properties of nickel ferrite ferrofluids.* Journal Of Magnetism And Magnetic Materials, 1999. **201**: p. 195-199.

8. Hasmonay, E., Depeyrot, J., Sousa, M.H., Tourinho, F.A., Bacri, J.C., Perzynski, R., Raikher, Y.L., and Rosenman, I., *Magnetic and optical properties of ionic ferrofluids based on nickel ferrite nanoparticles.* Journal Of Applied Physics, 2000. **88**(11): p. 6628-6635.

9. Hasmonay, E., Dubois, E., Neveu, S., Bacri, J.C., and Perzynski, R., *Alternating magneto-birefringence of ionic ferrofluids in crossed fields.* The European Physical Journal B - Condensed Matter and Complex Systems, 2001. **21**(1): p. 19.

10. Martin, J.E., Hill, K.M., and Tigges, C.P., *Magnetic-field-induced optical transmittance in colloidal suspensions.* Physical Review E, 1999. **59**(5): p. 5676-5692.

11. Davies, P., Popplewell, J., Martin, G., Bradbury, A., and Chantrell, R.W., *Monte-Carlo Simulations Of The Structure Of Magnetic Fluid Composites.* Journal Of Physics D-Applied Physics, 1986. **19**(3): p. 469-&.

12. Toussaint, R., Akselvoll, J., Helgesen, G., Skjeltorp, A.T., and Flekkoy, E.G., *Interaction model for magnetic holes in a ferrofluid layer.* Physical Review E, 2004. **69**(1).

13. Miguel, M.C. and Rubi, J.M., *On the dynamics of magnetic colloidal particles and holes.* Physica A, 1996. **231**(1-3): p. 288-294.

14. Charles, S.W., *Alignment Of Biological Assemblies Using Magnetic Fluids - A Review.* Journal Of Magnetism And Magnetic Materials, 1990. **85**(1-3): p. 277-284.

15. Allen, M.P. and Tildesley, D.J., *Computer Simulation of Liquids*. 1987: Oxford Science Publications.

16. Satoh, A., *A New Technique For Metropolis Monte-Carlo Simulation To Capture Aggregate Structures Of Fine Particles - Cluster-Moving Monte-Carlo Algorithm.* Journal Of Colloid And Interface Science, 1992. **150**(2): p. 461-472.

17. Frenkel, D. and Smit, B., *Understanding molecular simulations*. 2002: Academic Press.

18. Satoh, A., Chantrell, R.W., Kamiyama, S., and Coverdale, G.N., *Three dimensional Monte Carlo simulations of thick chainlike clusters composed of ferromagnetic fine particles.* Journal Of Colloid And Interface Science, 1996. **181**(2): p. 422-428.

19. Satoh, A., Chantrell, R.W., Kamiyama, S.I., and Coverdale, G.N., *Two-dimensional Monte Carlo simulations to capture thick chainlike clusters of ferromagnetic particles in colloidal dispersions.* Journal Of Colloid And Interface Science, 1996. **178**(2): p. 620-627.

20. Metropolis, N., Rosenbluth, A.W., Rosenbluth, M.N., Teller A.H., and Teller E., *Equation of State Calculations by Fast Computing Machines.* Journal of Chemical Physics, 1953. **21**(6): p. 1087-1092.

21. Newman, M.E. and Barkema, G.T., *Monte Carlo Methods in Statistical Physics*. 1999: Clarendon Press.

22. Landau, D. and Binder, K., *A Guide to Monte Carlo Simulations in Statistical Physics.* 2000.

23. Hiemenz, P.C. and Rajagopalan, R., *Principles of Colloid and Surface Chemistry*. 1997: Marcel Dekker, Inc.

24. Rosensweig, R.E., *Ferrohydrodynamics*. 1985: Cambridge University Press: Cambridge.

25. Castro, L.L., da Silva, M.F., Bakuzis, A.F., and Miotto, R., *Mono-disperse ferrofluids clusterization: a Monte Carlo study.* Journal of Magnetism and Magnetic Materials, 2005. **289**: p. 230-233.

26. Gonzalez, L., Fateen, S.E.K., Smith, K., and Hatton, T.A., *Magnetophoresis of Nonmagnetic, Submicrometer Particles in Magnetic Fluids.* Singapore-MIT Alliance (SMA) Symposium, 2004.

Chapter 3

3. Evaluation of chemical potential of non-magnetic species in magnetic fluids

3.1 Introduction

The focus of this section of work is separation conducted such that the medium rather than the particles to be separated is magnetic. These have been termed magnetic separations of the second kind [1]. The magnetic fluid is used to generate a "magnetic pressure", which is utilized to move the non-magnetic species in the direction opposite to the magnetic field gradient. Fateen [2] studied the forced diffusion of polystyrene beads in magnetic fluids. Fateen validated his work experimentally by using digital imaging techniques to study the dynamic evolution of the concentration profile of fluorescently-tagged polymer beads. He also performed a feasibility study by designing a simple separation device to isolate 200 nm from 500 nm particles. Gonzalez [3, 4] studied the focusing and trapping of sub-micron non-magnetic particles in magnetic fluids under the presence of magnetic fields. He developed a microchip that produced spatially increasing magnetic field gradients that trapped polystyrene beads in different locations of the chip, based on the relative size of the beads. Brownian dynamic simulations were used to match his experimental results with theoretical predictions.

Our interest lies in evaluating the forces a non-magnetic particle experiences when subjected to external magnetic fields in magnetic fields. The forces are evaluated by taking the gradient of chemical potential. For a system of non-magnetic particles immersed in magnetic particles the gradient in chemical potential can be defined as:

$$\underline{\nabla}\mu_1 = \left(\frac{\partial \mu_1}{\partial x_1}\right)_{T,p,H} \underline{\nabla} x_1 + \left(\frac{\partial \mu_1}{\partial H}\right)_{T,p,x_1} \underline{\nabla} H + \left(\frac{\partial \mu_1}{\partial p}\right)_{T,H,x_1} \underline{\nabla} p \tag{3.1}$$

Gonzalez [3] has shown that the last term in the above equation the pressure gradient term in the end can be simplified to show that a non-magnetic particle experiences a magnetophoretic force of

$$\boldsymbol{F} = -\mu_0 V_p M_f \nabla \boldsymbol{H} \tag{3.2}$$

where μ_0 is the permeability of free space, V_p is the volume of the particle, M_f is the magnetization of the magnetic fluid and $\nabla \boldsymbol{H}$ is the gradient of the magnetic field. However, the variation of the chemical potential with the magnetic field has been ignored in the past. This variation becomes significant when the non-magnetic particles are of the same size as that of magnetic particles and has been demonstrated in this work. We have studied the significance of this force as a function of magnetic field strength, non-magnetic particle size and the magnetic particle size.

3.2 Theory

Thermodynamic properties such as free energy, chemical potential, entropy and related quantities cannot be directly evaluated by taking averages of function of the phase space coordinates of a system [5]. However, there do exist some indirect ways to evaluate the excess chemical potential of a species in the system. The chemical potential can be calculated thereafter by adding the ideal gas chemical potential.

One of the most commonly used methods for evaluating chemical potential is the particle insertion method or the Widom method [6]. Chemical potential can be defined as

$$\mu_i = \left(\frac{\partial F}{\partial N_i}\right)_{VTN_{j\neq i}} \tag{3.3}$$

where, F is the Helmholtz free energy and N_i is the number of moles of species 'i'. This form of definition for chemical potential was chosen so as to relate it with an *NVT*

ensemble. The Helmholtz free energy of the system can be related the classical partition function as

$$F(N,V,T) = -k_B T \ln Q \tag{3.4}$$

The classical partition function of a system with N atoms in a cubic volume with a side of length L can be given as:

$$Q(N,V,T) = \frac{V^N}{\Lambda^{3N} N!} \int_0^1 \cdots \int_0^1 d\mathbf{s}^N \exp[-\beta U(\mathbf{s}^N; L)] \tag{3.5}$$

where Λ is the thermal de Broglie wavelength, U is the energy of the system with the scaled coordinates defined as $s^N = r^N/L$. Now relating this Helmholtz free energy definition of chemical potential, we have

$$\mu = -k_B T \ln\left(\frac{Q_{N+1}}{Q_N}\right) \tag{3.6}$$

On substituting the definition of classical partition function we have

$$\mu = \underbrace{-k_B T \ln\left(\frac{V/\Lambda^3}{N+1}\right)}_{\mu_{id}} \underbrace{- k_B T \ln\left\{\frac{\int d\mathbf{s}^{N+1} \exp[-\beta U(\mathbf{s}^{N+1})]}{\int d\mathbf{s}^N \exp[-\beta U(\mathbf{s}^N)]}\right\}}_{\mu_{ex}} \tag{3.7}$$

Here the first term represents the ideal gas contribution of the chemical potential, while the second term is the contribution from the excess part. On separating the potential energy term as a function of the $N+1$ particle system into a function of the N particle system and the interaction energy of the $(N+1)^{th}$ particle with the rest N particle system (ΔU) we can define the excess chemical potential as

$$\mu_{ex} = -k_B T \ln \int d\mathbf{s}^{N+1} \langle \exp(-\beta \Delta U) \rangle_N \tag{3.8}$$

Here the angular brackets imply a canonical ensemble averaging over the N particle ensemble. To evaluate this integral, a conventional NVT Monte Carlo simulation is carried out for the N particle system using the Metropolis algorithm [7]. After frequent

intervals, a random co-ordinate s^{N+1} is generated uniformly and the interaction energy of this 'inserted' particle ΔU is computed. It is important to note that none of these trial moves is accepted, or in other words we are always sampling a N particle system.

However, for systems with higher particle densities this technique fails because most of the insertion moves are rejected [8, 9]. Also, this method fails to calculate the chemical potential of the larger species when simulating a system with two species having contrastingly different sizes. Shing and Gubbins [9] used the method of particle removal to calculate the chemical potential. The calculation of excess chemical potential is slightly different from the particle insertion method.

$$\mu^{ex}{}_{insertion} = -kT \ln\left\langle \exp\left(-U_t / kT\right)\right\rangle \tag{3.9}$$

$$\mu^{ex}{}_{removal} = kT \ln\left\langle \exp\left(U_t / kT\right)\right\rangle \tag{3.10}$$

where, U_t is the energy of the test particle (inserted or removed). However, this method leads to a systematic discrepancy, that the test particle is already biased with the pre-existing energy distribution. A simple derivation using statistical mechanics shows that for the particle removal method, test particles with high energy contributions play a significant part in evaluation of chemical potential which are not adequately sampled. In other words it is unsafe to ignore the outcome of an unlikely event, which makes a large contribution. To elucidate this bias a system of hard spheres is considered. For the particle removal method U_t is equal to zero and hence the value of excess chemical is zero. However, for the particle insertion method it would be a finite value dependent on the particle density. A detailed description of the discrepancies between the two models has been discussed by Parsonage [10, 11]. Kofke and Cummings [12] have further described the precision and accuracy of staged free energy perturbation methods involving insertion and deletion for computing the residual chemical potential.

Mon and Griffith [13] explored the method of gradual insertion of a new particle to evaluate chemical potential for dense systems. This method is a variation of the 'umbrella sampling method' proposed by Shing and Gubbins [8]. However this method is computationally expensive and needs long run times to obtain statistically significant

data. Lyubartsev and co-workers [14-17] used the method of expanded ensemble to evaluate free energy and chemical potential. The expanded ensemble is composed as a sum of canonical ensembles with gradually inserting the $(N+1)^{th}$ particle. The probability distribution over the sub-ensembles is directly related to the ratio of the partition functions and hence to the free energy difference. This method is computationally less expensive than the gradual insertion method, but still significantly higher than particle insertion method. A variation of expanded ensemble method utilizing preferential sampling method was used by Vrabec [18]. The method of expanded ensemble has been extensively used in polymeric systems [19, 20].

A slightly different variation of expanded ensemble was used by Labik [21] to evaluate the chemical potential by using the 'scaled particle theory'. The essence of this method was to measure the probability of successful insertion of solute particles smaller than the particle diameter and then performing a cubic interpolation. This theory was used by Smith and co-workers [22] used the 'scaled particle theory' to calculate the chemical potentials of binary hard-sphere mixtures. This was further extended by Smith [23] for ternary mixture of fused hard spheres. Malijevsky [24] used a refined scaled particle method to calculate the chemical potential of ternary hard sphere mixtures. Boulougouris [25, 26] used a variation of the particle removal method to calculate the chemical potential of binary mixtures.

Lotfi and Fischer [27] used perturbation theory and simulations to evaluate the chemical potential of Lennard-Jones mixtures. However, the chemical potential evaluated from this method becomes inaccurate at decreasing densities. Nezbada and Kolafa [28] developed a method for evaluation of chemical potential for mixtures of significantly different compounds using a variation of the gradual particle insertion method. Nonetheless they had extremely long run times, resulting in poor statistical reliability. Gao and co-workers [29] used umbrella sampling to investigate Solute-solvent size ratio dependence of the solute residual chemical potential in subcritical solvents.

Biased Monte Carlo methods were used by Orkoulas [30] and de Pablo [31], which also suffer from the aforementioned drawbacks. Stamatopoulou and Ben-Amotz [32] carried out excess chemical potential calculations for different shaped solutes, such as linear and

hexagonal hexa-atomic solutes using the Widom test particle insertion method. Koda and Ikeda [33] used the scaled particle theory to calculate the chemical potential of hard sphero-cylinders.

Some other methods which have been used in the literature are the methods proposed by Attard [34], Wolf and co-workers [35], Powles [36], Parsonage [37], Henderson [38], Sokhan [39], Kofke [40, 41], Borowko [42] and Athenes [43]. However they all suffer from limitations unsuitable for our system.

3.3 Proposed method

We propose a new method to measure the variation of chemical potential with the magnetic field. We can relate the differential of Helmholtz free energy as:

$$dF = -SdT - PdV + \mu_0 \overline{H} d(MV) + \sum_i \mu_i dn_i \tag{3.11}$$

where S is the entropy, T is the temperature, P is the pressure, V is the volume, $\overline{H}$ is the partial molar magnetic field strength, M is the magnetization, μ_i is the chemical potential and n is the number of moles of species i in the system.

Applying Maxwell's relationship we get

$$\left(\frac{\partial \mu_i}{\partial (MV)}\right)_{T,V,n_j} = \mu_0 \left(\frac{\partial H}{\partial n_i}\right)_{T,V,M,n_{j\neq i}} \tag{3.12}$$

Since the volume of the system is constant we can move V out of the differential we have

$$\frac{1}{V}\left(\frac{\partial \mu_i}{\partial M}\right)_{T,V,n_j} = \mu_0 \left(\frac{\partial H}{\partial n_i}\right)_{T,V,M,n_{j\neq i}} \tag{3.13}$$

Now we add H as another variable on the left hand side of the equation to get

$$\frac{\frac{1}{V}\left(\frac{\partial \mu_i}{\partial H}\right)_{T,V,n_j}}{\left(\frac{\partial M}{\partial H}\right)_{T,V,n_j}} = \mu_0 \left(\frac{\partial H}{\partial n_i}\right)_{T,V,M,n_{j\neq i}} \tag{3.14}$$

On rearranging equation (3.14) we get

$$\left(\frac{\partial \mu_i}{\partial H}\right)_{T,V,n_j} = \mu_0 V \left(\frac{\partial H}{\partial n_i}\right)_{T,V,M,n_{j\neq i}} \left(\frac{\partial M}{\partial H}\right)_{T,V,n_j} \tag{3.15}$$

Now by triple product rule we have

$$\left(\frac{\partial H}{\partial n_i}\right)_M \left(\frac{\partial n_i}{\partial M}\right)_H \left(\frac{\partial M}{\partial H}\right)_{n_i} = -1 \tag{3.16}$$

Considering the equation at constant yemperature, volume and constant mole fraction for all other species, we have

$$\left(\frac{\partial H}{\partial n_i}\right)_M \left(\frac{\partial n_i}{\partial M}\right)_H \left(\frac{\partial M}{\partial H}\right)_{n_i}\Bigg|_{T,V,n_{j\neq i}} = -1 \tag{3.17}$$

Substituting equation (3.17) in equation (3.15) we have

$$\left(\frac{\partial \mu_i}{\partial H}\right)_{T,V,n_j} = \frac{\mu_0 V \left(\frac{\partial M}{\partial H}\right)_{T,V,n_j}}{\left(\frac{\partial n_i}{\partial M}\right)_{H,T,V,n_{j\neq i}} \left(\frac{\partial M}{\partial H}\right)_{T,V,n_j}} \tag{3.18}$$

This further simplifies to

$$\left(\frac{\partial \mu_i}{\partial H}\right)_{T,V,n_j} = \mu_0 V \left(\frac{\partial M}{\partial n_i}\right)_{H,T,V,n_{j\neq i}} \tag{3.19}$$

With this expression we have been able to relate a quantity on the left hand side which is difficult to measure with the help of simulation with a quantity on the right hand side, which relates the change in magnetization of the system with the changing mole fraction of non-magnetic species which can be evaluated easily through computer experiments.

3.4 Simulation Procedure

We have used Monte Carlo simulations in an NVT ensemble to evaluate the quantity of interest. We perform simulations with varying concentration of non-magnetic particles and observe the change in magnetization of the system. The simulation box contains magnetic particles at a concentration of about 1.5 volume % with periodic boundary conditions at 298K.

The interactions that we consider in the simulation are magnetic inter-particle interactions, magnetic particle and external field interaction for magnetic particles. For both magnetic and nonmagnetic particles we consider, Van der Waals forces of interaction and steric repulsion forces. We have used Metropolis algorithm [7], which means that all particle moves that lead to lowering of energy of the system are accepted, while moves which lead to an increase in energy are accepted with a finite probability. Magnetization is evaluated by averaging over the entire ensemble of particles.

3.5 Results

We perform a sample run for a system consisting of 100 magnetic particles, 20 nm in size with systems varying from no non-magnetic particles to 900 non-magnetic particles. In the Figure 3-1, we observe that the normalized magnetization of the particle decreases with increasing number of non-magnetic particles. The normalized magnetization here represents the ensemble average of the cosine of the angle θ the dipole makes with the external magnetic field.

$$\bar{m} = \langle \cos\theta \rangle \tag{3.20}$$

The magnetic particles on application of an external magnetic field align themselves in chain-like structures in an energetically favorable manner. The presence of non-magnetic in the system increases the hindrance between the magnetic-particles, making it difficult for them to interact, leading to lower magnetization. Hence, with increased non-magnetic particle strength the normalized magnetization of the system decreases.

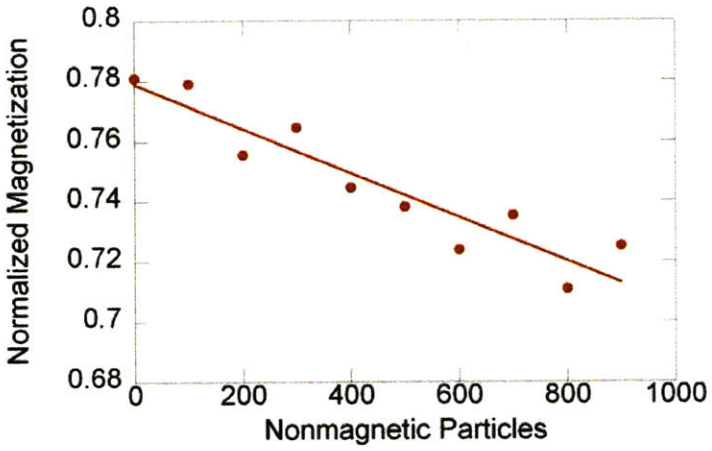

Figure 3-1: Normalized magnetization decreases with increased non-magnetic particle strength.

In order to evaluate the chemical potential driving force arising from the magnetic field, F_H we need to evaluate the slope of the line plotting magnetization against the non-magnetic particle strength. As a simplistic model we have fitted a straight line to the data for the evaluation of the force. To demonstrate the significance of F_H, we define a dimensionless quantity f as:

$$f = \frac{F_H}{F_P} \tag{3.21}$$

where F_P is the magnetophoretic force that originates from the pressure gradient, defined as $-\mu_0 \bar{V}_P M_f \nabla \boldsymbol{H}$. To understand the origin of both these forces let us look at Figure 3-2. When a magnetic field gradient is applied, the magnetic particles move in the direction of the gradient, displacing the non-magnetic particles in the opposite direction (shown in the top figures). Also, on application of an external magnetic field, magnetic particles (large

enough to interact with each other) align themselves in chain-like structures. The particles are more constrained when present in chain like structures at higher magnetic field and hence to reduce their entropy the force F_M, pushes the particles to lower magnetic field regions. Hence, any non-magnetic particles present in the system would go towards the region of lower magnetic strength (lower left hand illustration in Figure 3-2) as compared to region of higher magnetic strength (lower right hand illustration in Figure 3-2). Hence, both the effects create the driving forces F_M and F_P in the direction opposite to that of the magnetic field gradient in the system.

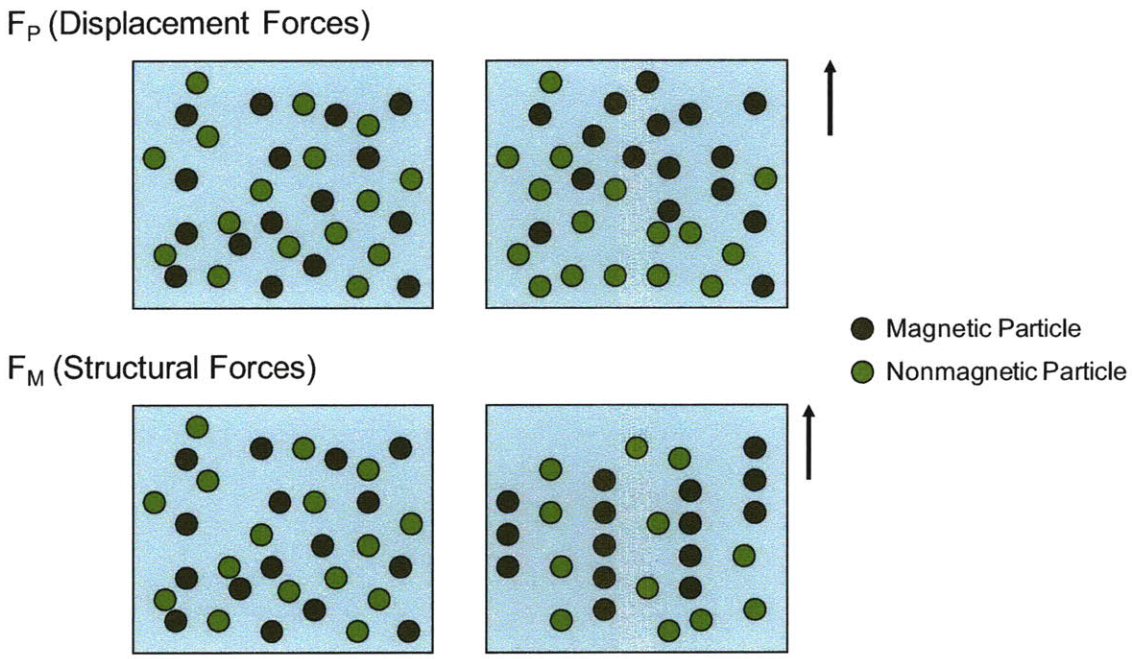

Figure 3-2: Understanding the origin of the driving forces for nonmagnetic particles. F_P arises from the magnetic particles pushing the non-magnetic particles in the direction opposite to the gradient, while F_M arises from the interaction effects between the particles. The arrow shown here depicts the direction of magnetic field gradient.

3.5.1 Variation with magnetic particle size

The results in Figure 3-3 show the variation of the dimensionless magnetic driving force for the non-magnetic particle, f with the magnetic particle diameter. The size of the non-

magnetic particle is the same as that of the magnetic particle. The simulation was performed for a dimensionless magnetic field strength, ξ of 1.35. The dimensionless magnetic field strength is defined as

$$\xi = \frac{mH}{k_B T} \tag{3.22}$$

where m is the magnetic moment of an individual magnetic nanoparticle defined as $m = \mu_0 MV$, V is the volume of the particle, M is the saturation magnetization of magnetite, H is the applied external field, k_B is the Boltzmann's constant and T is the temperature of the system.

We observe that this force is small for smaller magnetic particle sizes, since there are no chain-like structures as the magnetic inter-particle interactions are weak. The scale on the top shows λ, the ration of inter-particle magnetic forces to thermal forces.

$$\lambda = \frac{m^2}{4\pi\mu_0 (d + 2\delta)^3 k_B T} \tag{3.23}$$

where δ is the surfactant layer thickness. At around 18 nm particle size we observe a sudden increase in the force which occurs with the chain formation in system. On further increasing the magnetic particle size, we do not observe a significant change in the driving force since the chain structures for 20 nm particles are very similar to that of say 25 nm particles. Also, it is important to note the significance of the driving forces arising from these structural effects, which are comparable to that of the displacement forces arising from the magnetic particles.

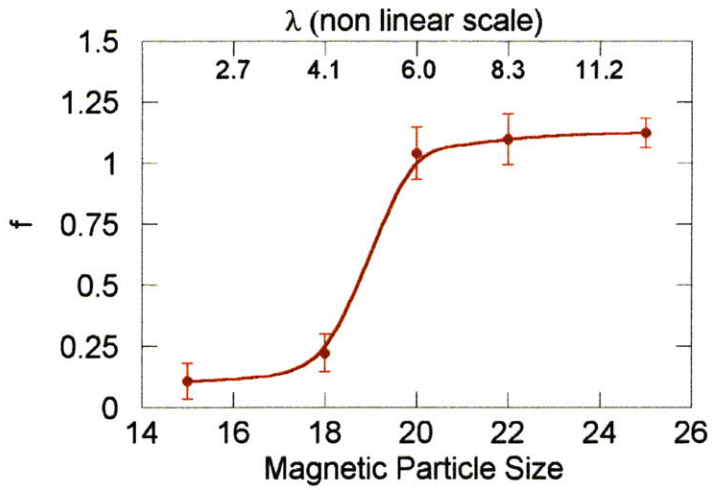

Figure 3-3: Variation of the dimensionless magnetic driving force with the magnetic particle size shows a sharp increase at a size of approximately 18 nm. The scale on the top λ is the ratio of magnetic inter-particle forces to thermal forces.

3.5.2 Variation with non-magnetic particle size

Next, we observe the variation of f with increasing non-magnetic particle size. The simulation results shown in Figure 3-4 are for 20 nm magnetic particles and a magnetic field strength ξ of 1.35. With an increasing non-magnetic particle size, f decreases. This primarily occurs because the displacement driving force F_P increases linearly with volume of the particle. Since f is inversely proportional to F_P, it decreases with increasing magnetic particle size. This is in accordance with the continuum approximation model for the driving forces, according to which the structural driving forces are almost absent when the non-magnetic particle size is much larger than the magnetic particle size in the magnetic fluid.

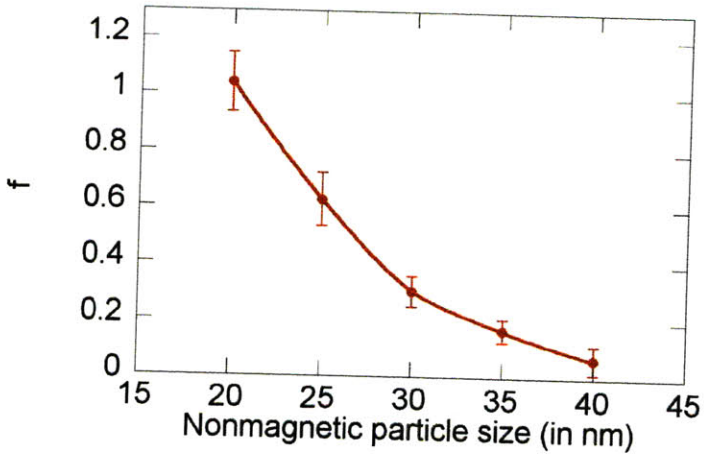

Figure 3-4: The dimensionless driving force, f decreases with increasing nonmagnetic particle size in accordance with the continuum approximation for magnetic nanoparticles of size 20 nm and magnetic field strength ξ of 1.35.

3.5.3 Variation with magnetic field strength

On increasing the magnetic field strength, f decreases as shown in Figure 3-5. When we initially apply a field, we see formation of chain-like structures. On increasing the field strength to higher values we do not see a considerable change in the structures. Hence, the driving forces at higher magnetic field strengths arising from the magnetic field gradients are fairly small. Another way to think about this result is that the magnetization of the magnetic nanoparticles is high because of the stronger magnetic field and the field arising from inter-particle interactions is not significant in increasing the magnetization of these particles.

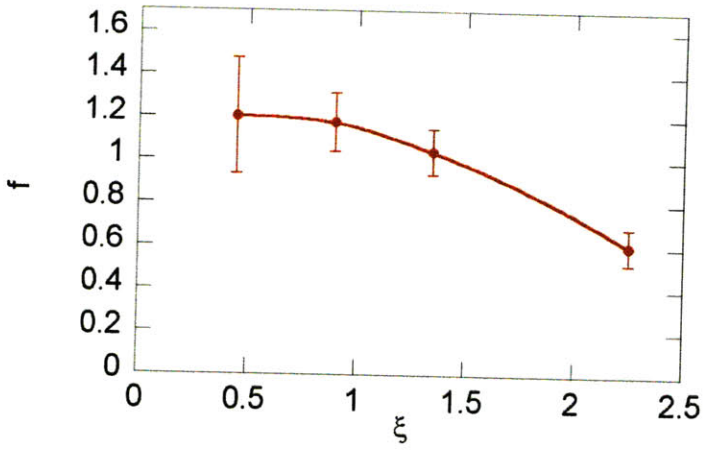

Figure 3-5: The dimensionless driving force, f decreases with increasing magnetic field strength. These results are for magnetic nanoparticles and non-magnetic particles of size 20 nm.

3.6 Conclusions

In this work we have identified and developed a novel method to evaluate driving forces on non-magnetic origination from the structural effects of magnetic particles in magnetic fluids. The method involved identifying this variation of chemical potential with the magnetic field to quantities, such as magnetization of magnetic nanoparticles which can be measured using Monte Carlo simulation.

With this new method we were able to demonstrate that this force arising from the structural effects is equally important as compared to the displacement force, $\boldsymbol{F} = -\mu_0 V_p M_f \nabla \boldsymbol{H}$, arising from the displacement of magnetic particles when non-magnetic particle are similar to the size of magnetic particles. Both these forces push the non-magnetic particles in the direction opposite to that of the external magnetic field gradient.

It was observed that this force was small compared to the displacement force when magnetic particles are small (~15 nm for magnetite), since at this size range the inter-particle interaction between the magnetite particles is not large enough to form chain-like structures. At around 18 nm we see a sharp increase in these forces as we see the

transition from a disordered structure to an ordered structure for the magnetic nanoparticles. Any further increase does not lead to a significant increase in the structural driving forces.

On increasing the size of the non-magnetic particle, for a fixed size of magnetic particles, the ratio of force arising from the structural effects as compared to the displacement force decreases. This is in agreement with the continuum approximation, which when evaluates the force on the non-magnetic particles considering the magnetic fluid as a continuum neglects and forces arising from the structural effects of the magnetic particles in the fluids. Also, it was observed that this ratio also decreases with increasing magnetic field strength.

It is essential in developing separation devices for non-magnetic particles using magnetic fluids, that we understand the magnetophoretic forces these particles experience. To model these forces we need computational tools that evaluate these driving forces. In this work we have developed a novel method to calculate these forces by evaluating the gradients in chemical potential of non-magnetic particles in magnetic fluids. A detailed parametric study for these forces is further required to understand this further.

3.7 Bibliography

1. Khalafalla, S.E., *Magnetic Separation Of 2nd Kind - Magnetogravimetric, Magnetohydrostatic, And Magnetohydrodynamic Separations.* Ieee Transactions On Magnetics, 1976. **12**(5): p. 455-462.

2. Fateen, S., *Magnetophoretic Focusing of Submicron Particles Dispersed in a Polymer-Based Magnetic Fluid*, in *Doctoral Thesis*. 2002, MIT: Cambridge.

3. Gonzalez, L., Fateen, S.E.K., Smith, K., and Hatton, T.A., *Magnetophoresis of Nonmagnetic, Submicrometer Particles in Magnetic Fluids.* Singapore-MIT Alliance (SMA) Symposium, 2004.

4. Gonzalez, L.A., *Negaative Magnetophoresis of Submicron Species in Magnetic Nanofluids*. 2009, Massachusetts Institute of Technology: Cambridge.

5. Frenkel, D. and Smit, B., *Understanding molecular simulations*. 2002: Academic Press.

6. Widom, B., *Some topics in the theory of fluids.* Journal Of Chemical Physics, 1963. **39**: p. 2808.

7. Metropolis, N., Rosenbluth, A.W., Rosenbluth, M.N., Teller A.H., and Teller E., *Equation of State Calculations by Fast Computing Machines.* Journal of Chemical Physics, 1953. **21**(6): p. 1087-1092.

8. Shing, K.S. and Gubbins, K.E., *The Chemical-Potential From Computer-Simulation Test Particle Method With Umbrella Sampling.* Molecular Physics, 1981. **43**(3): p. 717-721.

9. Shing, K.S. and Gubbins, K.E., *The Chemical-Potential In Dense Fluids And Fluid Mixtures Via Computer-Simulation.* Molecular Physics, 1982. **46**(5): p. 1109-1128.

10. Parsonage, N.G., *Determination Of The Chemical-Potential By The Particle Insertion Method And By Its Inverse.* Journal Of The Chemical Society-Faraday Transactions, 1995. **91**(17): p. 2971-2973.

11. Parsonage, N.G., *Chemical-potential paradox in molecular simulation - Explanation and Monte Carlo results for a Lennard-Jones fluid.* Journal Of The Chemical Society-Faraday Transactions, 1996. **92**(7): p. 1129-1134.

12. Kofke, D.A. and Cummings, P.T., *Precision and accuracy of staged free-energy perturbation methods for computing the chemical potential by molecular simulation.* Fluid Phase Equilibria, 1998. **151**: p. 41-49.

13. Mon, K.K. and Griffiths, R.B., *Chemical-Potential By Gradual Insertion Of A Particle In Monte-Carlo Simulation.* Physical Review A, 1985. **31**(2): p. 956-959.

14. Lyubartsev, A.P., Laaksonen, A., and Vorontsovvelyaminov, P.N., *Free-Energy Calculations For Lennard-Jones Systems And Water Using The Expanded Ensemble Method - A Monte-Carlo And Molecular-Dynamics Simulation Study.* Molecular Physics, 1994. **82**(3): p. 455-471.

15. Lyubartsev, A.P., Laaksonen, A., and VorontsovVelyaminov, P.N., *Determination of free energy from chemical potentials: Application of the expanded ensemble method.* Molecular Simulation, 1996. **18**(1-2): p. 43-58.

16. Lyubartsev, A.P., Martsinovski, A.A., Shevkunov, S.V., and Vorontsovvelyaminov, P.N., *New Approach To Monte-Carlo Calculation Of The Free-Energy - Method Of Expanded Ensembles.* Journal Of Chemical Physics, 1992. **96**(3): p. 1776-1783.

17. Shevkunov, S.V., Martsinovskii, A.A., and Vorontsov-Vel'yaminov, P.N., *Calculating the critical size and properties of a microdrop by the Monte Carlo method in a generalized ensemble.* High Temperature, 1988. **26**(2).

18. Vrabec, J., Kettler, M., and Hasse, H., *Chemical potential of quadrupolar two-centre Lennard-Jones fluids by gradual insertion.* Chemical Physics Letters, 2002. **356**(5-6): p. 431-436.

19. Escobedo, F.A. and Depablo, J.J., *Monte-Carlo Simulation Of The Chemical-Potential Of Polymers In An Expanded Ensemble.* Journal Of Chemical Physics, 1995. **103**(7): p. 2703-2710.

20. Tej, M.K. and Meredith, J.C., *Simulation of nanocolloid chemical potentials in a hard-sphere polymer solution: Expanded ensemble Monte Carlo.* Journal Of Chemical Physics, 2002. **117**(11): p. 5443-5451.

21. Labik, S. and Smith, W.R., *Scaled Particle Theory And The Efficient Calculation Of The Chemical-Potential Of Hard-Spheres In The Nvt Ensemble.* Molecular Simulation, 1994. **12**(1): p. 23-31.

22. Barosova, M., Malijevsky, M., Labik, S., and Smith, W.R., *Computer simulation of the chemical potentials of binary hard-sphere mixtures.* Molecular Physics, 1996. **87**(2): p. 423-439.

23. Labik, S., Jirasek, V., Malijevsky, A., and Smith, W.R., *Modifications of the SP-MC method for the computer simulation of chemical potentials: ternary mixtures of fused hard sphere fluids.* Molecular Physics, 1998. **94**(2): p. 385-393.

24. Malijevsky, A., Labik, S., and Malijevsky, A., *Computer simulation of chemical potentials of ternary hard-sphere fluid mixtures.* Physical Chemistry Chemical Physics, 2004. **6**(8): p. 1742-1744.

25. Boulougouris, G.C., Economou, I.G., and Theodorou, D.N., *Calculation of the chemical potential of chain molecules using the staged particle deletion scheme.* Journal Of Chemical Physics, 2001. **115**(17): p. 8231-8237.

26. Boulougouris, G.C., Economou, I.G., and Theodorou, D.N., *On the calculation of the chemical potential using the particle deletion scheme.* Molecular Physics, 1999. **96**(6): p. 905-913.

27. Lotfi, A. and Fischer, J., *Chemical-Potentials Of Model And Real Dense Fluid Mixtures From Perturbation-Theory And Simulations.* Molecular Physics, 1989. **66**(1): p. 199-219.

28. Nezbeda, I. and Kolafa, J., *A New Version of the Insertion Particle Method for Determining the Chemical Potential by Monte Carlo Simulation.* Molecular Simulation, 1991. **5**: p. 391-403.

29. Gao, G.T., Woller, J.B., Zeng, X.C., and Wang, W.C., *Solute-solvent size ratio dependence of the solute residual chemical potential in subcritical solvents.* Molecular Physics, 1997. **90**(1): p. 141-145.

30. Orkoulas, G. and Panagiotopoulos, A.Z., *Chemical-Potentials In Ionic Systems From Monte-Carlo Simulations With Distance-Biased Test Particle Insertions.* Fluid Phase Equilibria, 1993. **83**: p. 223-231.

31. Depablo, J.J., Laso, M., and Suter, U.W., *Estimation Of The Chemical-Potential Of Chain Molecules By Simulation.* Journal Of Chemical Physics, 1992. **96**(8): p. 6157-6162.

32. Stamatopoulou, A. and BenAmotz, D., *Chemical potentials of hard polyatomic solutes in hard sphere fluids.* Journal Of Chemical Physics, 1997. **106**(3): p. 1181-1186.

33. Koda, T. and Ikeda, S., *Test of the scaled particle theory for aligned hard spherocylinders using Monte Carlo simulation.* Journal Of Chemical Physics, 2002. **116**(13): p. 5825-5830.

34. Attard, P., *Simulation Of The Chemical-Potential And The Cavity Free-Energy Of Dense Hard-Sphere Fluids.* Journal Of Chemical Physics, 1993. **98**(3): p. 2225-2231.

35. Fay, P.J., Ray, J.R., and Wolf, R.J., *Detailed Balance Method For Chemical-Potential Determination In Monte-Carlo And Molecular-Dynamics Simulations.* Journal Of Chemical Physics, 1994. **100**(3): p. 2154-2160.

36. Powles, J.G., Holtz, B., and Evans, W.A.B., *New Method For Determining The Chemical-Potential For Condensed Matter At High-Density.* Journal Of Chemical Physics, 1994. **101**(9): p. 7804-7810.

37. Parsonage, N.G., *Computation of the chemical potential in high density fluids by a Monte Carlo method.* Molecular Physics, 1996. **89**(4): p. 1133-1144.

38. Henderson, J.R., *Inverse potential distribution theory for models with hard cores.* Molecular Physics, 1997. **90**(4): p. 581-583.

39. Sokhan, V.P., *The chemical potential of dense liquids by the coupled test particle method.* Molecular Simulation, 1997. **19**(3): p. 181-204.

40. Lu, N.D. and Kofke, D.A., *Optimal intermediates in staged free energy calculations.* Journal Of Chemical Physics, 1999. **111**(10): p. 4414-4423.

41. Lu, N.D., Kofke, D.A., and Woolf, T.B., *Improving the efficiency and reliability of free energy perturbation calculations using overlap sampling methods.* Journal Of Computational Chemistry, 2004. **25**(1): p. 28-39.

42. Borowko, M., Zagorski, R., and Malijevsky, A., *Computer simulation of the chemical potential of binary Lennard-Jones mixtures.* Journal Of Chemical Physics, 2000. **112**(5): p. 2315-2318.

43. Athenes, M., *Computation of a chemical potential using a residence weight algorithm.* Physical Review E, 2002. **66**(4).

Chapter 4

4. Anisotropic diffusion of non-magnetic particles in magnetic fluids

4.1 Introduction

For designing separation systems, it is important that we understand the diffusion characteristics of the non-magnetic particles. Knowledge of these diffusion coefficients is also important in understanding self assembly of non-magnetic particles in magnetic fluids. In this work, we have evaluated the diffusion coefficients of the non-magnetic particles in a system of magnetic and non-magnetic particles. We expect these diffusion coefficients to be anisotropic because of the constraints imposed by magnetic particles in such systems, as shown in Figure 4-1. Magnetic nanoparticles having sufficiently strong inter-particle interaction (more than 20 nm in size for magnetite particles at room temperature) tend to align themselves as chains upon application of a magnetic field. The diffusion coefficient in the direction of the magnetic field will therefore be higher than that in the direction perpendicular to the field because diffusion across the chains is more difficult than diffusion parallel to the chains.

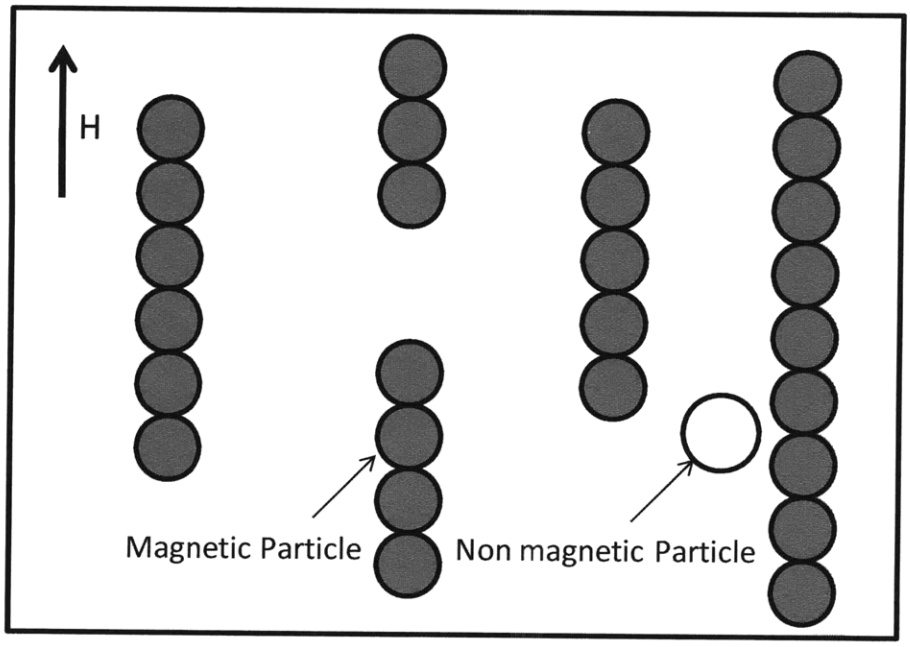

Figure 4-1: Diffusion of non-magnetic particle (white) in a system of magnetic particles (grey) aligned under the influence of magnetic field.

4.2 Diffusion in constrained systems

Diffusion in constrained systems has been of considerable interest in the literature. Rallison [1] studied the diffusion of particles around a circular ring, and one dimensional and two dimensional rod suspensions using theory and stochastic simulations. He evaluated the self diffusion coefficients of these particles, which was observed to decrease with sampling time intervals. Guzowski [2] has evaluated the short time diffusion coefficients in a system consisting of freely moving rods and a single spherical particle, which was found to be a linear function of the rod concentration. Diffusion of spheres in a network of rods has been studied by Kang and workers [3, 4] using fluorescence correlation spectroscopy for small tracer particles, dynamic light scattering for intermediate sized particles and video microscopy for larger particles. Kluijtmans [5] studied the long time self diffusion and sedimentation in a dilute suspension of rigid rods. Tracy studied the diffusion characteristics of rod-sphere composites. Cavicchi [6] evaluated anisotropic diffusion coefficients in block copolymer cylinders by using forced Rayleigh scattering. Phillips and co-workers [7] have evaluated the effect of

hydrodynamic interaction on the hindered transport of macromolecules in fibrous media. Lord Rayleigh [8] has studied the influence of obstacles in a rectangular order on the properties of the medium. This system compares well with the diffusion of spheres in system of magnetic particle chains, which can be considered as rigid cylinders.

In this work, we perform Brownian dynamics simulations to evaluate the diffusion coefficients of the non-magnetic particles in magnetic fluids. We have used the Gunsteren and Berendsen [9] algorithm to perform the stochastic dynamic simulations. The methodology is explained in detail in the following section. The results demonstrate a strong anisotropy in the diffusion coefficients in directions parallel and perpendicular to the field. We have studied the effect of magnetic fluid concentration, magnetic particle size and non-magnetic particle size on the anisotropy coefficient, defined as the ratio of diffusion coefficients perpendicular and parallel to the magnetic field.

4.3 Methodology

For a dispersion of nanoparticles in a low molecular weight solvent, the time scales for motion of solvent molecules and of nanoparticles are vastly different. Therefore, the short time steps needed to model the fast solvent behavior may severely restrict the overall time span that can be modeled. Brownian Dynamic Simulations remove this difficulty by treating the solvent molecules statistically rather than explicitly [10]. A combination of stochastic and frictional terms eliminates the need for an explicit treatment of the solvent molecules in our simulation [11].

A system consisting of N nanoparticles in a solvent can be described by the Langevin equation [9]:

$$m_i \dot{v}_i(t) = m_i \gamma_i v_i(t) + F_i\{x(t)\} + R_i(t) \tag{4.1}$$

The index i labels particles and Cartesian components (i= 1, 2, . .., 3N). v_i is the x, y or z component of the velocity, m_i is the mass of the particle and γ_i is the friction coefficient of the particle. $\boldsymbol{F_i}$ represent the systematic force acting on the particle which depends on the coordinates of all the particles, represented by $x(t)$. The non-systematic effect of the

solvent on the solute is represented by R_i. The friction coefficient is related to the viscosity by:

$$\gamma_i = \frac{6\pi\eta a_i}{m_i} \tag{4.2}$$

where η is the viscosity of the dispersion medium and m_i and a_i being the particle's mass and radius. This process takes place on a characteristic time scale $\tau_B = m_i / 6\pi\eta a_i = 1/\gamma_i$ [12].

The random force should be stationary, Markovian, Gaussian with a zero mean and should have no correlation with prior velocities. The stochastic term, $R_i(t)$ needs to exhibit the following statistical properties [13].

$$\left\langle R_i(0) R_j(t) \right\rangle = 2 m_i \gamma_i k T_{ref} \delta_{ij} \delta(t) \tag{4.3}$$

$$W(R_i) = \left[2\pi \left\langle R_i^2 \right\rangle \right] \exp\left\{ -R_i^2 / \left(2 \left\langle R_i^2 \right\rangle \right) \right\} \tag{4.4}$$

$$\left\langle R_i \right\rangle = 0 \tag{4.5}$$

$$\left\langle v_i(0) R_j(t) \right\rangle = 0, t \geq 0 \tag{4.6}$$

$$\left\langle F_i(0) R_j(t) \right\rangle = 0, t \geq 0 \tag{4.7}$$

where $\langle .... \rangle$ denotes the average over an ensemble, i and j classify the components of the ensemble, k_b is the Bolzmann's constant, T is the temperature, δ_{ij} is the Kronecker delta function, and $W(R_i)$ is the probability density function of the random force.

Brownian Dynamic equations are the simplest form of stochastic equations which have no correlation in time and space [14]. Various algorithms have been employed to solve these Brownian dynamic equations. Ermak and McCammon's [15, 16] first order algorithm to has been employed extensively in the past. Ermak's algorithm is restricted by the fact that time steps have to be very small ($\Delta t \ll \gamma^{-1}$); else it leads to drift in the quantities calculated. The efficiency can be improved by using second or third order

algorithms and longer time steps [17]. Quite a few such methods [18-22] use extensions of the Runge-Kutta Method to involve stochastic terms. These algorithms are not limited by the time step, but by the rate of change of the systematic force.

In this work we have used a third order algorithm devised by Van Gunsteren and Berendsen in 1982 [9] which is based on the well known Molecular Dynamics Verlet algorithm [23, 24]. This algorithm is numerically equivalent to the Brownian Dynamic algorithm proposed by Allen [25, 26]. The proposed algorithm reduces to the Verlet algorithm under the conditions of zero friction. Also, Van Gunsteren and Berendsen do not assume that the stochastic forces to remain constant within each time step [13]. Thus, one can take larger simulation steps as compared to schemes which assume constant stochastic forces within a time step [27].

The discretized equation for the particle trajectories can be formulated solving the linear, non-homogeneous first order differential equation (Equation (4.1)).

$$\begin{aligned} x(t_n+\Delta t) = {} & x(t_n)\left[1+e^{-\gamma\Delta t}\right] - x(t_n-\Delta t)e^{-\gamma\Delta t} + m^{-1}F(t_n)(\Delta t)^2(\gamma\Delta t)^{-1}\left[1+e^{-\gamma\Delta t}\right] + \\ & m^{-1}\dot{F}(t_n)(\Delta t)^3(\gamma\Delta t)^{-2}\left[\frac{1}{2}\gamma\Delta t\left[\left(1+e^{-\gamma\Delta t}\right)-\left(1-e^{-\gamma\Delta t}\right)\right]\right] + \\ & X_n(\Delta t) + e^{-\gamma\Delta t}X_n(-\Delta t) + O\left[(\Delta t)^4\right] \end{aligned} \tag{4.8}$$

where $X_n(\Delta t) = (m\gamma)^{-1}\int_{t_n}^{t_n+\Delta t}\left[1-e^{-\gamma(t_n+\Delta t-t)}\right]R(t)dt$.

4.4 Algorithm

The computation scheme implemented in our algorithm (except the first step) can be summarized as follows:

1. The values of $x(t_n)$, $x(t_{n-1})$, $X_{n-1}(\Delta t)$ and $F(t_{n-1})$ are assumed
2. Systematic forces in the system $F(t_n)$ are assumed.
3. The derivative of the systematic forces are computed as follows:

$$\dot{F}(t_n) = \left[F(t_n) - F(t_{n-1})\right]/\Delta t \tag{4.9}$$

4. Y is sampled from a Gaussian with zero mean and width of $\sigma^2 = \frac{kT_{ref}}{m\gamma^2} E(\gamma(\Delta t) / C(\gamma(\Delta t)$

5. The stochastic term, $X_n(-\Delta t)$ is computed as:

$$X_n(-\Delta t) = X_{n-1}(\Delta t)\, G(\gamma\Delta t)/C(\gamma\Delta t) + Y \tag{4.10}$$

where

$$C(\gamma\Delta t) = 2\gamma\Delta t - 3 + 4\exp(-\gamma\Delta t) - \exp(-2\gamma\Delta t) \tag{4.11}$$

$$G(\gamma\Delta t) = \exp(\gamma\Delta t) - 2\gamma\Delta t - \exp(-\gamma\Delta t) \tag{4.12}$$

6. Finally $\boldsymbol{X}_n(\Delta t)$ is sampled from a Gaussian with a zero mean and a width of $\sigma^2 = \frac{kT_{ref}}{m\gamma^2} C(\gamma(\Delta t)$.

7. The new positions are calculated using equation (4.8)

For the first time step $x(t_{-1})$, $X_{-1}(\Delta t)$ and $F(t_{-1})$ are unknown. Hence, for the first step the update is performed as follows:

$$\begin{aligned} x(t_1) = x(t_0) + v(t_0)\Delta t\left(\gamma\Delta t\right)^{-1}\left[1 - e^{-\gamma\Delta t}\right] + \\ m^{-1}F(t_0)(\Delta t)^2(\gamma\Delta t)^{-2}\left[\gamma\Delta t - \left[1 - e^{-\gamma\Delta t}\right]\right] + X_o(\Delta t) \end{aligned} \tag{4.13}$$

Where $X_0(\Delta t)$ is sampled from a Gaussian mean and a width of $\sigma^2 = \frac{kT_{ref}}{m\gamma^2} C(\gamma(\Delta t)$.

The system simulated has periodic boundary conditions. Hence, the algorithm needs to be used appropriately for updating particle positions when crossing the boundaries of the considered simulation cell.

4.5 Force model

The systematic forces considered in our simulation were as follows:

4.5.1 Magnetic dipole-dipole forces

The magnetic particles were considered to be spherical in shape with central point dipoles. The force acting on them was calculated to be [28]:

$$\boldsymbol{F}_{ij}^{\,m} = -\frac{3\mu_0 m^2}{4\pi d^4}\frac{1}{\left(r_{ij}/d\right)^4}\left[-(\boldsymbol{n}_i.\boldsymbol{n}_j)\boldsymbol{t}_{ij} + 5(\boldsymbol{n}_i.\boldsymbol{t}_{ij})(\boldsymbol{n}_j.\boldsymbol{t}_{ij})\boldsymbol{t}_{ij} - \left\{(\boldsymbol{n}_j.\boldsymbol{t}_{ij})\boldsymbol{n}_i + (\boldsymbol{n}_i.\boldsymbol{t}_{ij})\boldsymbol{n}_i\right\}\right] \quad (4.14)$$

where $\boldsymbol{n}_i$ is the unit vector pointing in the direction of magnetic moment, $\boldsymbol{m}_i$ (m= $|\boldsymbol{m}_i|$) of particle i, $\boldsymbol{r}_{ij}$ is the vector pointing to the center of particle j from the center of particle i, $\boldsymbol{t}_{ij}$ is the unit vector given by $\boldsymbol{r}_{ij}/r_{ij}$, d is the diameter of the particle core.

4.5.2 Van der Waals forces of attraction

The Van der Waals forces of attraction calculated using the potential function is:

$$\boldsymbol{F}_{ij}^{\,vdw} = -\frac{A_H}{6}\frac{(d_i d_j)^3 \boldsymbol{r}_{ij}}{\left[r_{ij}^{\,2} - \left(\frac{d_i - d_j}{2}\right)^2\right]^2\left[r_{ij}^{\,2} - \left(\frac{d_i + d_j}{2}\right)^2\right]^2} \quad (4.15)$$

where A_H is the Hamaker constant.

4.5.3 Interaction energy of overlap

In a single time step, after all particles are moved, the particles may overlap and it is important to adjust them. Some of the common approaches that have been used in the past are those by Cichocki and Hinsen [29], Schaerlt and Sillescu [30] and Strating [31]. We assume that the particles are coated with a surfactant (or a steric layer) and the force of repulsion is given by:

$$\boldsymbol{F}_{ij}^{S} = k_b T \frac{\pi d^2 N_s}{2\delta} \boldsymbol{t}_{ij} \ln\left(\frac{d+2\delta}{r_{ij}}\right) \left(d \le r_{ij} \le d+\delta\right) \tag{4.16}$$

where δ is the surfactant layer thickness and N_s is the number of adsorbed surfactant molecules per unit area.

Since there are no magnetic field gradients and we have assumed that all the magnetic particles are aligned in the direction of the applied magnetic field, the non-magnetic particles do not experience any systematic magnetophoretic forces.

4.6 Evaluation of diffusion coefficient

Self diffusion coefficients were evaluated from the root mean square displacement [32]

$$D^s = \frac{\left\langle \Delta r_i^2 \right\rangle}{2\Delta t_s} \tag{4.17}$$

where r_i is the displacement in the i^{th} component (i=x,y or z) in a given sampling time Δt_s. When Δt_s is short, the result is close to the diffusion coefficient calculated from the Stokes-Einstein equation (4.2), which applies to dilute system. However, for a long time interval, the diffusion coefficient, has a lower value because the diffusive motion is then hindered by other particles [33].

$$\left\langle r_i^2 \right\rangle \sim 2D^s{}_o t \; for \; \tau_B << t << \tau_\phi \tag{4.18}$$

$$\left\langle r_i^2 \right\rangle \sim 2D^s{}_\infty t \; for \; \tau_\phi << t \tag{4.19}$$

where $\tau_\phi = a^2\phi^{-\frac{2}{3}}/D_0$ is the time to diffuse across a particle separation distance $a\phi^{-\frac{1}{3}}$, and φ is the volume fraction of the spheres in the suspension.

For intermediate time scales, the self-diffusion coefficient is time dependent. Various empirical and theoretical approaches have been used to describe this time dependence. One such empirical approach has been used by Pusey [34, 35] to describe the time dependence of diffusion coefficient is:

$$D^S(t) = D^S{}_\infty + (D^S{}_0 - D^S{}_\infty)\lambda(t) \tag{4.20}$$

where λ(t) is an exponential or stretched exponential decay. Though such approaches A theoretical approach was used by Cichocki and Felderhoff [36] using a two pole approximation.

Several prior studies have provided theoretical estimates of the long time self diffusion coefficients. Batchelor [37, 38] has worked using the 'relaxation affect' approach to calculate the diffusion coefficients of interacting spheres in dilute suspensions. A very common approach used by other researchers has been using the 'memory effect' [39-42]. Both the approaches describe the same physical effect. The relaxation approach involves evaluating the mobility of a tagged particle from the thermodynamic driving force which is used to evaluate the diffusion coefficient. Memory effect utilizes the Smoluchowski effect to describe the motion of a tagged colloidal particle and the root mean square displacement is used to evaluate the diffusion coefficient. For the case of hard spheres without hydrodynamic interaction, Lekkerkerker [32], Ackerson and Fleishman [39], and Hanna, Hess and Klein [43] have derived the self diffusion coefficient to be

$$D^S{}_\infty = D_0(1-2\phi) \tag{4.21}$$

where φ is the volume fraction of the hard spheres.

4.7 Error estimation of the diffusion coefficients

The confidence intervals were calculated by evaluating the Chi square values for the variance. The probability (P) that the value of σ^2 lies between $\frac{(n-1)S^2}{\chi_U{}^2}$ and $\frac{(n-1)S^2}{\chi_L{}^2}$ is $1-\alpha$ [44].

$$P\left[\frac{(n-1)S^2}{\chi_L{}^2} \le \sigma^2 \le \frac{(n-1)S^2}{\chi_U{}^2}\right] = 1-\alpha \tag{4.22}$$

Where S^2 is the sample variance, n is the number of data points, and the values of χ^2 can be looked up in tables or evaluated with the help of MATLAB® using the command 'chi2inv'. The value of χ^2 is dependent on both n and α.

4.8 Simulation Parameters

The simulations were performed for magnetic particles in the size range of 10 nm (λ=0.48) and 30 nm (λ=24.38), where $\lambda = m^2/4\pi\mu_0(d+2\delta)^3 kT$ compares the inter-particle magnetic forces to the thermal forces. Here, m is the magnetic moment of the dipoles defined by $m = \mu_0 MV$, d is the diameter of the magnetic particle , V is the volume of the particle, M is the saturation magnetization of magnetite, and δ is the surfactant layer thickness which was taken to be 2 nm. This definition of λ is similar to one used by Rosensweig [45], but adjusted to include the surfactant layer thickness. The non-magnetic particles are in the range of 10 nm to 60 nm. Only mono-disperse spheres were considered.

The viscosity of the medium was considered to be 0.002 Pa-s. The simulation time step was in the range of 10^{-10} to 10^{-9} seconds depending on the system simulated. The step size is constrained by the fact that a larger step size may lead to a larger overlap of the particles, giving it unrealistically high forces and displacements. The density for magnetic particles and non magnetic particles were taken to be 6000 kg/m^3 and 2500 kg/m^3 respectively. Simulations were carried out at a temperature of 300K and a strong magnetic field was applied in the z-direction. Error bars correspond to a 99% confidence level, as determined by the Chi squared analysis [44].

The simulation was carried out in two phases, the equilibration phase and the sampling phase. In the equilibration phase, starting with a random initial configuration of the particles, we simulate till the system achieves equilibration. In the next stage, the sampling phase, we measure the quantities of interest, which in this case are the position vectors for the non-magnetic particles. These position vectors are used to calculate the diffusion constants. We use periodic boundary conditions with a Cartesian co-ordinate system in the above simulations.

4.9 Results and Analysis

4.9.1 Validation

The base case (Figure 4-2) used only non-magnetic particles, 30 nm in diameter, with a 2 nm surfactant coating. The concentration of the non-magnetic particle was taken to be 0.5% by volume, ensuring that any effects of concentration on the diffusion coefficient were minimal. The diffusion coefficient plotted in Figure 4-2 has been non-dimensionalized by D_o, the diffusion coefficient from the Stokes-Einstein equation [46]. The dotted lines, the coefficient values in the three different co-ordinates, show no anisotropy. This is as expected. The solid line represents the averaged (over the three different co-ordinate axis) values of the diffusion coefficient. One might observe that the error bounds increase with increasing value of Δt_s. The system is simulated for 10^{-2} seconds of real time, which means that for higher values of Δt_s, there would be fewer data points, since there are a fixed number of data points and sampling is less frequent. This leads to a lower confidence and larger error bars for data with larger sampling time intervals. Also the time is plotted on a logarithmic axis to cover a wider range of sampling time intervals. The y-axis has been made dimensionless using τ_ϕ, the time required for particles to travel the inter-particle separation:

$$\Delta t_\phi = \frac{\Delta t_s}{\tau_\phi} \tag{4.23}$$

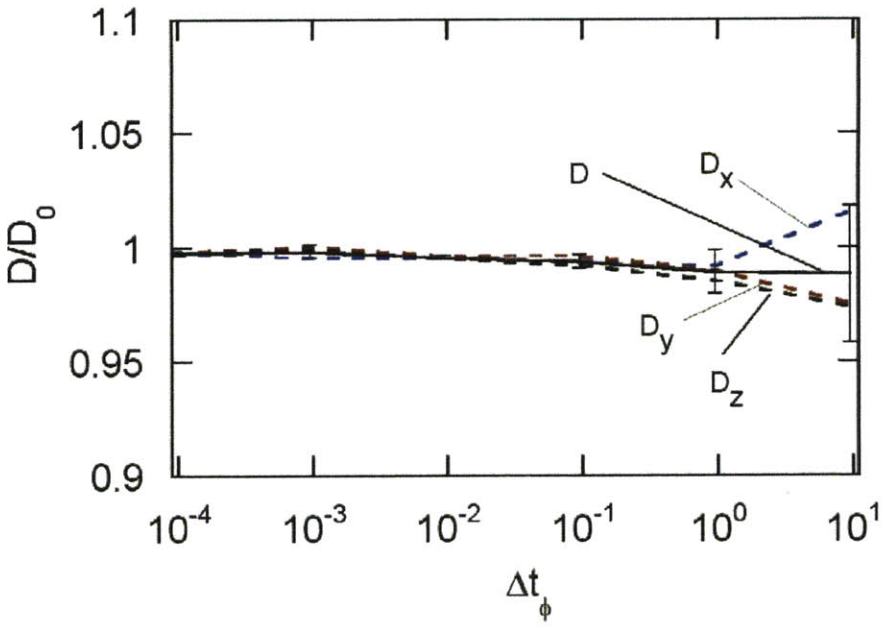

Figure 4-2: Dimensionless diffusion coefficient of 30nm non-magnetic particles (0.5% volume concentration) decreases as a function of sampling time, Δt_s.

However, for the rest of the simulations we need to simulate the systems at a higher level of concentration for the non-magnetic particles to obtain statistically significant data on non-magnetic particles. A larger simulation box (to reduce the concentration, for the same number of non-magnetic particles) is not feasible because then one would need to simulate a considerably larger number of magnetic particles (for a higher magnetic particle concentration to observe the anisotropic effects), leading to very long simulation times.

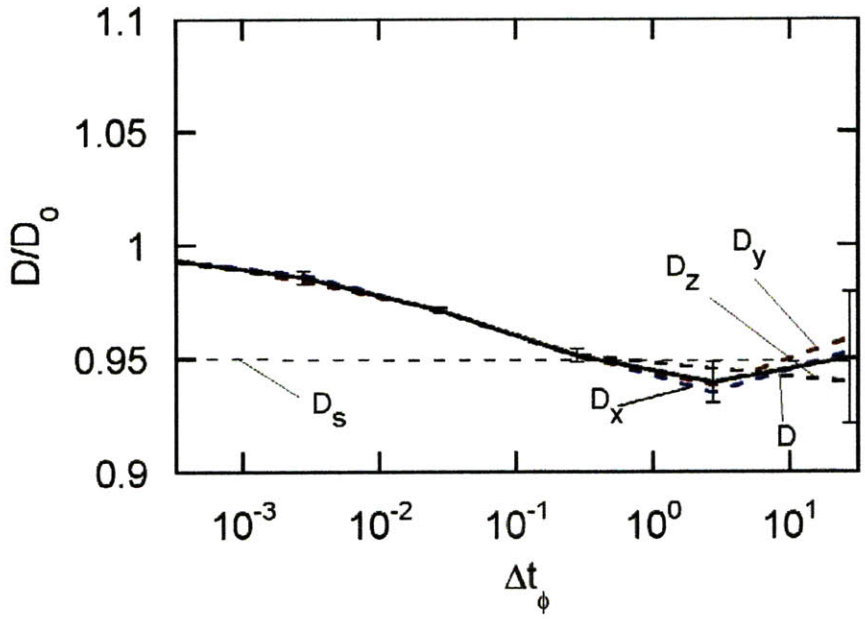

Figure 4-3: Diffusion coefficient decreases with higher non-magnetic particle concentration. The plot shows the diffusion coefficient as a function of sampling time for 30nm non-magnetic particles at 2.5% volume concentration.

Figure 4-3 shows similar results for higher concentration of non-magnetic particles. Higher concentration implies that these particles bump into each other more often restricting their mobility and hence lower diffusion coefficient values. Again, we observe that the results are isotropic. At short sampling times, we see that the effects of concentration are very small. The non-magnetic particles can travel very small distances in short sampling times and hence do not experience the effect of other particles around it. We compare our results with the long time diffusivity values, D^S_∞ obtained from literature, we had discussed previously (Equation (4.21)). The results are in broad agreement within the error bounds of the diffusion coefficient values.

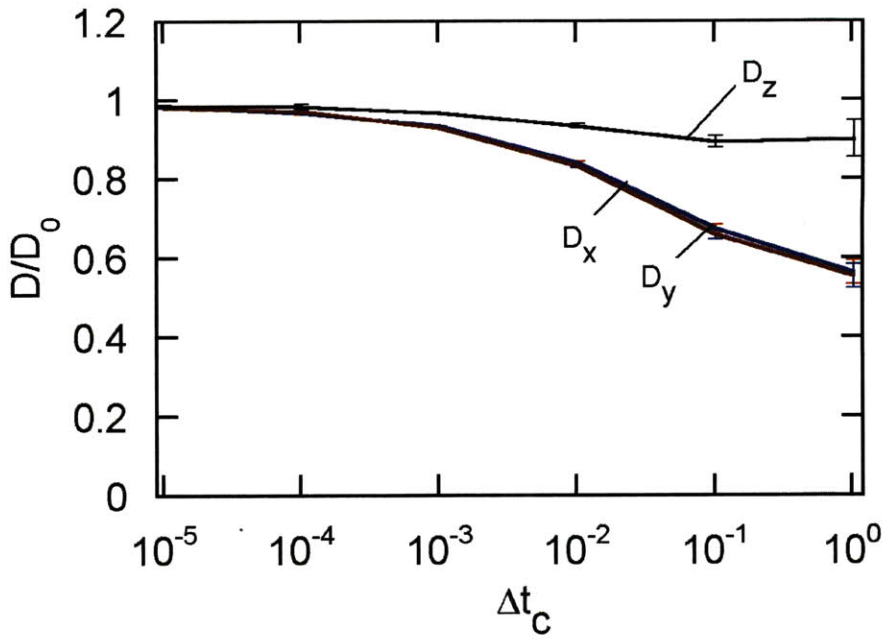

Figure 4-4: Anisotropic diffusion coefficients are observed for 30 nm non-magnetic particles (2.5% by volume) in a suspension of 30 nm magnetic particles (10% by volume) with the magnetic field being applied in the *z*-direction.

4.9.2 Anisotropy in a sample system

A system consisting of 30 nm magnetite particles at 10% volume concentration and 30 nm magnetite particles at 2.5% volume concentration was simulated (Figure 4-4). The particles have a 2 nm surfactant layer on them. The *y*-axis has been made dimensionless using $\Delta\tau_C$, the time required for non-magnetic particles to travel the distance between the magnetic nanoparticle chains:

$$\tau_c = \frac{d_c^{\,2}}{2D} \tag{4.24}$$

Where dc is the distance between chains of magnetic nanoparticles and D is the diffusivity of the non-magnetic particle.

$$\Delta t_c = \frac{\Delta t_s}{\tau_c} \tag{4.25}$$

These magnetite particles have fairly strong inter-particle interactions (λ=24.38) and chain up on application of magnetic fields. A uniform magnetic field was applied along the z-direction, which leads to formation of chain-like structures. Hence, the non-magnetic particles will experience a greater obstruction when diffusing in the x-y plane as compared to the z-direction, since the chains are aligned along the z direction. Again, these effects are non-existent at short time scales, since the diffusing particles do not get to see the effects of the chains. As seen in Figure 4-4, behavior at short times is similar to that of Figure 4-3, but for the long time diffusion coefficients exhibit strong anisotropy. To obtain asymptotic behavior, we need to simulate system with sampling time intervals much higher than the current scheme

4.9.3 Freeze Method

With the current computation scheme it is difficult to go beyond a Δt_c of 1 since it would lead to very long simulation times. Hence, we developed a "freeze method" to evaluate the diffusion for longer sampling times. In this method, the equilibration phase is performed in an identical manner as the usual case. However, during the sampling phase, we freeze the magnetic particles. This is a reasonable because 30 nm magnetic particles form chain-like structures which are fairly rigid and change very little in the course of 10 ms or so during the sampling phase. Hence, during the sampling phase we do not need to evaluate the new co-ordinates for the magnetic particles, thus reducing the computational times. For the system simulated in Figure 4-4, we were able to speed it up by a factor of 5. The results thus obtained are shown in Figure 4-5.

In Figure 4-5, we observe that the freeze method compares very well with the previously discussed regular simulation method. We also notice that freeze method always slightly under-predicts the diffusion constant as compared with the more rigorous method. Since the magnetic particles are not allowed to move, the constraints for the non-magnetic particles become more rigid, hence leading to the lower values for diffusion coefficients. Also, the freeze method will not work for magnetic particles which have low inter-particle interactions, since they will not form chain like structures and will move around in the time scales we would be evaluating the diffusion coefficients.

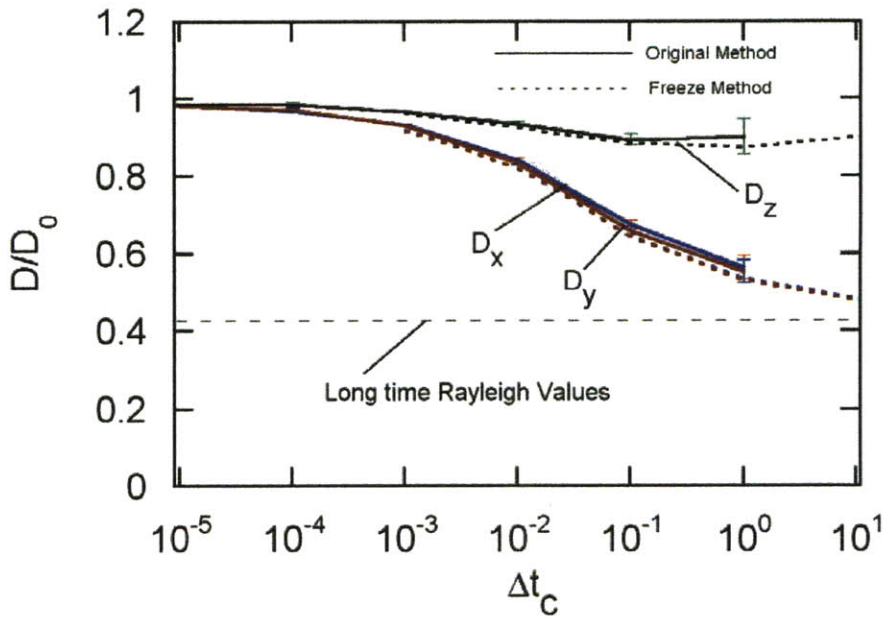

Figure 4-5: Comparing the results obtained from the freeze method (dotted lines) to the regular computation scheme. By using the freeze method we could obtain the data point for Δt_c for one higher magnitude as compared to the regular method.

We had mentioned that we would expect asymptotic behavior for sampling times well in excess of 1. Using this method we were able to obtain the values for the diffusion coefficients for values of Δt_c up to 10. An asymptotic behavior for the diffusion coefficients in the x or the y direction was not fully observed, initiating a need to calculate these constants for higher values of Δt_s. Since the diffusion coefficient is reduced in the perpendicular direction and if the scaling was done with these adjusted diffusion coefficients it would yield a Δt_c of 5. Hence, we expect that we would need to simulate for even larger time intervals to expect asymptotic behavior. However, we were constrained by the computational power we to go any further.

A quantity of interest, the Anisotropy Coefficient, α defined as:

$$\alpha = \frac{D_x + D_y}{2D_z} \tag{4.26}$$

Plotting α for the two methods helps describe the same results as above in a more comprehensive manner and helps compare multiple data on the same plot. In Figure 4-6, we observe that the results obtained from the freeze method and the regular simulation methods are in close agreement with each other.

Also, we try to compare our results for the perpendicular direction by the analytical expressions obtained by Rayleigh in 1892 [8]. Rayleigh calculated expressions for the case of diffusion in a rectangular array of cylinders. We modified the expressions calculated by Rayleigh to include that the diffusing particles in our simulations have a finite size. Since our diffusing particles have the same diameter as those of particle chains, we use twice the diameter in our calculations to account for the excluded volume. The dotted line in Figure 4-5 shows the long time diffusion values calculated for the parameters used in our simulations. Again, in our case we do not have perfect rectangular array of cylinders, but this result does give us benchmark values which is broadly in agreement with our simulations. Another set of results is to compare our results is the anisotropy coefficient obtained by Phillips [7]. The coefficients, so obtained were fairly similar to that obtained by Rayleigh, but slightly lower (of the order of 10%), since they include for the hydrodynamic interactions among the particles.

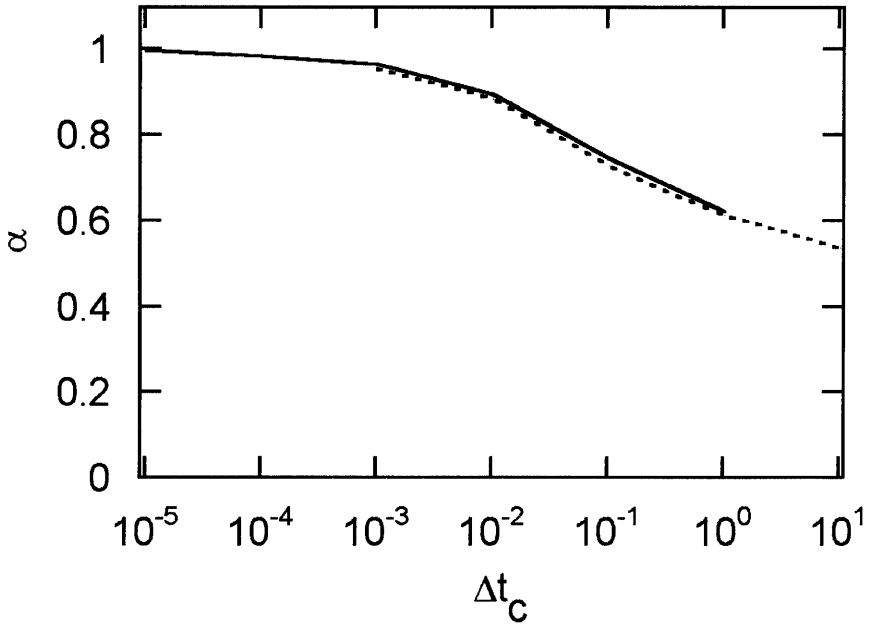

Figure 4-6: Anisotropic coefficient, α as a function of sampling time interval. The solid line represents the data shown in Figure 4-4, while the dotted line shows the data from the freeze method (Figure 4-5)

4.9.4 Anisotropy as a function of magnetic particle concentration

Anisotropy coefficient decreases with increasing magnetic particle concentration, as shown in Figure 4-7. As the concentration of the magnetic particles increases, there are more chain-like structures present in the system. The constraints the chains have on the non-magnetic particles in direction perpendicular to the magnetic field, leads to a decrease in their mobility and hence the diffusion coefficients in the perpendicular direction. On the other hand the mobility in the direction parallel to the chains is only marginally affected, leading to a decrease in the anisotropy coefficient. We have also compared the anisotropy with the long time diffusion coefficients calculated using Rayleigh's method.

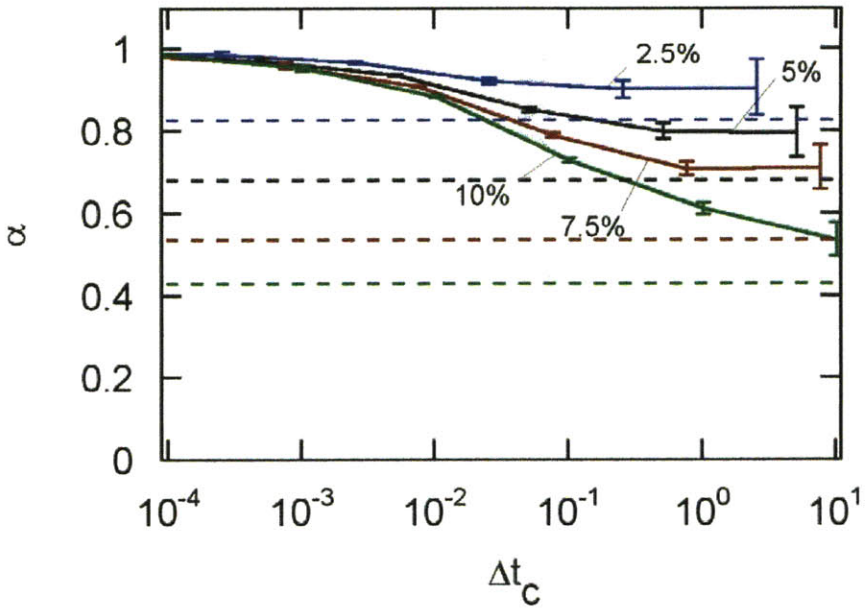

Figure 4-7: Anisotropy coefficient, α decrease with increasing magnetic particle concentration (by volume). The dotted lines represent the long time diffusion coefficients calculated using Rayleigh's method as described before. Magnetic and non-magnetic particles simulated are both 30 nm in diameter. The concentration of non-magnetic particles is 2.5% by volume..

4.9.5 Anisotropy as a function of magnetic particle size

Variation of the anisotropy coefficient with magnetic particle size shows a very interesting behavior (Figure 4-8). We simulated similar systems with magnetic particles with the same size as that of non-magnetic particles. The concentration for magnetic particles was 10% while that of non-magnetic particles was 2.5% by volume. The magnetic particles considered were 10 nm (λ=0.48), 20 nm (λ=6.09) and 30 nm (λ=24.38) in diameter. We did not use the freeze method for the following simulations because the magnetic particles for the 10 nm particles do not form chain like rigid structures but tend to move around the simulation box. Also, we need to take smaller simulation time steps because the mobility of smaller particles, either magnetic or non magnetic is higher. Large time steps can lead to overlaps between particles and hence erroneous results.

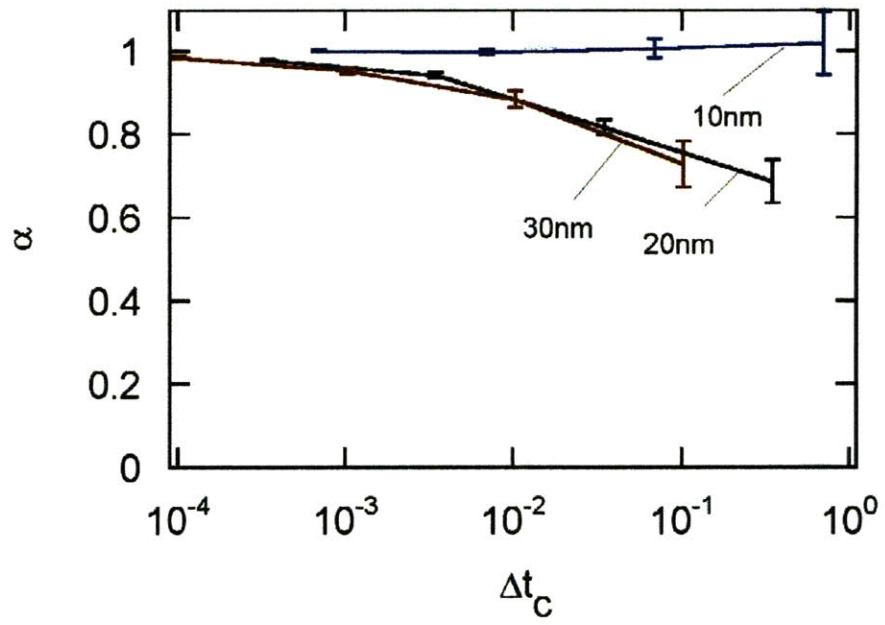

Figure 4-8: Variation of anisotropy coefficient with the sampling time for different sized magnetic particles. The non-magnetic particles are taken to be the same size as that of magnetic particles. The volume fractions are 2.5% for the non-magnetic particles and 10% for all the magnetic particles.

For 10 nm particles the inter particle magnetic interactions are weak. When a magnetic field is applied we do not observe the formation of any chain-like structures. Hence, for the 10 nm particles the anisotropy coefficient is close to 1. On comparing the results obtained for 30 nm particles and 20 nm particles, we observe that there is a strong chain formation for both the systems. In other words, the systems look very similar to each other, with a difference in scale. Hence, the anisotropic coefficient for both the systems are very similar and the anisotropy curves almost overlap on each other. This argument can be further extended to say that anisotropy curves for particles larger than 20 nm will overlap on each other.

4.9.6 Anisotropy as a function of non-magnetic particle size

Anisotropy coefficient decreases with an increase in the size of non-magnetic particles. The plot shown in Figure 4-9 depicts this behavior for a system with 30 nm magnetic particles at 10% volume concentration and varying non magnetic particle size. Small non magnetic particles tend to navigate themselves around the chains a lot easier as compared to larger particles. For the given system, the separation between the chains is a little less than 100 nm. Hence, we see that the 60 nm non-magnetic particles face a lot of constraint while passing through the magnetic particle chains in the direction perpendicular to the magnetic field leading to lower anisotropy coefficients for larger particles.

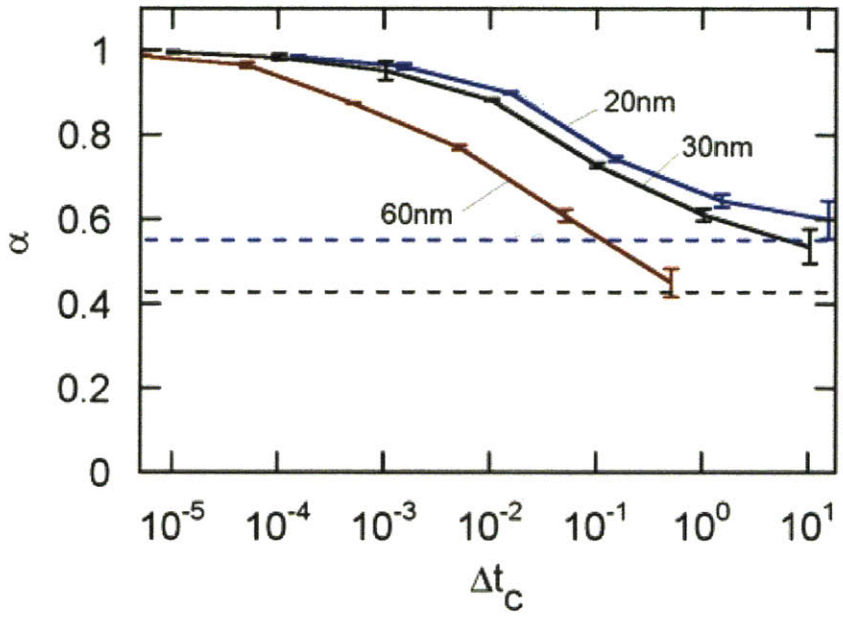

Figure 4-9: Variation of anisotropy coefficient with the sampling time for different sizes of non-magnetic particles. The magnetic particles were 30 nm in diameter and 10% in volume concentration. All systems had the same number concentration for non-magnetic particles, corresponding to 2.5% volume fraction for the 30 nm non-magnetic particles

4.10 Conclusions

Understanding the transport behavior of non-magnetic species is important in design of separation and other devices employing magnetic fluids. Magnetic fluids have a unique property that their structure can be reversibly altered by application and removal of an externally applied magnetic field. Different applications can utilize the anisotropic transport properties induced by the structural arrangement of magnetic nanoparticles. In this work, we have successfully designed computational tools to evaluate the diffusion coefficient of non-magnetic particles in magnetic fluids. The evaluated diffusion coefficient will be used in developing macroscopic models for such devices. Also, a systematic study on parameters such as particle size, surfactant thickness, and particle concentrations would help us design suitable magnetic fluids for the corresponding applications.

We have explored the diffusion characteristics of non-magnetic particles in magnetic fluids using Brownian Dynamics simulation. The diffusion coefficients were evaluated as a function of sampling time intervals. To evaluate long time diffusion coefficients, we have developed a new 'freeze method' for our simulations. Also, runs with non-magnetic particles only were compared with previous theoretical works.

We observed that the diffusion coefficients in the direction perpendicular to the magnetic field were lower than that in the direction parallel to magnetic field, due to the formation of chain like structures by the magnetic nanoparticles. The anisotropy was stronger for magnetic fluids with higher volume fraction for the magnetic nanoparticles. The results were at large in correspondence with the long time anisotropic values evaluated for diffusion across cylinders evaluated by Rayleigh. Larger non-magnetic particles tend to have a higher anisotropic coefficient, since they find the motion across the chains to be more constrained. Anisotropy coefficient was close to 1, for smaller magnetic particles which do not chain when a magnetic field is applied. For similar systems having magnetic nanoparticles larger than 20 nm in size, the anisotropy curves are very similar each other, since the inter-particle magnetic forces are sufficiently higher than thermal forces for the magnetic particles making them fairly similar in the structural arrangement.

Also, the anisotropic coefficients for particles larger than 20 nm were much less than one, emphasizing the need to evaluate the diffusion coefficients for the different directions when developing macroscopic models for separation devices. This work was limited to presence of strong magnetic fields, but can be further extended to low magnetic fields by including appropriate magnetic relaxation mechanisms for the magnetic nanoparticles. We also neglected hydrodynamic interactions between the particles. These interactions should also be included to simulate a more realistic behavior.

4.11 Bibliography

1. Rallison, J.M., *Brownian Diffusion In Concentrated Suspensions Of Interacting Particles.* Journal Of Fluid Mechanics, 1988. **186**: p. 471-500.

2. Guzowski, J., Cichocki, B., Wajnryb, E., and Abade, G.C., *The short-time self-diffusion coefficient of a sphere in a suspension of rigid rods.* Journal Of Chemical Physics, 2008. **128**(9).

3. Kang, K., Gapinski, J., Lettinga, M.P., Buitenhuis, J., Meier, G., Ratajczyk, M., Dhont, J.K.G., and Patkowski, A., *Diffusion of spheres in crowded suspensions of rods.* Journal Of Chemical Physics, 2005. **122**(4).

4. Kang, K., Wilk, A., Patkowski, A., and Dhont, J.K.G., *Diffusion of spheres in isotropic and nematic networks of rods: Electrostatic interactions and hydrodynamic screening.* Journal Of Chemical Physics, 2007. **126**(21).

5. Kluijtmans, S., Koenderink, G.H., and Philipse, A.P., *Self-diffusion and sedimentation of tracer spheres in (semi)dilute dispersions of rigid colloidal rods.* Physical Review E, 2000. **61**(1): p. 626-636.

6. Cavicchi, K.A. and Lodge, T.P., *Anisotropic self-diffusion in block copolymer cylinders.* Macromolecules, 2004. **37**(16): p. 6004-6012.

7. Phillips, R.J., Deen, W.M., and Brady, J.F., *Hindered Transport Of Spherical Macromolecules In Fibrous Membranes And Gels.* Aiche Journal, 1989. **35**(11): p. 1761-1769.

8. Rayleigh, J.W., *On the Influence of Obstacles Arranged in Rectangular Order upon the Properties of a Medium.* Phil. Mag, 1892. **5**(34): p. 481-502.

9. Vangunsteren, W.F. and Berendsen, H.J.C., *Algorithms For Brownian Dynamics.* Molecular Physics, 1982. **45**(3): p. 637-647.

10. Rudisill, J.W. and Cummings, P.T., *Brownian Dynamics Simulation Of Model Polymer Fluids In Shear-Flow.1. Dumbbell Models.* Journal Of Non-Newtonian Fluid Mechanics, 1992. **41**(3): p. 275-288.

11. Allen, M.P. and Tildesley, D.J., *Computer Simulation of Liquids*. 1987: Oxford Science Publications.

12. Lellig, C., Wagner, J., Hempelmann, R., Keller, S., Lumma, D., and Hartl, W., *Self-diffusion of rodlike and spherical particles in a matrix of charged colloidal spheres: A comparison between fluorescence recovery after photobleaching and fluorescence correlation spectroscopy.* Journal Of Chemical Physics, 2004. **121**(14): p. 7022-7029.

13. Chen, J.C. and Kim, A.S., *Brownian Dynamics, Molecular Dynamics, and Monte Carlo modeling of colloidal systems.* Advances in Colloid and Interface Science, 2004. **112**(1-3): p. 159.

14. Branka, A.C. and Heyes, D.M., *Algorithms for Brownian dynamics simulation.* Physical Review E, 1998. **58**(2): p. 2611-2615.

15. Ermak, D.L. and McCammon, J.A., *Brownian Dynamics With Hydrodynamic Interactions.* Journal Of Chemical Physics, 1978. **69**(4): p. 1352-1360.

16. Ermak, D.L., *Computer-Simulation Of Charged-Particles In Solution.1. Technique And Equilibrium Properties.* Journal Of Chemical Physics, 1975. **62**(10): p. 4189-4196.

17. Heyes, D.M. and Branka, A.C., *More efficient Brownian dynamics algorithms.* Molecular Physics, 2000. **98**(23): p. 1949-1960.

18. Helfand, E., *Brownian Dynamics Study Of Transitions In A Polymer-Chain Of Bistable Oscillators.* Journal Of Chemical Physics, 1978. **69**(3): p. 1010-1018.

19. Honeycutt, R.L., *Stochastic Runge-Kutta Algorithms.1. White-Noise.* Physical Review A, 1992. **45**(2): p. 600-603.

20. White, T.O., Ciccotti, G., and Hansen, J.P., *Brownian dynamics with constraints.* Molecular Physics, 2001. **99**(24): p. 2023-2036.

21. Abe, Y., Ayik, S., Reinhard, P.G., and Suraud, E., *On stochastic approaches of nuclear dynamics.* Physics Reports-Review Section Of Physics Letters, 1996. **275**(2-3): p. 49-196.

22. Iniesta, A. and Delatorre, J.G., *A 2nd-Order Algorithm For The Simulation Of The Brownian Dynamics Of Macromolecular Models.* Journal Of Chemical Physics, 1990. **92**(3): p. 2015-2018.

23. Verlet, L., *Computer "Experiments" on Classical Fluids. I. Thermodynamical Properties of Lennard-Jones Molecules.* Physical Review, 1967. **159**(1): p. 98.

24. Verlet, L., *Computer "Experiments" on Classical Fluids. II. Equilibrium Correlation Functions.* Physical Review, 1968. **165**(1): p. 201.

25. Allen, M.P., *Brownian Dynamics Simulation Of A Chemical-Reaction In Solution.* Molecular Physics, 1980. **40**(5): p. 1073-1087.

26. Allen, M.P., *Algorithms For Brownian Dynamics.* Molecular Physics, 1982. **47**(3): p. 599-601.

27. Turq, P., Lantelme, F., and Levesque, D., *Transport Properties And The Time Evolution Of Electrolyte-Solutions In The Brownian Dynamics Approximation.* Molecular Physics, 1979. **37**(1): p. 223-236.

28. Satoh, A., Chantrell, R.W., Coverdale, G.N., and Kamiyama, S., *Stokesian dynamics simulations of ferromagnetic colloidal dispersions in a simple shear flow.* Journal Of Colloid And Interface Science, 1998. **203**(2): p. 233-248.

29. Cichocki, B. and Hinsen, K., *Dynamic Computer-Simulation Of Concentrated Hard-Sphere Suspensions.1. Simulation Technique And Mean-Square Displacement Data.* Physica A, 1990. **166**(3): p. 473-491.

30. Schaertl, W. and Sillescu, H., *Brownian Dynamics Simulations Of Colloidal Hard-Spheres - Effects Of Sample Dimensionality Of Self-Diffusion.* Journal Of Statistical Physics, 1994. **74**(3-4): p. 687-703.

31. Strating, P., *Brownian dynamics simulation of a hard-sphere suspension.* Physical Review E, 1999. **59**(2): p. 2175-2187.

32. Lekkerkerker, H.N.W. and Dhont, J.K.G., *On The Calculation Of The Self-Diffusion Coefficient Of Interacting Brownian Particles.* Journal Of Chemical Physics, 1984. **80**(11): p. 5790-5792.

33. Rallison, J.M. and Hinch, E.J., *The Effect Of Particle Interactions On Dynamic Light-Scattering From A Dilute Suspension.* Journal Of Fluid Mechanics, 1986. **167**: p. 131-168.

34. Pusey, P.N., *Intensity Fluctuation Spectroscopy Of Charged Brownian Particles - Coherent Scattering Function.* Journal Of Physics A-Mathematical And General, 1978. **11**(1): p. 119-135.

35. Pusey, P.N., *Dynamics Of Interacting Brownian Particles.* Journal Of Physics A-Mathematical And General, 1975. **8**(9): p. 1433-1440.

36. Cichocki, B. and Felderhof, B.U., *Time-Dependent Self-Diffusion Coefficient Of Interacting Brownian Particles.* Physical Review A, 1991. **44**(10): p. 6551-6558.

37. Batchelor, G.K., *Brownian Diffusion Of Particles With Hydrodynamic Interaction.* Journal Of Fluid Mechanics, 1976. **74**(MAR9): p. 1-29.

38. Batchelor, G.K., *Diffusion In A Dilute Polydisperse System Of Interacting Spheres.* Journal Of Fluid Mechanics, 1983. **131**(JUN): p. 155-175.

39. Ackerson, B.J. and Fleishman, L., *Correlations For Dilute Hard-Core Suspensions.* Journal Of Chemical Physics, 1982. **76**(5): p. 2675-2679.

40. Jones, R.B. and Alavi, F.N., *Rotational Diffusion Of A Tracer Colloid Particle.4. Brownian Dynamics With Wall Effects.* Physica A, 1992. **187**(3-4): p. 436-455.

41. Marqusee, J.A. and Deutch, J.M., *Concentration-Dependence Of The Self-Diffusion Coefficient.* Journal Of Chemical Physics, 1980. **73**(10): p. 5396-5397.

42. Tough, R.J.A., *Self-Diffusion In A Suspension Of Interacting Brownian Particles.* Molecular Physics, 1982. **46**(3): p. 465-474.

43. Hanna, S., Hess, W., and Klein, R., *Self-Diffusion Of Spherical Brownian Particles With Hard-Core Interaction.* Physica A, 1982. **111**(1-2): p. 181-199.

44. Mendenhall, W., Wackerly, D.D., and Scheaffer, R.L., *Mathematical Statistics with Applications*. 1990: PWS-Kent Publishing Company.

45. Rosensweig, R.E., *Ferrohydrodynamics*. 1985: Cambridge University Press: Cambridge.

46. Kubo, R., *The fluctuation-dissipation theorem.* Reports on Progress in Physics, 1966(1): p. 255.

Chapter 5

5. Neel relaxation of magnetic particle clusters

5.1 Introduction

Magnetic fluids have been employed in adsorptive non-magnetic particle separations[1-5]. One of the challenges one faces in the design of magnetic nanoparticles is that the particles should be large enough so that they get trapped in the High Gradient Magnetic Separation (HGMS) column [6, 7] in separation phase, yet should be easily removed in the elution phase when the magnetic field is switched off. In other words, they should have high net magnetic moment, but should have small relaxation times. Ditsch [2, 8] has used magnetic nanoparticle clusters to achieve the same effect. Having multiple smaller (8-10 nm) particles in the cluster ensures that the clusters are entrapped in the HGMS column, yet are removed easily when the magnetic field is removed. The objective of this work is to study the relaxation of magnetic nanoparticle clusters. A better understanding of the relaxation will help us design, tailor and synthesize magnetic nanoparticle clusters which will have optimal properties for magnetic separations.

5.2 Relaxation mechanisms for magnetic nanoparticles

Studies have been performed on relaxation of magnetic nanoparticles in ferrofluids [9-13]. There are two basic mechanisms by which the colloidal ferrofluid can relax when the applied magnetic field is changed: Brownian and Néel relaxation. Brownian relaxation refers to the bulk rotational diffusion of the particle while Néel relaxation refers to the

rotation of internal magnetization vector or the magnetic domain of the magnetic particle [14].

The Brownian rotational diffusion time, τ_B having a hydrodynamic origin was calculated by Frenkel [15] to be:

$$\tau_B = \frac{3V\eta_0}{k_B T} \tag{5.1}$$

where V is the particle volume, η_0 is the viscosity of carrier liquid, k_B is the Boltzmann's constant and T is the temperature of the system. Néel relaxation is caused by reorientation of the magnetization vector by overcoming an energy barrier [16]. The magnetic moment of the particles also have preferred orientations, called the 'easy axis' of magnetization. The easy axis of magnetization arises from a combination of shape and magnetocrystalline anisotropy [17]. For example, a sphere of magnetite, there would be six easy directions of magnetization.

The energy barrier between the two opposite orientations is given by $K_{eff}V$, where K_{eff} is the anisotropy constant of the material. When $k_B T \gg K_{eff} V$, the thermal energy is large enough to overcome the energy barrier. The characteristic Néel relaxation time, τ_N inside a single grain is given by:

$$\tau_N = \frac{1}{f_0} e^{\frac{K_{eff}V}{k_B T}} \tag{5.2}$$

where f_0 is the frequency having an approximate value of 10^9 Hz.

Normally, both Brownian and Néel mechanisms contribute to the relaxation of the magnetic nanoparticles. The effective relaxation time, τ_{eff} for the particles can be calculated to be [10]

$$\tau_{eff} = \frac{\tau_N \tau_B}{\tau_N + \tau_B} \tag{5.3}$$

In case $\tau_N \ll \tau_B$, or if the rotation is inhibited (freezing/drying of sample, or formation of large agglomerates, relaxation occurs by Néel mechanism and the process is called intrinsic superparamagnetism. However, when $\tau_N \gg \tau_B$, Brownian motion is primarily responsible for relaxation and the material exhibits extrinsic superparamagnetism. In general, Néel relaxation dominates for smaller particles while Brownian relaxation dominates for larger particles. For magnetite, this transition occurs around a particle diameter of 10 nm [14]. Particles with relaxation times faster than the measurement time are referred to as superparamagnetic. Both Néel and Brownian relaxation can be described as exponential decays for identical particles, but for real systems it is usually non-exponential because of the distribution of sizes and shapes of the particles.

In our model, we assume a simplistic case in which all orientations would have an equal probability. In other words, we ignore the easy axis of magnetization. Our interest lies in qualitative understanding of relaxation behavior of magnetic cluster based on their size, arrangement configurations and geometry. We have studied the effect the magnetic inter-particle interactions play on the relaxation time of these clusters.

5.3 Simulation methodology

Rotational Brownian Dynamics simulations are used to describe the time evolution of the orientation distributions of particles [18]. These simulations are frequently used to study the relaxation effects in a variety of systems such as liquid crystals [19, 20], ferromagnetic colloidal dispersions [21, 22], quantum spin systems [23], etc. Dickinson [24, 25] studied the effect of translational motion on the rotational Brownian motion. In our work, we consider the magnetic particle clusters to be stationary (no translational motion) and hence we consider only the pure rotational movement of the magnetic domains.

The rotational motion expressed in the Langevin equation can be written as:

$$I_i \frac{d\omega_i}{dt} = -\zeta_R \omega_i + T_i + R_i \tag{5.4}$$

where i ($1 \le i \le 3N$), labels the particle number and the three axis (x,y, and z) in an N particle system. I_i is the moment of inertia associated with index i, T_i is the sum of external and interparticle torques, ω_i is the angular velocity, and R_i is the stochastic force acting in direction i.

Using the above equation, we can evaluate the angular time step in a given time interval Δt by [24, 25]

$$\varphi_i - \varphi_i^0 = (k_B T)^{-1} D_i^R T_i \Delta t + R_i\left(D_i^R, \Delta t\right) \tag{5.5}$$

Where D_i^R is the rotational diffusion coefficient, k_B is the Boltzmann's constant and T is the temperature of the system. The Brownian displacement force can be related to the rotational diffusion coefficient as

$$\left\langle R_i(0) R_j(t) \right\rangle = 2 D_i^R \Delta t \delta_{ij} \tag{5.6}$$

Now the rotational diffusion coefficient can be related to the Brownian relaxation time by the following relationship

$$D^R = \frac{1}{2\tau_B} \tag{5.7}$$

However, in our system we do not allow the physical rotation of the particles or particle clusters, but just the rotation of the magnetic domains resulting in Néel relaxation. Hence, we just use the same system of equations as above with an effective diffusion rotation coefficient of

$$D^R{}_{eff} = \frac{1}{2\tau_N} \tag{5.8}$$

For the above simulation the time step, Δt_s was restricted by the condition, $\Delta t_s \ll \tau_N$. This condition ensures that the systematic forces, magnetic torque in our case do not change appreciable over the give time step. We have used a time step of $\tau_N / 100$ for all our simulations.

5.4 Torque Models

The torque acting on a magnetic dipole due to an external magnetic field $\boldsymbol{H}$ is

$$\boldsymbol{T} = \boldsymbol{m} \times \boldsymbol{H} \tag{5.9}$$

Here the magnetic dipole moment m is defined as

$$m = |\boldsymbol{m}| = \mu_0 M_s V \tag{5.10}$$

in which μ_0 is the permeability of free space, M_s is the saturation magnetization of the material and V is the volume of the magnetic particle. To derive the torque acting on a particle α due to magnetic field from a particle β, we have

$$\boldsymbol{T}_{\alpha\beta} = \boldsymbol{m}_\alpha \times \boldsymbol{H}_\beta \tag{5.11}$$

The magnetic field, $\boldsymbol{H}_\beta$ originating from a dipole is

$$\boldsymbol{H}_\beta = \frac{3(\boldsymbol{m}_\beta \cdot \boldsymbol{t})\boldsymbol{t} - \boldsymbol{m}_\beta}{4\pi\mu_0 r^3} \tag{5.12}$$

On grouping m can be written as:

$$\boldsymbol{H}_\beta = \frac{3m}{4\pi\mu_0 r^3}\left[(\boldsymbol{n}_\beta \cdot \boldsymbol{t})\boldsymbol{t} - \boldsymbol{n}_\beta\right] \tag{5.13}$$

in which $\boldsymbol{n}_\beta$ is the unit vector denoted in the direction of the magnetic moment $\boldsymbol{m}_\beta$, $\boldsymbol{t}$ is the unit vector given by $\boldsymbol{r}/r$, where $\boldsymbol{r}$ is the position vector of the co-ordinates at which the field being measured with the centre of dipole being the origin and r is the magnitude of the position vector. So the torque on particle α due to the particle β, $\boldsymbol{T}_{\alpha\beta}$ can be written as:

$$\boldsymbol{T}_{\alpha\beta} = \frac{m^2}{4\pi\mu_0 r^3}\left(\boldsymbol{n}_\alpha \times \left[3(\boldsymbol{n}_\beta . \boldsymbol{t}_{a\beta})\boldsymbol{t}_{a\beta} - \boldsymbol{n}_\beta\right]\right) \tag{5.14}$$

$$\boldsymbol{T}_{\alpha\beta} = -\frac{m^2}{4\pi\mu_0 r^3}\left(\boldsymbol{n}_\alpha \times \boldsymbol{n}_\beta - 3(\boldsymbol{n}_\beta . \boldsymbol{t}_{a\beta})(\boldsymbol{n}_\alpha \times \boldsymbol{t}_{a\beta})\right) \tag{5.15}$$

It is also important to note that this torque vector is not symmetric. In other words $\boldsymbol{T}_{\alpha\beta}$ is not identical to $\boldsymbol{T}_{\beta\alpha}$.

5.5 Simulation parameters and details

We carried out 10,000 parallel simulations to generate reasonable statistics about the relaxation behavior. In all the simulations we start an initial configuration with all the dipoles aligned along the z-axis at time t=0 and we allow them to relax thereafter, with or without a remnant magnetization field. The simulations are carried out a room temperature of 298K. Also, it is assumed that the particles are single domain, which is considerably fair for the particle size range simulated. We measure the magnetization of the particles over the simulated ensemble as a function of time. The two primary structures we start with are chains and spheres as shown in Figure 5-1. The reason we simulate these shapes is because they are commonly observed in magnetic fluids. For larger magnetic particles chain-like structures are stable and frequently observed. The parameters that we vary are the size of the cluster, the size of the individual nanoparticles, and the structural arrangement. The simulations have been carried out for the magnetite as the material for the particles, but can be easily repeated for other magnetic materials, such as cobalt.

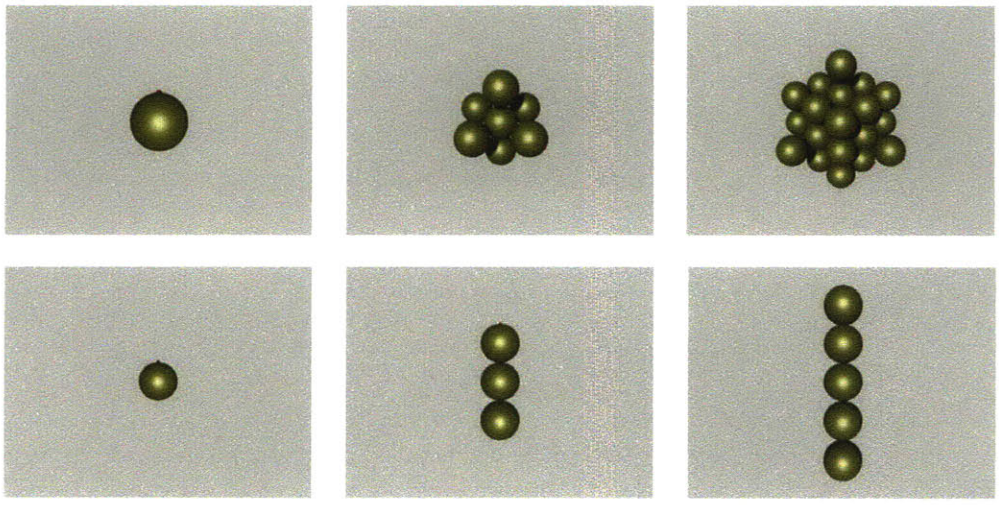

Figure 5-1: Sample structural configurations simulated: Top row shows spherical clusters (n=1, 7, 33). Bottom row shows chain like structures (n=1, 3, 5).

5.6 Results

5.6.1 Chain-like clusters: effect of chain length

In our first set of simulations, we have captured the relaxation behavior of chain like magnetic nanoparticle clusters on removal of magnetic field which was originally applied along the z-axis. The clusters are composed of 10 nm magnetite particles of varying chain lengths. The normalized magnetization, m_{dim} is defined as

$$m_{\text{dim}} = \langle \cos\theta \rangle \tag{5.16}$$

in which θ is the angle the dipole makes with the z axis and $\langle ... \rangle$ represents the ensemble average. The dimensionless time, t_{dim} is defined as:

$$t_{\text{dim}} = \frac{t}{\tau_N} \tag{5.17}$$

in which τ_N is the characteristic relaxation time for a single isolated particle of the same diameter. In the results shown in Figure 5-2 it would be the relaxation time for a 10 nm particle.

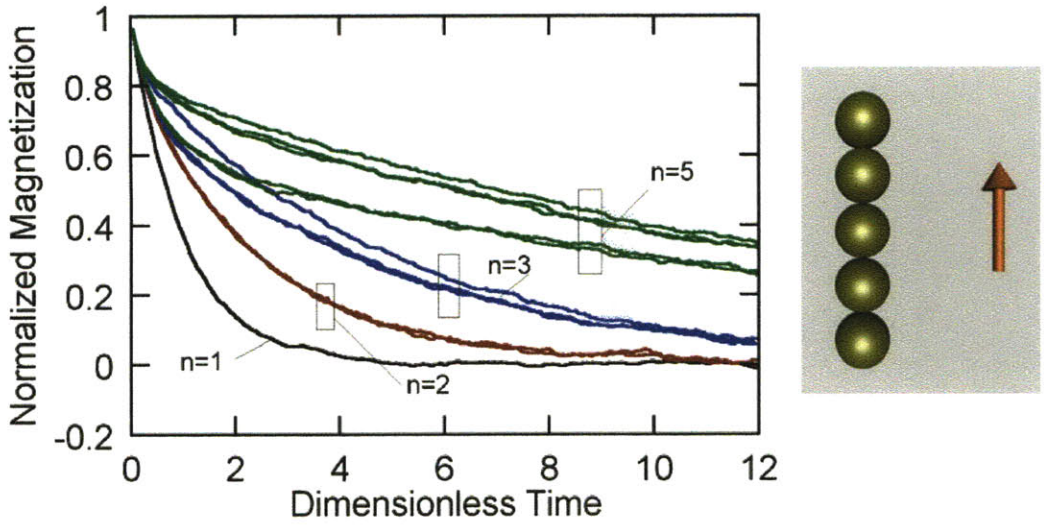

Figure 5-2: Relaxation dynamics of individual particles in cluster chains on removal of magnetic field (at time t=0). The labels 'n' represent the number of particles in cluster chains. The arrow next to cluster indicates the direction of initially applied external magnetic field.

The single particle cluster (n=1) relaxes exponentially with a characteristic time of τ_N as expected, shown in Figure 5-2. For the two particle cluster, the relaxation is slower than compared to an isolated single particle. This is because both the particles are in a stable configuration aligned in the direction of initial applied field. Also, they exhibit identical relaxation behavior because they have the same spatial configuration. Observing the three particle chain cluster, the relaxation is even slower than the two particle cluster. Also, here we see two distinct relaxation curves. One is for the particles on the outside and the other is for the particle in the centre. The relaxation for the particle in the centre is slower than the particles on the outside, since it is stabilized by two dipoles right next to it (one above and one below). The particles on the outside have only one immediate neighbor and a particle two diameters away leading to a lower stabilization and faster relaxation as compared to the particle in the middle. Similarly in the five particle cluster chain we see three distinct modes, one for the particles on the outside, one for particle in the absolute center and one for the particles in between.

Another interesting behavior is that the initial relaxation behavior may not determine the final relaxation behavior. If we compare the relaxation of the particle in the centre of the three particle cluster to that of the particles on the outside of the five particle cluster, we see that initially the five particle cluster end particles relaxes faster than the center particle of the cluster. However, the final relaxation is slower for the central particle in the three chain particle cluster. To understand it, let's try to consider the inter-particle interactions. The central particle in the three chain particle cluster interacts with the outer particles in the three particle cluster, which relax faster and have lower magnetization, also bringing the magnetization down for the central particle. However, the outer particles in the five particle cluster interact with the inner particles, which have relaxed slower and have higher magnetization, leading to an increased magnetization and slower relaxation for outside particles of the five particle cluster.

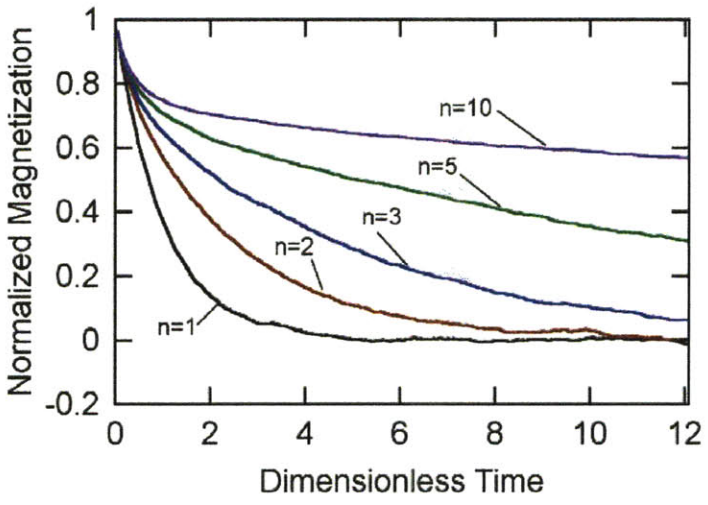

Figure 5-3: Relaxation behavior of magnetic chains averaged over all the particles. '*n*' represents the number of individual particles in the chains.

Figure 5-3 plots the average magnetization of particle clusters against dimensionless time. The averaging is done over all the particles in a given cluster. We see that the relaxation times are a strong function of the cluster size. The more the number of particles in the chain, greater is the stabilization and slower the relaxation. This means

that in order to design clusters for efficient separations they should not be preferably in linear shapes, which will lead to difficulties in the elution step of the separation.

5.6.2 Chain-like structures: effect of particle size

We also studied the effect of particle size on the relaxation times of magnetic particle clusters in chain forms as shown in Figure 5-4. We observe that the dimensionless relaxation times for the clusters are a very strong function of particle size, since inter-particle interactions vary as the third power of diameter of the particle. For 6 nm particles (Figure 5-4a), the relaxation behavior for a 10 particle cluster is very similar to the relaxation characteristic for an individual particle. However, for larger particles the relaxation becomes a lot slower as when compared to the behavior of a single particle. Observing it for the 12 nm particles (Figure 5-4d), the relaxation time for the 10 particle chain is order of magnitudes slower than that of the individual particle. Hence, if we expect a system to have long magnetic nanoparticle chains, the size of the individual particles should be maintained below 8 nm for elution step to be effective.

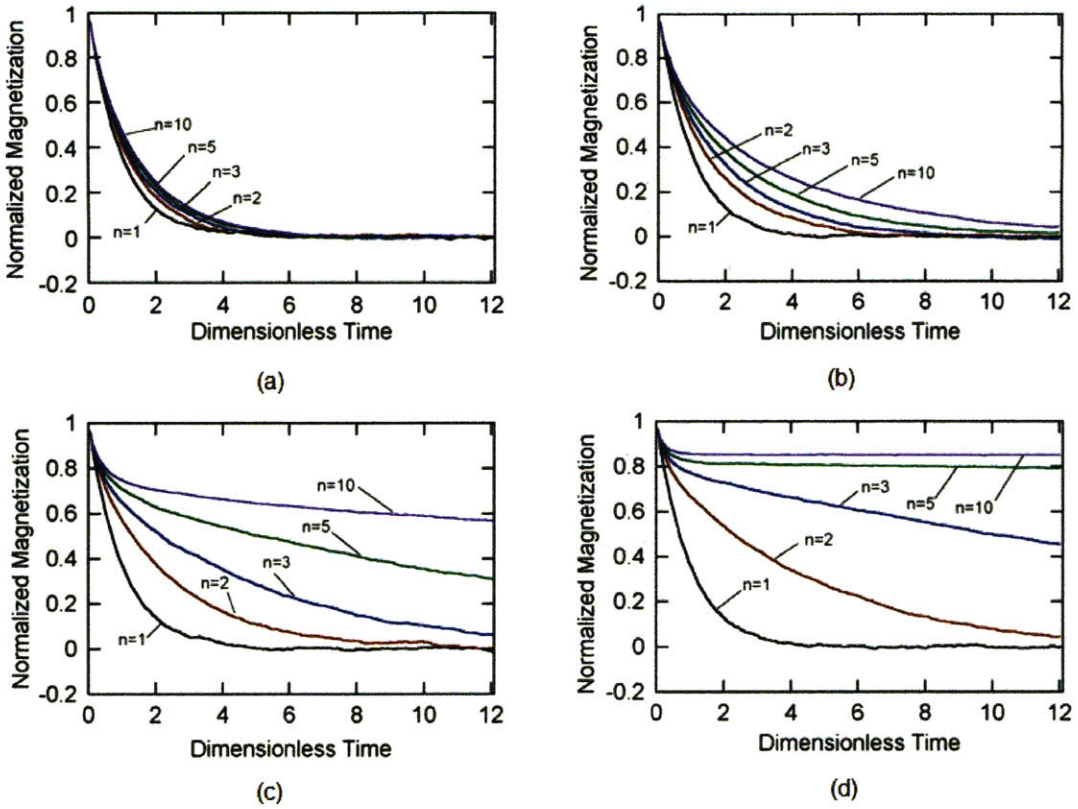

Figure 5-4: Relaxation behavior of magnetic chains with individual particle size of 6nm (a), 8nm (b), 10nm (c) and 12nm (d). '*n*' represents the number of individual particles in the chains.

5.6.3 Spherical clusters

The relaxation behavior of spherical clusters is very similar to that of the individual particles themselves as shown in Figure 5-5. Even on increasing the cluster size to 33 particles, we do not see any appreciable change in the relaxation times. This is a result of the arrangement or the packing of the clusters. If we observe an individual particle, it has a couple of particles present directly above and below it which provide a stabilizing force while the four particles around its equatorial plane, provide a destabilizing force. These stabilizing and destabilizing forces negate each other, providing a relaxation behavior very similar to that of individual particles. Comparing the result for 10 nm particles in spherical and linear arrangement, we see that the relaxation of spherical clusters is orders

of magnitude faster that linear clusters. Hence, spherical clusters would be more efficient in the elution step as compared to linear clusters.

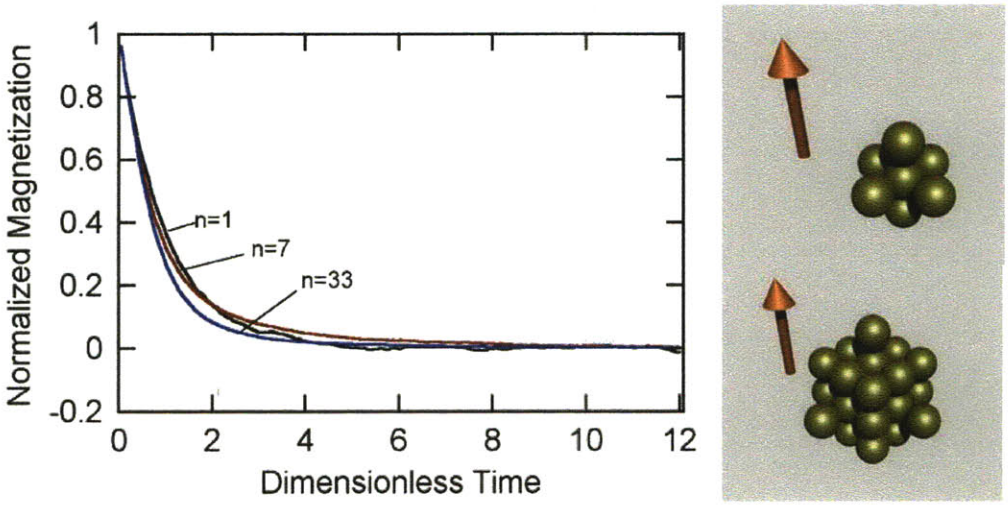

Figure 5-5: Relaxation behavior of spherical cluster consisting of 1 (n=1), 2 (n=7) and 3 (n=33) layers of 10 nm particles. The pictures on the right show the arrangement of the particles in the cluster for 7 and 33 particles respectively.

5.6.4 Planar structures: Orientation

To understand how the effect of particles in different configuration affect the relaxation behavior we have performed a study for planar structures parallel and perpendicular to the initially applied external magnetic field, shown by the arrows in Figure 5-6. The planar structures are of interest to us because they are frequently observed on the wires in HGMS columns. For the rectangular perpendicular arrangement (top right hand corner in Figure 5-6), the relaxation is much faster as compared to an individual particle. Since the particles are present in the equatorial plane of one another, they provide a destabilizing force to each other, leading to faster relaxation. Looking at the situation when the plane of magnetic particles is parallel to the initially applied external magnetic field (bottom right hand corner in Figure 5-6), the relaxation is slower than that of individual particles since the particles present above and below each other prevent a stabilizing force. However, on comparing this result with chain like structures of similar length, we observe this relaxation is still faster. One can visualize this structure to as that of multiple

chains sitting alongside each other. Though the particles in chains by themselves provide a stabilizing force, the presence of chains alongside each other is energetically unfavorable. We also compare the results for different sized clusters, n=25 and n=100 to understand the significance of edge effects. For the perpendicular arrangement, we observe that for 100 particles the relaxation is a little faster than for 25 particles, while for the parallel arrangement it is slightly slower.

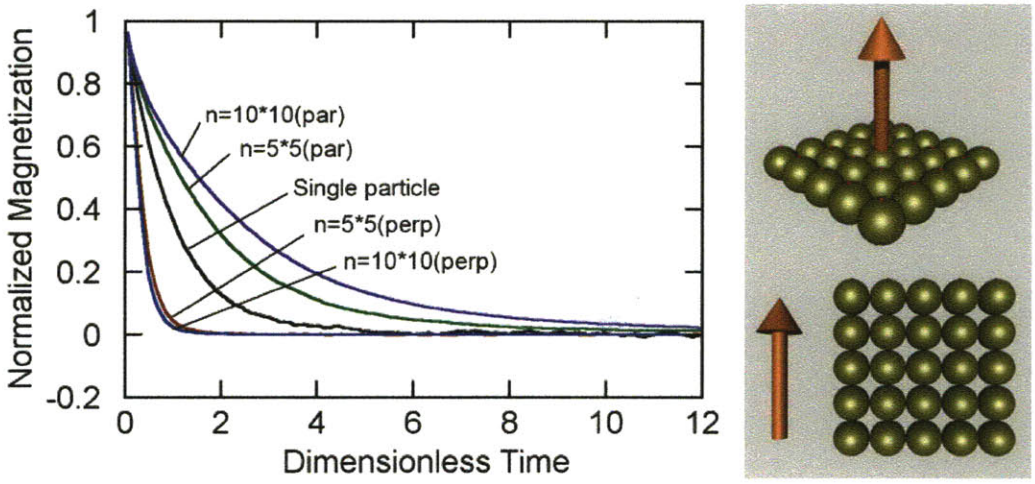

Figure 5-6: Relaxation behavior for rectangular planar arrangements parallel and perpendicular to the initial applied field. The results are shown for 25 and 100 particle clusters.

5.6.5 Planar Structures: Arrangement

Next, we compare the relaxation behavior for the rectangular and hexagonal packing arrangement for the planar clusters. For the parallel configuration we observe that the relaxation behavior for the hexagonal arrangement is slightly faster than the rectangular arrangement (Figure 5-7). In hexagonal arrangement, each particle has six immediate neighbors next to it, while in rectangular arrangement there are only four immediate neighbors, leading to slightly stronger destabilizing forces and shorter relaxation times in the case of hexagonal arrangement of particles. For the perpendicular configuration, let us compare the rectangular and hexagonal arrangements as packing of linear chains. In the rectangular arrangements the chains can be visualized to be lying next to each other, as

shown in bottom right hand corner of Figure 5-6, while in the hexagonal arrangement they are present in alternating fashion (bottom right hand corner of Figure 5-7). Since in the hexagonal arrangements particle are not occupying positions next to each other, but at 45 degrees, the configuration is more stable. Hence the relaxation for the hexagonal arrangement is slower.

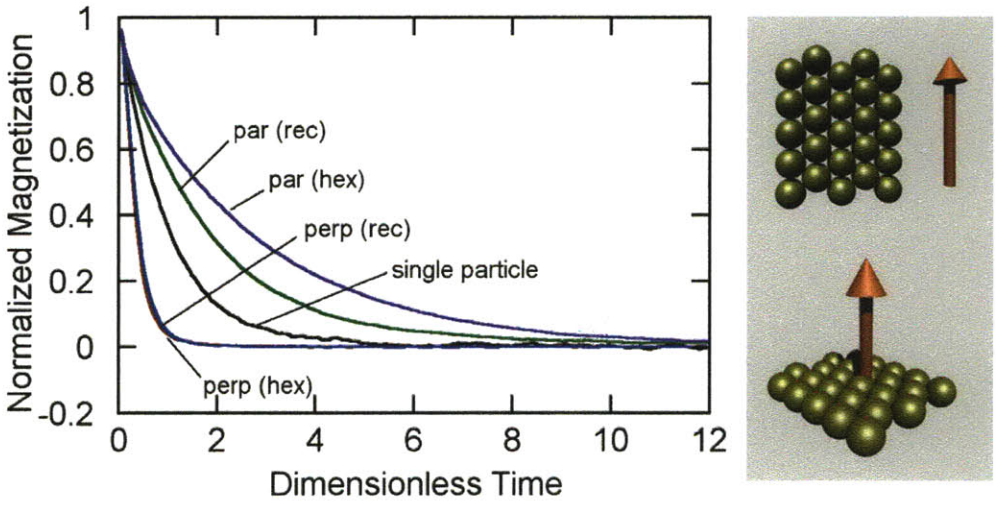

Figure 5-7: Comparing the relaxation behavior for the rectangular and hexagonal configuration in planar magnetic nanoparticle structure for 25 particle clusters. The figures on the right show the hexagonal packing considered for the particle clusters for the parallel and perpendicular arrangements.

5.6.6 Planar Structures: Size of magnetic nanoparticles

We have also examined the effect of particle size on the magnetic relaxation behavior of planar structures. In Figure 5-8, we can compare the difference in relaxation times for 6 nm magnetic particle clusters to that of 10 nm particle size clusters. The inter-particle effects are much smaller for the 6 nm particles as compared to that of 10 nm particles and hence the relaxation times for the 6 nm particle clusters is very similar to that of 6 nm individual particles.

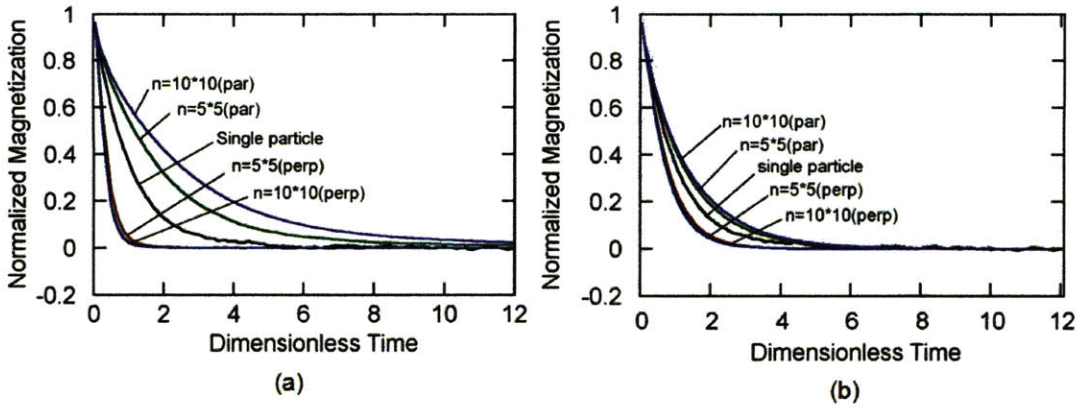

Figure 5-8: Relaxation behavior for planar magnetic nanoparticle clusters consisting of (a) 10 nm particles and (b) 6 nm particles.

5.6.7 Remnant Magnetization

5.6.7.1 Chain-like structures

Iron wires are frequently used to pack the HGMS column to trap the magnetic nanoparticles. Iron is ferromagnetic and has a high amount of remnant magnetization even on removal of external magnetic fields. This could prove to be a reason for concern during the elution step. We have studied the relaxation behavior of magnetic nanoparitcle clusters under the influence of remnant magnetic fields. In these simulations, we have included the external torque term defined in Equation (5.9).

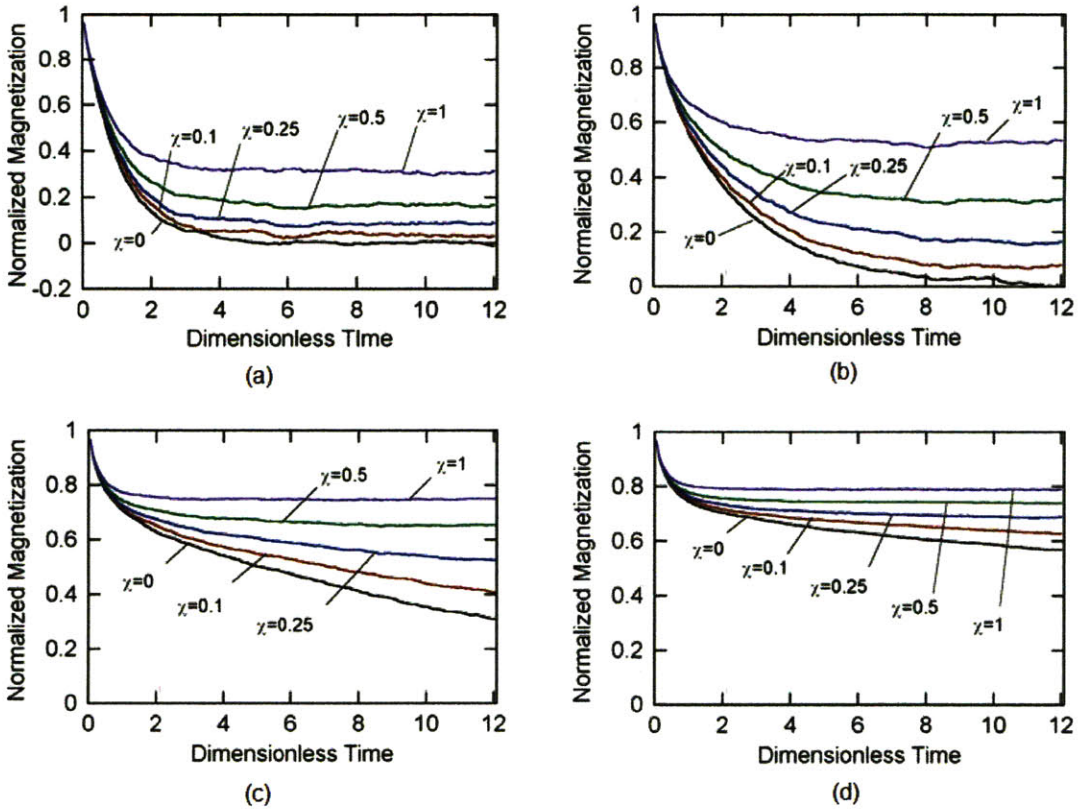

Figure 5-9: Relaxation behavior under the presence of a varying external magnetic field for 10 nm chain-like magnetic clusters having (a) 1 particle, (b) 2 particles, (c) 5 particles and (d) 10 particles.

In Figure 5-9, we have shown the relaxation behavior of chain-like magnetic clusters for varying external magnetic field strengths. χ, the dimensionless external magnetic field strength is defined as:

$$\chi = \frac{mH_e}{kT} \tag{5.18}$$

where m is the magnetic moment of the particle as defined by (5.10), H_e is the applied field strength. We observe that for the same magnetic field strength, the longer chains have a higher magnetization values, implying difficulty in elution. Say, on comparing magnetization values for χ=1, it is a little more than twice for 10 nm individual particles (m_{dim}~0.4) to that of 10 nm particles in the 10 particle chains (m_{dim}~0.8).

5.6.7.2 Spherical Clusters

Next, we perform a similar study as show in Figure 5-9 for spherical shaped clusters having individual magnetic nanoparticles with a diameter of 10 nm. We observe that for the spherical clusters the relaxation is very similar to that of individual particles (Figure 5-10). Also, the final magnetization values are identical to that of individual nanoparticles. The reasoning for these results is along similar lines to that of results obtained in Figure 5-5 that the particles above and below a given particle nullify the stabilizing and destabilizing effect.

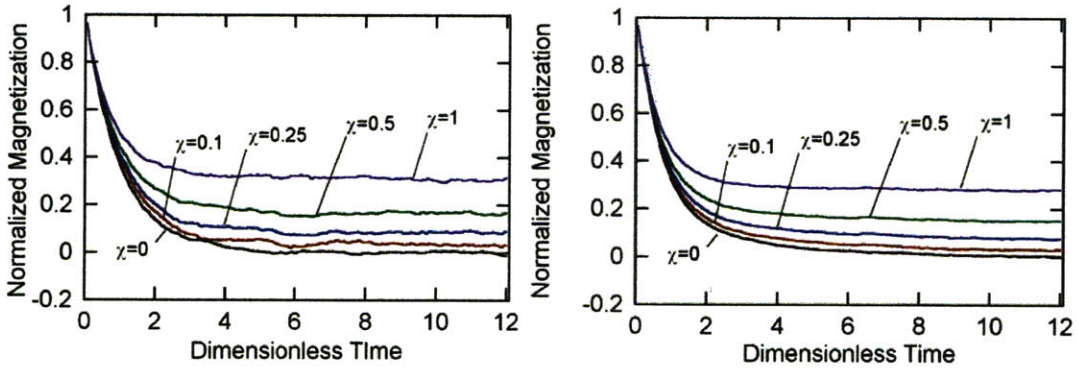

Figure 5-10: Relaxation behavior under the presence of a varying external magnetic field for 10 nm spherical clusters for (a) 1 particle and (b) 7 particles.

5.7 Conclusions

It is important to understand the relaxation process of magnetic nanoparticle clusters employed in high gradient magnetic separation columns so as to design magnetic nanoparticles which can prove to be most efficient in separation as well as elution step. In this work we have modeled the Néel relaxation processes using stochastic dynamics simulations, in the presence and absence of an external magnetic field. Our simulations are restricted to capture only Néel relaxation and not Brownian relaxation processes, because when these particles are present in sludge like mixtures or are trapped on the iron wires in the column, the rotational Brownian motion is physically restricted and the primary method of relaxation is via the rotation of magnetic domains or in other words by Néel relaxation.

The parameters that we consider in these simulations are the size of the magnetic nanoparticle clusters, size of the individual nanoparticles, shapes of these clusters, arrangement and orientation of the clusters with regards to the external magnetic field. We observed that relaxation characteristic of spherical clusters is very identical to that of individual particles in isolation. Even under the presence of an external magnetic field, the final magnetization is very similar for both spherical clusters and isolated magnetic nanoparticles.

For chain-like clusters we observe that relaxation times increases with increasing chain lengths. For particles less than 8 nm in size this increase in relaxation times is fairly small because the inter-particle magnetic interactions are small as compared to the thermal forces. However, for particles larger than 8 nm, the relaxation time drastically increases with increasing chain length. For a 10 nm particle size, the relaxation time for a 10 particle chain is orders of magnitude higher than that of an individual particle. Also, the final magnetization under the presence of an external magnetic field is considerably higher for particles present in chain like structures as compared to individual particles.

Magnetic nanoparticle cluster in planar arrangements relax extremely quickly when the plane is present perpendicular and slower when the plane is present parallel to the initially applied magnetic field. The configuration of these planes when hexagonal, relaxes faster than rectangular configuration when the plane is perpendicular and slower when the plane is parallel to the initially applied magnetic field.

It was observed the initial relaxation behavior of the magnetic nanoparticles may not determine the final relaxation behavior. The end particles on the five particle chain like cluster initially relax faster than the centre particle in the three particle chain like cluster, but after a while, the behavior is inverted. This behavior is a result of the interaction between the different particles in the magnetic nanoparticle chains.

To design magnetic nanoparticle clusters for separations, one would like them to get trapped easily during the separation step and to be released quickly during the elution step. In other words, one is looking for clusters that relax quickly when the magnetic field is removed. Analyzing the results so obtained from these stochastic dynamic

simulations, we recommend that spherical nanoparticle clusters to be employed for magnetic separations. If there is a need to use, or in the process we obtain chain like structures, the individual particle size should be restricted to less than 6 nm, if using magnetite for efficient elution.

This work can be further extended to include the rotational Brownian motion when the clusters are not physically constrained to move. Also, we have neglected the effect of "easy axis" of magnetization. More complicated models need to be developed to include such effects. However, the simple model that we developed has led to an increased insight in design of magnetic fluids.

5.8 Bibliography

1. Bucak, S., Jones, D.A., Laibinis, P.E., and Hatton, T.A., *Protein separations using colloidal magnetic nanoparticles.* Biotechnology Progress, 2003. **19**(2): p. 477-484.

2. Ditsch, A., Lindenmann, S., Laibinis, P.E., Wang, D.I.C., and Hatton, T.A., *High-gradient magnetic separation of magnetic nanoclusters.* Industrial & Engineering Chemistry Research, 2005. **44**(17): p. 6824-6836.

3. Hubbuch, J.J. and Thomas, O.R.T., *High-gradient magnetic affinity separation of trypsin from porcine pancreatin.* Biotechnology And Bioengineering, 2002. **79**(3): p. 301-313.

4. Watarai, H. and Namba, M., *Magnetophoretic behavior of single polystyrene particles in aqueous manganese(II) chloride.* Analytical Sciences, 2001. **17**(10): p. 1233-1236.

5. Watarai, H., Suwa, M., and Iiguni, Y., *Magnetophoresis and electromagnetophoresis of microparticles in liquids.* Analytical And Bioanalytical Chemistry, 2004. **378**(7): p. 1693-1699.

6. Moeser, G.D., Roach, K.A., Green, W.H., Hatton, T.A., and Laibinis, P.E., *High-gradient magnetic separation of coated magnetic nanoparticles.* Aiche Journal, 2004. **50**(11): p. 2835-2848.

7. Gerber, S. and Briss, R.R., *High Gradient Magnetic Separation.* 1983, Chichester; New York: Research Studies Press.

8. Ditsch, A., Yin, J., Laibinis, P.E., Wang, D.I.C., and Hatton, T.A., *Ion-exchange purification of proteins using magnetic nanoclusters.* Biotechnology Progress, 2006. **22**(4): p. 1153-1162.

9. Fannin, P.C. and Charles, S.W., *The Study Of A Ferrofluid Exhibiting Both Brownian And Neel Relaxation.* Journal Of Physics D-Applied Physics, 1989. **22**(1): p. 187-191.

10. Kotitz, R., Fannin, P.C., and Trahms, L., *Time-Domain Study Of Brownian And Neel Relaxation In Ferrofluids.* Journal Of Magnetism And Magnetic Materials, 1995. **149**(1-2): p. 42-46.

11. Kotitz, R., Weitschies, W., Trahms, L., and Semmler, W., *Investigation of Brownian and Neel relaxation in magnetic fluids.* Journal Of Magnetism And Magnetic Materials, 1999. **201**: p. 102-104.

12. Malaescu, I. and Marin, C.N., *Study of magnetic fluids by means of magnetic spectroscopy.* Physica B-Condensed Matter, 2005. **365**(1-4): p. 134-140.

13. Vaishnava, P.P., Tackett, R., Dixit, A., Sudakar, C., Naik, R., and Lawes, G., *Magnetic relaxation and dissipative heating in ferrofluids.* Journal Of Applied Physics, 2007. **102**(6).

14. Rosensweig, R.E., *Ferrohydrodynamics*. 1985: Cambridge University Press: Cambridge.

15. Frenkel, J., *Kinetic Theory of Liquid.* 1955, New York: Dover Publications.

16. Néel, L., *Thermoremanent Magnetization of Fine Powders.* Reviews of Modern Physics, 1953. **25**(1): p. 293.

17. Fannin, P.C. and Charles, S.W., *On The Calculation Of The Neel Relaxation-Time In Uniaxial Single-Domain Ferromagnetic Particles.* Journal Of Physics D-Applied Physics, 1994. **27**(2): p. 185-188.

18. Coffey, W.T., Kalmykov, Y.P., and Titov, S.V., *Langevin equation method for the rotational Brownian motion and orientational relaxation in liquids.* Journal Of Physics A-Mathematical And General, 2002. **35**(32): p. 6789-6803.

19. Coffey, W.T., Kalmykov, Y.P., Ouari, B., and Titov, S.V., *Rotational diffusion and orientation relaxation of rodlike molecules in a biaxial liquid crystal phase.* Physica A-Statistical Mechanics And Its Applications, 2006. **368**(2): p. 362-376.

20. Coffey, W.T. and Kalmykov, Y.P., *On The Calculation Of The Dielectric-Relaxation Times Of A Nematic Liquid-Crystal From The Non-Inertial Langevin Equation.* Liquid Crystals, 1993. **14**(4): p. 1227-1236.

21. Satoh, A., Chantrell, R.W., and Coverdale, G.N., *Brownian dynamics simulations of ferromagnetic colloidal dispersions in a simple shear flow.* Journal Of Colloid And Interface Science, 1999. **209**(1): p. 44-59.

22. Ukai, T., Maekawa, T., and Morimoto, H., *Brownian dynamics analysis of magnetic order-disorder transition in a ferromagnetic colloidal system.* International Journal Of Modern Physics B, 2001. **15**(6-7): p. 817-822.

23. Kalmykov, Y.P., Coffey, W.T., and Titov, S.V., *Phase-space formulation of the nonlinear longitudinal relaxation of the magnetization in quantum spin systems.* Physical Review E, 2007. **76**(5).

24. Dickinson, E., Allison, S.A., and McCammon, J.A., *Brownian Dynamics With Rotation Translation Coupling.* Journal Of The Chemical Society-Faraday Transactions Ii, 1985. **81**(APR): p. 591-601.

25. Dickinson, E., *Brownian Dynamics With Hydrodynamic Interactions - The Application To Protein Diffusional Problems.* Chemical Society Reviews, 1985. **14**(4): p. 421-455.

Chapter 6

6. Magnetization characteristics of an array of magnetic nanoparticles under the presence of magnetic fields

6.1 Introduction

A HGMS column usually consists of magnetically susceptible wires or spheres packed in a column placed inside an electromagnet [1, 2]. When a magnetic field is applied, the wires dehomogenize the magnetic field in the column producing large magnetic field gradients in the column which can be used to trap particles on to the surface of these wires.

In the separations of non-magnetic particles using magnetic nanoparticles, the non-magnetic entity that needs to be separated is either physically or chemically attached preferentially to the magnetic nanoparticles. This entity then gets trapped in the HGMS column, while all other species are eluted out. The diffusion and equilibration steps are very fast of the order of few milliseconds, while HGMS usually poses as the rate limiting step [3]. Thus, it is important to understand the HGMS separations in further detail. The specific interest of this work is to understand the magnetization properties of magnetic nanoparticle clusters that get trapped on the wires in the HGMS columns. In this chapter, we have made an attempt to understand the effect of inter-particle magnetic interactions and the external magnetic field on the magnetization of these particle clusters.

These magnetic inter-particle interactions and contact forces between particles lead to formation of interesting particle structures, such as rings and chains [4]. Karpov [5]

studied the formation of three dimensional aggregates by considering the effect of interaction potential which consists of magnetic, electrostatic, elastic, gravitational and van der Waal forces. Neto [6] has studied the formation of complex superstructures such as spirals and spokes with magnetic nanoparticles using SANS, SAXS, and AFM. Richardi [7] and co-workers have studied the formation of magnetic nanoparticle structures when the suspension evaporates using Brownian dynamics simulation methods. Magnetic nanoparticle structures have been analyzed for which the local moment distribution is governed by the magnetic inter-particle dipolar interactions [8-12].

We have determined the effect of inter-particle interactions on the magnetization characteristics of magnetite nanoparticle clusters formed on cylindrical iron wires in an HGMS column. Understanding the effect of these interactions on the moment of particles and its effect on the structure is important so that they can be tailor-made for other applications such as colloidal photonic crystals [13, 14], catalytic coating of surfaces [15], nano-composites [16], etc. It is not possible to experimentally probe an array of magnetic nanoparticles to determine the magnetization values for each of these particles. Thus, we have developed a model to determine the magnetization characteristics of magnetic nanoparticles in regular arrays.

6.2 Theory

When a magnetic field $\boldsymbol{H}_i$ is applied, the average magnetic moment of a superparamagnetic nanoparticle for a given ensemble can be represented by [17]

$$\boldsymbol{m}_i = \frac{\mu_0 V \chi}{1+\beta H_i}\boldsymbol{H}_i = \begin{cases} \mu_0 V \chi \boldsymbol{H}_i & for\ H_i\beta \ll 1 \\ \mu_0 V (\chi/\beta)\hat{\boldsymbol{H}}_i & for\ H_i\beta \gg 1 \end{cases} \tag{6.1}$$

where $H_i = (\boldsymbol{H}_i \cdot \boldsymbol{H}_i)^{1/2}$ is the magnitude and $\hat{\boldsymbol{H}}_i$ the direction of the magnetic field $\boldsymbol{H}_i$, μ_0 is the permeability of free space, V is the effective volume of the core and χ is the magnetic susceptibility, given by the slope of the magnetization (M) curve at low magnetic fields, and i is the index for the particle number. The magnitude of the magnetic field at which the magnetization is half of its saturation value, $\mu_0 V(\chi/\beta)$ is $1/\beta$.

For non-interacting particles, the particles only experience the external magnetic field. However for a set of particles in close proximity of each other, not only do they experience the external magnetic field but also the magnetic fields associated with the particles around them. When an assembly of particles is in an externally applied field $\boldsymbol{H}_0$, the net magnetic field acting on a nanoparticle *i* is [18]

$$\boldsymbol{H}_i = \boldsymbol{H}_0 + \sum_{j \neq i} \boldsymbol{H}_{ij} \tag{6.2}$$

where H_{ij} is the field of the *j*th particle on the *i*th particle, and is given by [19]

$$\boldsymbol{H}_{ij} = \frac{1}{4\pi\mu_0} \frac{3\hat{\boldsymbol{r}}_{ij}(\hat{\boldsymbol{r}}_{ij} \cdot \boldsymbol{m}_j) - \boldsymbol{m}_j}{r_{ij}^3} \tag{6.3}$$

where $\hat{\boldsymbol{r}}_{ij}$ the unit vector connecting the particle '*i*' to particle '*j*', separated by a distance r_{ij}. Hence the average magnetic moment for a magnetic nanoparticle when present in a collection of magnetic nanoparticles is

$$\boldsymbol{m}_i = \frac{\mu_0 V \chi}{1 + \beta H_i} \left(\boldsymbol{H}_0 + \sum_{i \neq j} \frac{1}{4\pi\mu_0} \frac{3\hat{\boldsymbol{r}}_{ij}(\hat{\boldsymbol{r}}_{ij} \cdot \boldsymbol{m}_j) - \boldsymbol{m}_j}{r_{ij}^3} \right) \tag{6.4}$$

In our work, we will only consider low magnetic fields ($\beta H_0 \ll 1$) since the remnant magnetic fields from the iron wires are usually small. Such an approximation yields linear equations that can be solved explicitly.

$$\boldsymbol{m}_i = \mu_0 V \chi \left(\boldsymbol{H}_0 + \sum_{i \neq j} \frac{1}{4\pi\mu_0} \frac{3\hat{\boldsymbol{r}}_{ij}(\hat{\boldsymbol{r}}_{ij} \cdot \boldsymbol{m}_j) - \boldsymbol{m}_j}{r_{ij}^3} \right) \tag{6.5}$$

Converting the above equation in a dimensionless form we get

$$\boldsymbol{\mu}_i = \hat{\boldsymbol{H}}_0 + \frac{\chi}{3} \sum_{i \neq j} \frac{3\hat{\boldsymbol{r}}_{ij}(\hat{\boldsymbol{r}}_{ij} \cdot \boldsymbol{\mu}_j) - \boldsymbol{\mu}_j}{\left(r_{ij}/a\right)^3} \tag{6.6}$$

where the dimensionless magnetic moment $\boldsymbol{\mu}_i$, is defined as $\boldsymbol{\mu}_i = \boldsymbol{m}_i / \mu_0 V \chi H_0$, $\hat{\boldsymbol{H}}_0 = \boldsymbol{H}_0 / H_0$ is the unit vector pointing along the direction of magnetic field, and *a* is the

radius of the magnetic nanoparticle. Hence, if we are given a system with n particles, we can write n such linear equations, one each for the particle and obtain the magnetic moment values for each of the particles by solving the set of these equations.

6.3 Particle clusters on wire

In this work we have explored rectangular and hexagonal particle configurations in three dimensional magnetite clusters present on a magnetized iron wire as shown in Figure 6-1. We assume the clusters to be infinitely large in the x and y direction, reducing the problem to uni-dimensional with variation in magnetization only along the z direction as indicated in the figure below. We consider particles of different sizes in rectangular and hexagonal packing on a cylindrical iron wire. We also assume the wire diameter to be much larger than the particle size to assume planar geometries.

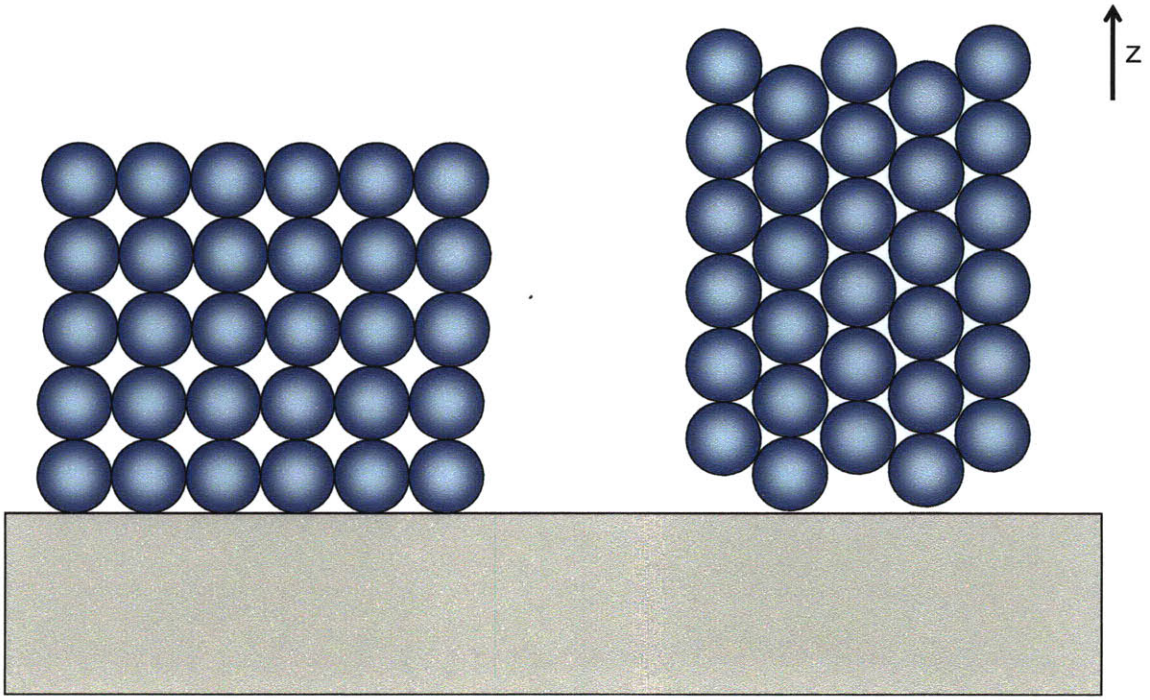

Figure 6-1: Particle clusters present on an iron wire in rectangular packing (on left) and hexagonal packing (on right).

6.3.1 Rectangular arrangement

The first arrangement we consider is the rectangular arrangement. As stated before, we have reduced the chosen system into a one dimensional problem. The magnetic moments would have a non-zero average value only in the *z*-direction. In other words, we have explored the variation of the magnetic moments as a function of *z*-direction. In the equations described below the subscript *i* refers to the layer number, with *i*=1 being the layer closest to the iron wire. The equation written below would be identical for any particle in row *i*, since we assume clusters to be infinitely large in the *x* and *y* planes.

$$\mu_i = 1 + \frac{\chi}{3}\sum_{j\neq i}\mu_j \sum_{\alpha}\sum_{\beta}\frac{3r^z{}_{\alpha\beta}r^z{}_{\alpha\beta}-1}{\left(r_{ij}/a\right)^3} + \frac{\chi}{3}\mu_i \sum_{\alpha}\sum_{\beta}\frac{3r^z{}_{\alpha\beta}r^z{}_{\alpha\beta}-1}{\left(r_{ij}/a\right)^3} \tag{6.7}$$

Here the double summation (α,β) is done over all the particles in that row in the *x* and *y* directions, $r^z{}_{ij}$ refers to the *z* component of the radial vector originating from the particle considered in the row *i* to a given particle in row *j* . Now considering the rectangular geometry of the system and substituting in all the summations we get

$$\mu_i = \hat{H}_0 + \sum_{j\neq i}\frac{\chi}{3}\mu_j a_{ij} + \frac{\chi}{3}\mu_i a_{ii} \tag{6.8}$$

where,

$$a_{ij} = \frac{1}{8}\sum_{\alpha=-\alpha_{\max}}^{\alpha_{\max}}\sum_{\beta=-\beta_{\max}}^{\beta_{\max}}\frac{\left(\dfrac{3(j-i)^2}{\alpha^2+\beta^2+(j-i)^2}-1\right)}{\left(\alpha^2+\beta^2+(j-i)^2\right)^{3/2}} \tag{6.9}$$

$$a_{ii} = \frac{1}{8}\sum_{\alpha=-\alpha_{\max}}^{\alpha_{\max}}\sum_{\beta=-\beta_{\max}}^{\beta_{\max}}\frac{-1}{\left(\alpha^2+\beta^2\right)^{3/2}} \tag{6.10}$$

The limits α_{max} and β_{max} extend from -∞ to +∞. When calculating a_{ii}, the coefficient excludes the summation for both α and β equal to zero, since that would imply the field of the particle itself. The coefficients a_{ij} and a_{ii} were numerically evaluated as a function of α_{max} (=β_{max}) as shown in Figure 6-2 and Figure 6-3. In Figure 6-2, we observe that $a_{1,2}$ (interaction between a given particle in row 1, with particles in row 2 starts with a positive value, as α_{max}=0 corresponds to the single particle sitting exactly above the given

particle in row 1. Thereafter, with increasing values of α_{max}, the interacting particles provide a destabilizing force, leading to a decrease in value of a_{12}. This value stabilizes to an asymptotic after more than 50 particles, since any more particles are far away from the given particle to make any significant difference. For the coefficient $a_{1,10}$, we observe that it increases for the first few particles, since the magnetic field originating from them is in the same direction as the particle itself, providing a stabilizing force (see right hand side illustration in Figure 6-3). For the particles further away, they are in an energetically unfavorable position, leading to a decrease in the value of the coefficient. We have used 30 layer and 60 layer particle clusters for the simulations and we have used 200 particles as our cut off radius for the evaluation of these coefficients.

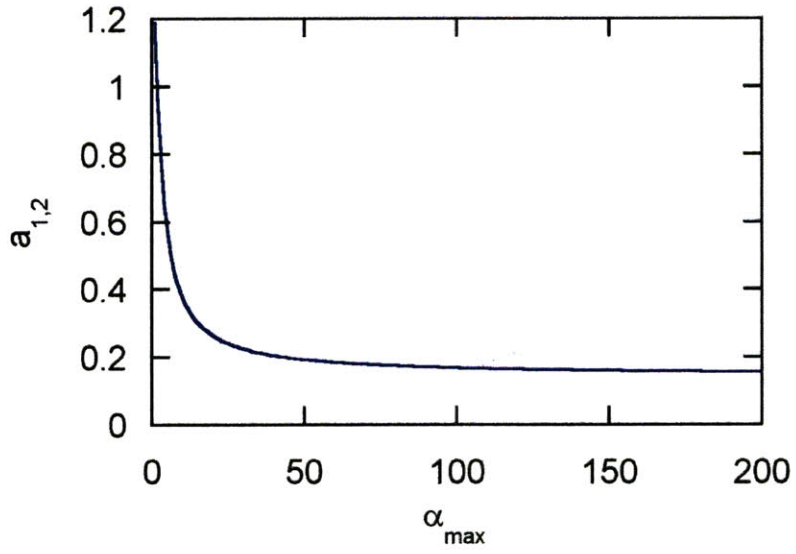

Figure 6-2: a_{12} as a function of α_{max}

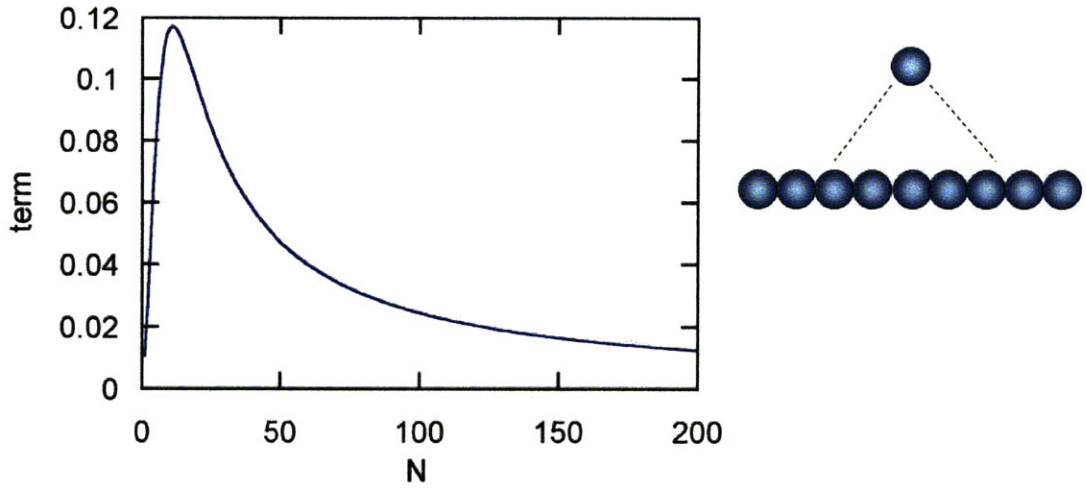

Figure 6-3: $a_{1,10}$ as a function of α_{max}

6.3.2 Hexagonal Configuration

The set of equations that we develop for the hexagonal configuration are very similar to the ones we developed for rectangular configuration (Equation (6.8)). The index of the rows in z direction is slightly different as shown in Figure 6-4 as compared to the rectangular arrangement.

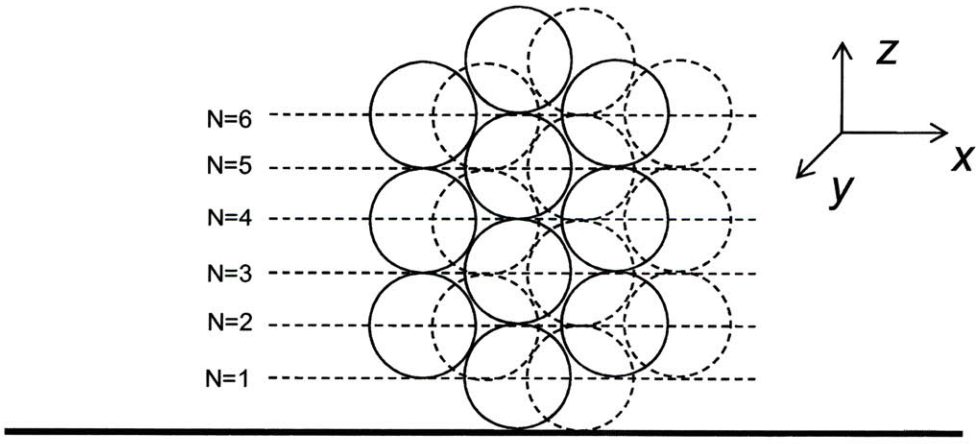

Figure 6-4: Arrangement of particles in a hexagonal cluster. N represents the layer number. The dotted circles represent the layer above and behind the given solid layer (x-z plane) in the y-axis.

With the hexagonal arrangement, the difference in geometry leads to a difference in the coefficients $a_{,j}$ and a_{ii} as:

$$a_{ii} = \frac{1}{8} \sum_{\alpha=-\alpha_{max}}^{\alpha_{max}} \sum_{\beta=-\beta_{max}}^{\beta_{max}} \frac{-1}{\left(x^2 + y^2\right)^{3/2}}$$

where,

$$y = \sqrt{\frac{2}{3}}\beta \qquad (6.11)$$

$$x = \sqrt{3}\alpha \; for \; \beta = even$$

$$x = \sqrt{3}\alpha + \frac{2}{\sqrt{3}} \; for \; \beta = odd$$

and,

$$a_{ij} = \frac{1}{8} \sum_{\alpha=-\alpha_{max}}^{\alpha_{max}} \sum_{\beta=-\beta_{max}}^{\beta_{max}} \frac{\left(\frac{3z^2}{x^2 + y^2 + z^2} - 1\right)}{\left(x^2 + y^2 + z^2\right)^{3/2}}$$

where,

$$z = \frac{(i-j)}{2}$$

$$y = \sqrt{\frac{2}{3}}\beta$$

$$for \; (i-j) = even$$

$$x = \sqrt{3}\alpha \; for \; \beta = even$$

$$x = \sqrt{3}\alpha + \frac{2}{\sqrt{3}} \; for \; \beta = odd$$

$$for \; (i-j) = odd$$

$$x = \sqrt{3}\alpha + \frac{\sqrt{3}}{2} \; for \; \beta = even$$

$$x = \sqrt{3}\alpha + \frac{1}{2\sqrt{3}} \; for \; \beta = odd \qquad (6.12)$$

6.4 Results

6.4.1 Rectangular configuration

We simulate a rectangular array of magnetic nanoparticles for 30 layers along the *z*-direction and measure the magnetic moment of particles for each of the layers, shown in Figure 6-5. For the same dimensionless magnetic field applied we observe that the dimensionless magnetization decreases with increasing magnetic particle size. This happens because the particles in the rectangular arrangement are not in a stable configuration since they are in equatorial position to each other with reference to the external magnetic field. Hence, the inter-particle magnetic interactions lower each other's magnetization values. Another way to represent the results shown in Figure 6-5, is by plotting the magnetization as a function of the distance from the wire surface (Figure 6-6). The dotted line represents the magnetization of particles if there was no inter-particle magnetic force. The magnetic field originating from a wire decays as the square of the inverse of the distance from the centre of the particle wire.

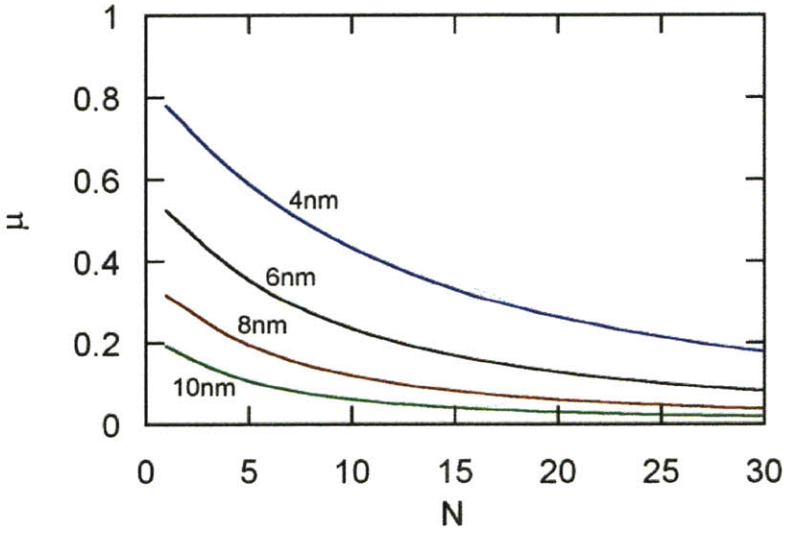

Figure 6-5: Dimensionless magnetization for rectangular array of magnetite nanoparticles consisting of 30 layers as a function of the layer number for particles with a diameter of 4, 6, 8 and 10 nm

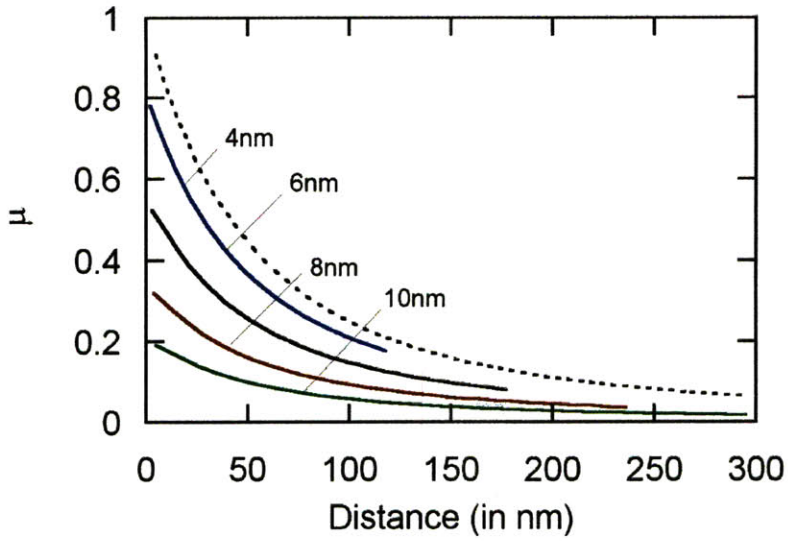

Figure 6-6: Dimensionless magnetization for rectangular array of magnetite nanoparticles consisting of 30 layers as a function of distance from the wire surface (d= 200 nm) with diameters of 4, 6, 8 and 10 nm. The dotted line represents the magnetization in absence of any inter-particle interactions.

6.4.2 Hexagonal Configuration

When simulating the hexagonal arrangement, for 4 and 6 nm particles we see results similar to that of rectangular arrangement, but for particles larger than 8 nm, we see an oscillatory behavior (Figure 6-7). To understand this oscillatory behavior we parsed the 10 nm results in two sets of data, one for each set of chains which are next to each other but are offset by half a particle diameter in the z-direction (Figure 6-4). One set of data is for odd layers (i=1,3,5….) and the other one is for even layers (i=2,4,6…..) show in Figure 6-8. We observe an alternating oscillatory behavior between the two set of data, i.e. if the magnetization is higher for a given particle, it will be lower for the particle in the adjacent column and vice-versa.

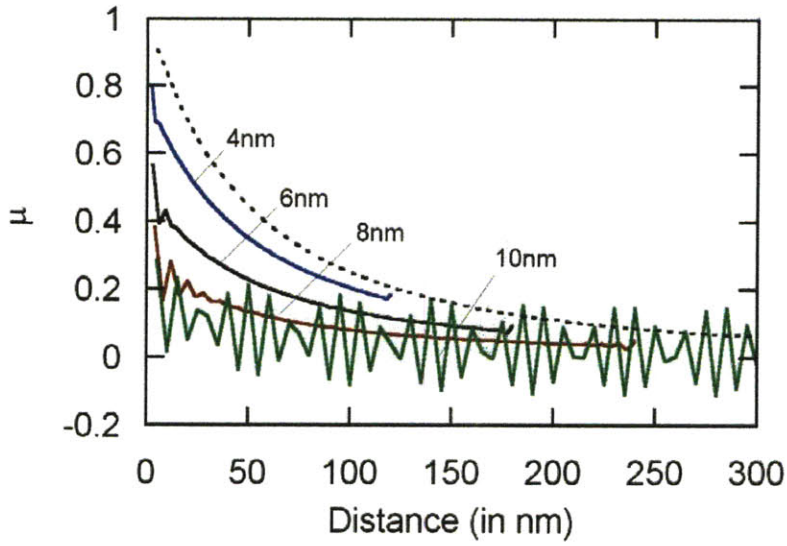

Figure 6-7: Dimensionless magnetization for hexagonal array of magnetite nanoparticles consisting of 30 layers as a function of distance from the wire surface (d= 200 nm) with diameters of 4, 6, 8 and 10 nm. The dotted line represents the magnetization in absence of any inter-particle interactions.

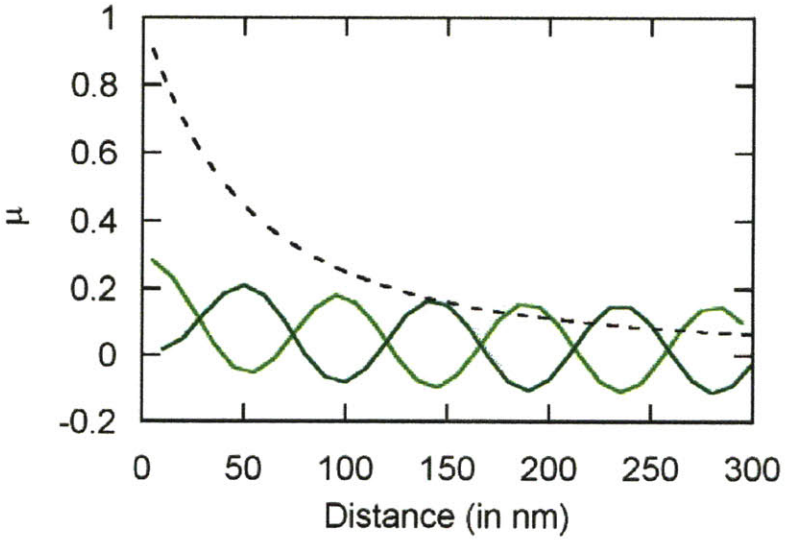

Figure 6-8: Oscillatory alternating behavior for 10 nm particle for the two adjacent columns. The dotted line represents the magnetization in absence of any inter-particle interactions.

6.4.3 Oscillatory behavior

To decouple the effect of changing magnetic field and inter-particle magnetic interactions, we perform the simulations at a constant magnetic field (Figure 6-9). The right hand side figures illustrate the magnitude and direction of the dipole moments. There is an external magnetic field present which would force the particle to point in the upward directions. However the particles in the adjacent column provide a magnetic field in the opposite (downward) direction in which they are pointing. Hence, the dipoles evolve themselves in such a unique magnetic moment configuration to maximize the stability. For the 12 nm particles the dipole interactions are significant enough, as compared to the external magnetic field, to make them point in the opposite direction to the external field. In other words the adjacent columns want to point in direction opposite to each other, but the presence of the external magnetic field in one direction wants both of them to point in the same upwards direction, resulting them to point in the periodic higher and lower values.

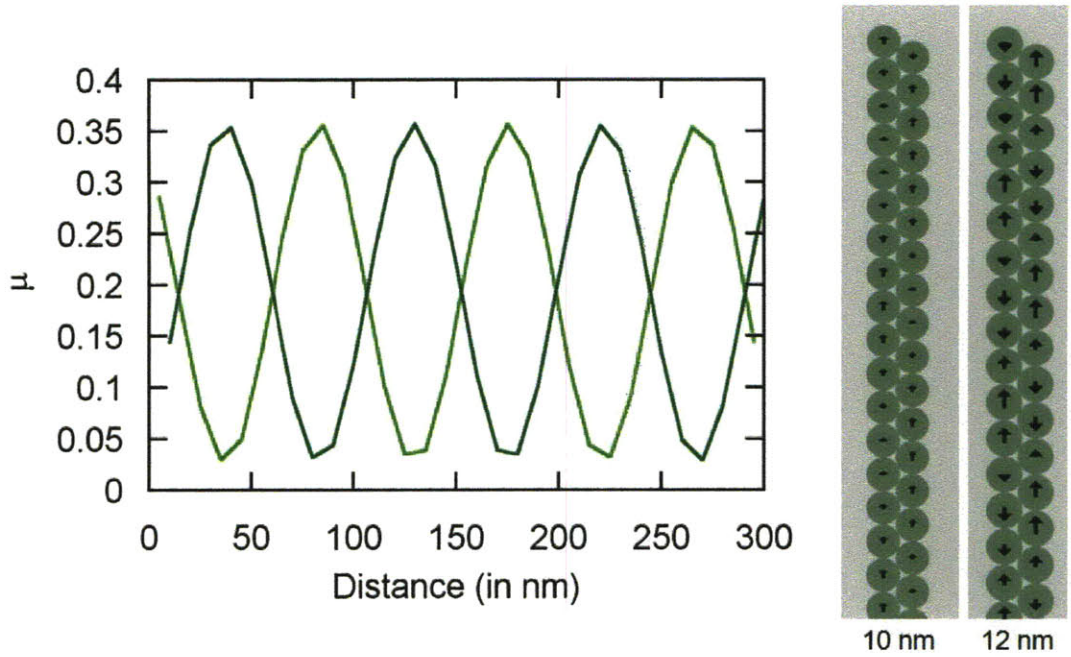

Figure 6-9: Oscillatory alternating behavior for 10 nm particle for the two adjacent columns at a constant magnetic field. The figures on the right depict the results in a pictorial fashion for 10 and 12 nm particles. The arrow heads show the direction of magnetic field, while the arrow length directly proportional to the magnitude of the magnetization of the dipole of the particle.

6.4.3.1 Effect of number of layers

We have also explored the effect of number of layers on the oscillatory behavior of the magnetic nanoparticle by repeating the simulation for twice the number of layers as compared to the previous simulation (Figure 6-10). We see that the oscillatory behavior is very similar to the results obtained in Figure 6-9 with an oscillatory period of close to 100 nm or 10 particle diameters.

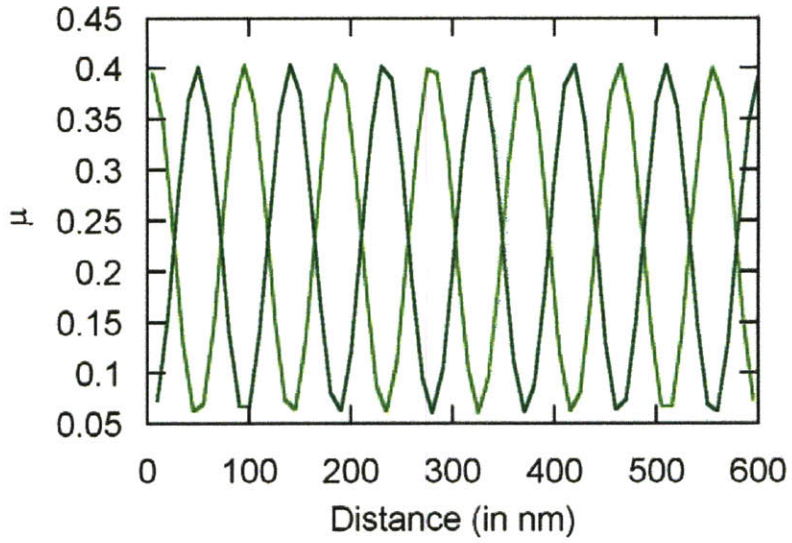

Figure 6-10: Oscillatory behavior for twice the number of layers in z-direction is very similar compared to the results simulated in Figure 6-9.

Also, it is important to note that the particle closest to the wire (N=1) always starts with the higher value as compared to the second particle (N=2) in this periodic oscillatory behavior. This happens since the particle in layer 1 (see Figure 6-4) has fewer immediate neighbors as compared to the particle in layer 2, which will provide a destabilizing influence.

6.4.3.2 Effect of size of magnetic nanoparticle

Next, we explore the influence of particle size on the oscillatory behavior (Figure 6-11). There are no oscillations for particle sizes of less than 9 nm. On increasing the particle size, at 9.25 mm particles we observe a sudden occurrence of the oscillations in the magnetization behavior. On increasing the particle size further we see a decrease in periodicity for this oscillatory magnetization.

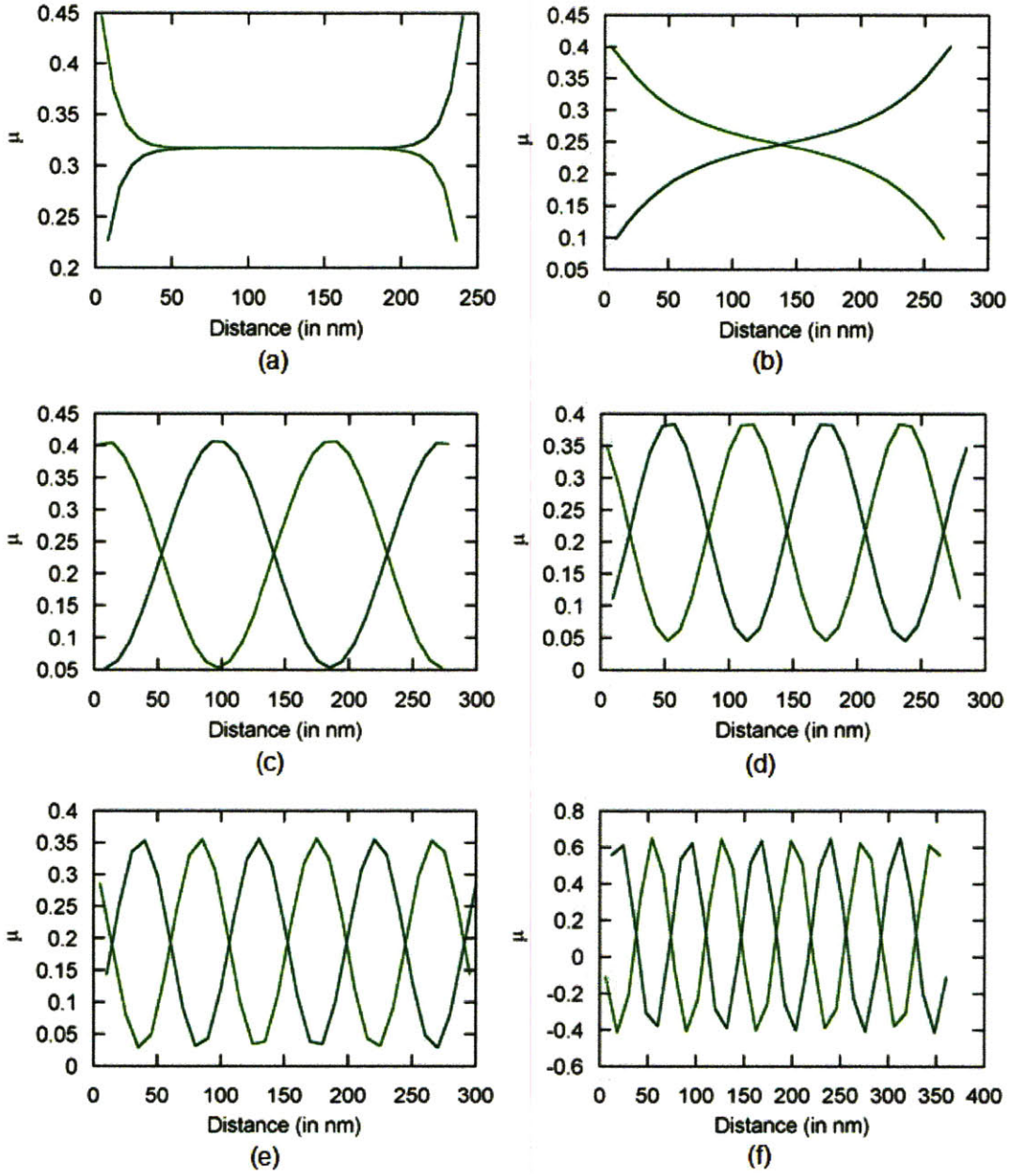

Figure 6-11: Oscillatory behavior as a function of magnetic particle size for (a) 8 nm, (b) 9 nm, (c) 9.25 nm, (d) 9.5 nm, (e) 10 nm and (f) 12 nm.

6.5 Theoretical Analysis

In order to understand why the diameter of ~9.25 nm proves to be the critical value for the oscillatory behavior we perform the following analysis. We take equation (6.8) and re-order it to obtain:

$$\left(-1+\frac{\chi}{3}a_{ii}\right)\mu_i+\frac{\chi}{3}a_{ij}\mu_j+\hat{H}_0=0 \tag{6.13}$$

Now, we write the entire set of equations in a form of a matrix to get

$$\frac{\chi}{3}\underbrace{\begin{bmatrix} -\frac{3}{\chi}+a_{11} & a_{12} & a_{13} & .. & .. \\ a_{21} & -\frac{3}{\chi}+a_{22} & a_{23} & .. & .. \\ a_{31} & a_{32} & -\frac{3}{\chi}+a_{33} & & \\ .. & .. & .. & & \\ .. & .. & .. & & \end{bmatrix}}_{A}\begin{bmatrix}\mu_1\\ \mu_2\\ \mu_3\\ ..\\ ..\end{bmatrix}+\begin{bmatrix}\hat{H}_0\\ \hat{H}_0\\ \hat{H}_0\\ ..\\ ..\end{bmatrix}=0 \tag{6.14}$$

On substituting the values of the coefficients, a_{ij}'s in the matrix A, with only the diagonal elements dependent on χ, we get

$$\begin{bmatrix} -\frac{3}{\chi}+(-0.71) & -0.45 & 0.086 & -0.0026 & .. \\ -0.45 & -\frac{3}{\chi}+(-0.71) & -0.45 & 0.086 & -0.0026 \\ 0.086 & -0.45 & -\frac{3}{\chi}+(-0.71) & -0.45 & 0.086 \\ -0.0026 & 0.086 & -0.45 & -\frac{3}{\chi}+(-0.71) & -0.45 \\ .. & .. & .. & .. & .. \end{bmatrix} \tag{6.15}$$

We observe that at the critical radius diameter of 9.25 nm, we get a value of χ=8.33 at which for any given row, the sum of alternate columns becomes equal (except the first and the last two rows present at the boundary). Physically it would mean that the

magnetic interactions between the two columns are balancing each other out, leading to this oscillatory behavior. As a test case, we set all the coefficients except a_{ij}, $a_{i(j-1)}$, $a_{i(j+1)}$ to zero. Again, we find that the critical value of radius is when a_{ij} is the sum of $a_{i(j-1)}$ and $a_{i(j+1)}$. This confirms our theory that we can predict the onset of oscillatory behavior when the sum of alternate column is same.

6.6 Conclusions

In this work, we have explored the magnetization of magnetite nanoparticles clusters present on iron wires in HGMS columns. We have developed a theoretical model to evaluate magnetic moments under the presence of low external magnetic field. We have studied the effect of particle configurations, arrangements and particle sizes on the magnetization behavior. For rectangular arrangement, we observed a decrease in magnetic moments with increasing particle size. For hexagonal arrangement, again we observed a reduction in magnetic moments, but we observe a novel oscillatory behavior for the magnetite particles more than 9.25 nm in diameter.

We were able to explain the onset of this oscillatory behavior by developing a matrix, A from the set of linear equations, which captures the inter-particle interactions between the different layers. The periodicity of the oscillations is a function of the particle size, but not a function of the number of layers in the z-direction of the particle cluster. However, we were unable to come up with a method to predict the periodicity of this oscillatory behavior.

Understanding of this oscillatory behavior can be of significance when modeling HGMS columns. During the elution stage, when we have fluid flow around these magnetic clusters, the clusters having such magnetic moment oscillations are more likely to break at locations having null magnetic moments. Thus, we can tailor the magnetic particle size in such a way to exploit this oscillatory behavior to enhance the removal of clusters from the magnetic wires, even under the presence of low remnant magnetic fields. More work is further need to have a more detailed understanding and prediction of this oscillatory behavior of magnetic moments.

6.7 Bibiliography

1. Moeser, G.D., Roach, K.A., Green, W.H., Hatton, T.A., and Laibinis, P.E., *High-gradient magnetic separation of coated magnetic nanoparticles.* Aiche Journal, 2004. **50**(11): p. 2835-2848.

2. Gerber, S. and Briss, R.R., *High Gradient Magnetic Separation.* 1983, Chichester; New York: Research Studies Press.

3. Ditsch, A., Lindenmann, S., Laibinis, P.E., Wang, D.I.C., and Hatton, T.A., *High-gradient magnetic separation of magnetic nanoclusters.* Industrial & Engineering Chemistry Research, 2005. **44**(17): p. 6824-6836.

4. Weis, J.J. and Levesque, D., *Chain Formation In Low-Density Dipolar Hard-Spheres - A Monte-Carlo Study.* Physical Review Letters, 1993. **71**(17): p. 2729-2732.

5. Karpov, S.V., Gerasimov, V.S., Isaev, I.L., and Obushchenko, A.V., *Simulation of the growth of nanoparticle aggregates reproducing their natural structure in disperse systems.* Colloid Journal, 2006. **68**(4): p. 441-450.

6. Neto, C., Bonini, M., and Baglioni, P., *Self-assembly of magnetic nanoparticles into complex superstructures: Spokes and spirals.* Colloids And Surfaces A-Physicochemical And Engineering Aspects, 2005. **269**(1-3): p. 96-100.

7. Richardi, J., Motte, L., and Pileni, M.P., *Mesoscopic organizations of magnetic nanocrystal: the influence of short-range interactions.* Current Opinion In Colloid & Interface Science, 2004. **9**(1-2): p. 185-191.

8. Tamura, I. and Mizushima, T., *Explanation for magnetic properties of interacting iron oxide nanocrystals.* Journal Of Magnetism And Magnetic Materials, 2002. **250**(1-3): p. 241-248.

9. Vasquez-Mansilla, M., Zysler, R.D., Apciprete, C., Dimitrijewits, M.I., Saragovi, C., and Greneche, J.M., *Magnetic interaction evidence in alpha-Fe2O3*

nanoparticles by magnetization and Mossbauer measurements. Journal Of Magnetism And Magnetic Materials, 1999. **204**(1-2): p. 29-35.

10. Iglesias, O. and Labarta, A., *Magnetic relaxation in a model of interacting nanoparticles in terms of microscopic energy barriers.* Physica Status Solidi A-Applied Research, 2004. **201**(15): p. 3329-3332.

11. Ghazali, A. and Levy, J.C., *Two-dimensional arrangements of magnetic nanoparticles.* Physical Review B, 2003. **67**(6).

12. Lamba, S. and Annapoorni, S., *Single domain magnetic arrays: role of disorder and interactions.* European Physical Journal B, 2004. **39**(1): p. 19-25.

13. Ge, J.P. and Yin, Y.D., *Magnetically responsive colloidal photonic crystals.* Journal Of Materials Chemistry, 2008. **18**(42): p. 5041-5045.

14. Lidorikis, E., Egusa, S., and Joannopoulos, J.D., *Effective medium properties and photonic crystal superstructures of metallic nanoparticle arrays.* Journal Of Applied Physics, 2007. **101**(5).

15. Gehl, B., Flege, J.I., Aleksandrovic, V., Schmidt, T., Kornowski, A., Bernstorff, S., Falta, J., Weller, H., and Baumer, M., *Plasma modification of CoPt3 nanoparticle arrays: A route to catalytic coatings of surfaces.* Journal Of Vacuum Science & Technology A, 2008. **26**(4): p. 908-912.

16. Guo, Z.H., Lei, K., Li, Y.T., Ng, H.W., Prikhodko, S., and Hahn, H.T., *Fabrication and characterization of iron oxide nanoparticles reinforced vinyl-ester resin nanocomposites.* Composites Science And Technology, 2008. **68**(6): p. 1513-1520.

17. Gonzalez, L.A., *Negative Magnetophoresis of Submicron Species in Magnetic Nanofluids*. 2009, Massachusetts Institute of Technology: Cambridge.

18. Singh, H. and Hatton, T.A., *Orientational dependence of apparent magnetic susceptibilities of superparamagnetic nanoparticles in planar structured arrays:*

Effect on magnetic moments of nanoparticle-coated core-shell magnetic beads. Journal Of Magnetism And Magnetic Materials, 2007. **315**(1): p. 53-64.

19. Rosensweig, R.E., *Ferrohydrodynamics*. 1985: Cambridge University Press: Cambridge.

Chapter 7

7. Concluding discussions

7.1 Summary of work

The goal of this work was to evaluate the thermodynamic and transport properties of non-magnetic particles in magnetic fluids. Also, we have evaluated the magnetization characteristics of magnetite particle nanoclusters. We have considered magnetic fluids to consist of discrete particles rather than to be continuum as considered by some of the previous works [1-5]. We consider non-magnetic particles to be of similar order of size as that of magnetic particles and hence the approximation is not valid for our work.

We performed Monte Carlo simulations [6] to evaluate the interactions between non-magnetic particles and magnetic nanoparticles (10 nm and 20 nm diameter) dispersed in organic phase. The presence of the non-magnetic particle in the system induces magnetic non-homogeneity. The magnetic nanoparticles present in the equatorial place of the non-magnetic particle with reference to the applied magnetic field have a higher magnetization as compared to the particles in the polar region. This effect was much more dominant for 20 nm particles than 10 nm particles, because the magnetic inter-particle interactions are much stronger for the larger particles. It was also observed that the radial distribution function for the magnetic nanoparticles in the equatorial plane next to the particle increases with increasing magnetic field strength, since the particles are more stable in this region.

We have evaluated magnetophoretic forces non-magnetic particles experience when subjected to magnetic field gradient. The forces arising from the inter-particle interactions between the magnetic nanoparticles were found to be significant, which have been neglected previously [2, 3], for larger magnetic particles, smaller non-magnetic

particles (as compared to the magnetic particles) and lower magnetic fields. A physical reasoning for the trends has been discussed in detail in Chapter 3.

We performed Brownian Dynamics simulations [7] to evaluate the diffusion coefficients for non-magnetic nanoparticles in magnetic fluids. The chain-like structures formed by magnetic nanoparticles introduce anisotropy in the system with the diffusion coefficients higher along the direction of external magnetic field and lower in the direction perpendicular. The anisotropy coefficient, defined as ratio of the diffusion coefficient in the parallel direction to the coefficient in the perpendicular direction, increases with higher magnetic particle concentration and larger size for the non-magnetic particles. Anisotropy is negligible for small sized magnetic particles for which the inter-particle interaction is smaller, increases with increasing magnetic particle size and becomes constant thereafter. Results have been compared with theoretical predictions [8, 9].

Néel Relaxation [10] was studied for magnetic nanoparticle clusters. Chain-like, spherical and planar clusters were evaluated for the relaxation times, as a function of cluster size and the individual magnetic nanoparticle size. For chain-like structures the relaxation times increase significantly on increasing the chain length and particle size. For spherical clusters the relaxation times were fairly similar to that of individual magnetic nanoparticles, irrespective of the cluster size. Hence, fast relaxation makes spherical clusters ideal candidates for HGMS separations [11-13], since they will be released quickly from the magnetic wires during the elution step.

Also, we studied the magnetization characteristics of magnetic clusters in presence of low remnant fields [14]. Rectangular and hexagonal packing arrangements were studied. The hexagonal arrangement revealed a novel oscillatory behavior in the magnetization characteristics. A theoretical model was developed to predict the magnetic particle size beyond which the oscillations are observed.

7.2 Future work

The interaction between the magnetic and non-magnetic particles was limited to only spherical particles for lack of computational power. This work can be further extended to

observe shape and orientation effects non-spherical particles may have. Also, a more detailed parametric study for the studied properties is needed. For example, our work for magnetization non-homogeneity is limited to only 10 nm and 20 nm sized particles. A parametric study would help us develop empirical models for the effects that we have observed. Also, for the evaluation of diffusion coefficients we need to run the simulations for longer times, so that we can evaluate the long time diffusion coefficients [15-18]. To perform these long time diffusion coefficient studies we either need to use faster algorithms or better computational resources. The thermodynamic and transport properties evaluated in this work have been limited to organic solvents. By including the electrostatic forces of interaction, this work can be extended to aqueous solutions.

Néel relaxation studies were limited to very simplistic models. A more complicated model needs to be developed to include the effect of the presence of 'easy axis of magnetization' [19]. This work can be further extended to include the rotational Brownian motion when the clusters are not physically constrained to move. Also, more work is further need to have a more detailed understanding and prediction of this oscillatory behavior of magnetic moments. We were able to predict the critical size at which the oscillations are induced, yet we need further work to predict the frequency/ wavelength of the oscillations.

The area of work to understand the interactions between magnetic and non-magnetic particles has a lot of unexplored opportunities. In this work we were able to explore only a few of these possibilities. Future work is needed to understand other thermodynamic and transport properties to help develop applications which will use magnetic fluids.

7.3 Bibliography

1. Fateen, S., *Magnetophoretic Focusing of Submicron Particles Dispersed in a Polymer-Based Magnetic Fluid*, in *Doctoral Thesis*. 2002, MIT: Cambridge.

2. Gonzalez, L., Fateen, S.E.K., Smith, K., and Hatton, T.A., *Magnetophoresis of Non-magnetic, Submicrometer Particles in Magnetic Fluids.* Singapore-MIT Alliance (SMA) Symposium, 2004.

3. Gonzalez, L.A., *Negative Magnetophoresis of Submicron Species in Magnetic Nanofluids*. 2009, Massachusetts Institute of Technology: Cambridge.

4. Skjeltorp, A.T., *Colloidal Crystals In Magnetic Fluid.* Journal Of Applied Physics, 1984. **55**(6): p. 2587-2588.

5. Skjeltorp, A.T., *Ordering Phenomena Of Particles Dispersed In Magnetic Fluids.* Journal Of Applied Physics, 1985. **57**(8): p. 3285-3290.

6. Frenkel, D. and Smit, B., *Understanding molecular simulations*. 2002: Academic Press.

7. Vangunsteren, W.F. and Berendsen, H.J.C., *Algorithms For Brownian Dynamics.* Molecular Physics, 1982. **45**(3): p. 637-647.

8. Phillips, R.J., Deen, W.M., and Brady, J.F., *Hindered Transport Of Spherical Macromolecules In Fibrous Membranes And Gels.* Aiche Journal, 1989. **35**(11): p. 1761-1769.

9. Rayleigh, J.W., *On the Influence of Obstacles Arranged in Rectangular Order upon the Properties of a Medium.* Phil. Mag, 1892. **5**(34): p. 481-502.

10. Néel, L., *Thermoremanent Magnetization of Fine Powders.* Reviews of Modern Physics, 1953. **25**(1): p. 293.

11. Ditsch, A., Lindenmann, S., Laibinis, P.E., Wang, D.I.C., and Hatton, T.A., *High-gradient magnetic separation of magnetic nanoclusters.* Industrial & Engineering Chemistry Research, 2005. **44**(17): p. 6824-6836.

12. Ditsch, A., Yin, J., Laibinis, P.E., Wang, D.I.C., and Hatton, T.A., *Ion-exchange purification of proteins using magnetic nanoclusters.* Biotechnology Progress, 2006. **22**(4): p. 1153-1162.

13. Moeser, G.D., Roach, K.A., Green, W.H., Hatton, T.A., and Laibinis, P.E., *High-gradient magnetic separation of coated magnetic nanoparticles.* Aiche Journal, 2004. **50**(11): p. 2835-2848.

14. Singh, H. and Hatton, T.A., *Orientational dependence of apparent magnetic susceptibilities of superparamagnetic nanoparticles in planar structured arrays: Effect on magnetic moments of nanoparticle-coated core-shell magnetic beads.* Journal Of Magnetism And Magnetic Materials, 2007. **315**(1): p. 53-64.

15. Batchelor, G.K., *Brownian Diffusion Of Particles With Hydrodynamic Interaction.* Journal Of Fluid Mechanics, 1976. **74**(MAR9): p. 1-29.

16. Batchelor, G.K., *Diffusion In A Dilute Polydisperse System Of Interacting Spheres.* Journal Of Fluid Mechanics, 1983. **131**(JUN): p. 155-175.

17. Cichocki, B. and Felderhof, B.U., *Time-Dependent Self-Diffusion Coefficient Of Interacting Brownian Particles.* Physical Review A, 1991. **44**(10): p. 6551-6558.

18. Lekkerkerker, H.N.W. and Dhont, J.K.G., *On The Calculation Of The Self-Diffusion Coefficient Of Interacting Brownian Particles.* Journal Of Chemical Physics, 1984. **80**(11): p. 5790-5792.

19. Fannin, P.C. and Charles, S.W., *On The Calculation Of The Neel Relaxation-Time In Uniaxial Single-Domain Ferromagnetic Particles.* Journal Of Physics D-Applied Physics, 1994. **27**(2): p. 185-188.

Appendix

A.1 Cluster Moving Algorithm

A new convenient cluster Algorithm was developed for the simulations. This method is modified insertion sort algorithm to easily identify the cluster and the data structure henceforth helps organize and perform cluster moves efficiently. To verify if two particle are a part of the same cluster we verify whether the two selected particles are in close proximity to each other, which is done be selecting an arbitrary clustering radius r_c. The most efficient way to demonstrate our algorithm is by illustrating with an example. Let us consider a system as shown in Figure A-1.

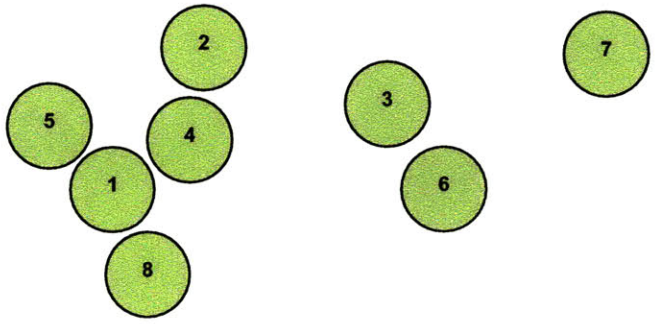

Figure A-1: An example cluster system chosen for our example. Particles 1,2,4,5 and 8 form one cluster while particles 3 and 6 form another cluster.

The first part of the algorithm involves initializing an array with particles at alternating position and zeros occupying the remaining positions as follows with the size of array being twice the size of number of particles.

1	0	2	0	3	0	4	0	5	0	6	0	7	0	8	0

The next step involves checking if the two particles belong to the same cluster. This process starts from the left hand side of the cluster. The comparison is made only if the two elements of the array are non zero. So for example the first comparison will be made between particles numbered 1 and 2.

1	0	2	0	3	0	4	0	5	0	6	0	7	0	8	0

Since these particles do not belong to the same cluster, no move is performed. The second step involves comparing 1 and 3 and after that the comparison is made between 1 and 4.

1	0	2	0	3	0	4	0	5	0	6	0	7	0	8	0

Here we see that 1 and 4 are within the clustering radius of each other and the first insertion move is performed. This implies inserting 4 immediately after element storing the index for particle 1 as follows:

1	4	0	2	0	3	0	0	5	0	6	0	7	0	8	0

We make further checks by further moving along the array. Hence the next comparison would be between 1 and 5. Another insertion move would be performed. These moves are performed till the second index reaches the end of the array. The array after the end of this operation will look as follows:

1	4	5	8	0	2	0	3	0	0	0	6	0	7	0	0

The second set of operation would begin from the second element in the array, which is '4' in this cited example and compare it with the next element.

1	4	5	8	0	2	0	3	0	0	0	6	0	7	0	0

The second script moves to the right as discussed before till the end of the array. These operations are performed until the entire array has been scanned for clusters.
The final output looks like:

1	4	2	5	8	0	0	3	6	0	0	0	0	7	0	0

The next step involves cluster size identification and ordering. The elements which are grouped together, or in other words elements not separated by zeros are particles of the same clusters. This algorithm is advantageous over some frequently used algorithms[1]
As it reduces the numbers of cluster calculations by half as the number of comparisons made in our algorithm are proportional to N^2 as compared to N^3 in the algorithm compared with [1]. Also by this algorithm we gather data for all the clusters simultaneously.

Particle Number	1	4	2	5	8	0	0	3	6	0	0	0	0	7	0	0
Size Vector	5	5	5	5	5	0	0	2	2	0	0	0	0	1	0	0
Position Vector	1	2	3	4	5	0	0	1	2	0	0	0	0	1	0	0

The second row added here denotes the size of the corresponding cluster and the third row stores the position vector of that particle in that cluster. The calculations of the position vector helps us in performing cluster orientation moves and the calculation of the size vector helps us to ensure that cluster size grows only by particle moves and not by cluster moves.

A.2 Bibliography

1. Stoddard, S.D., *Identifying Clusters In Computer Experiments On Systems Of Particles.* Journal Of Computational Physics, 1978. **27**(2): p. 291-293.